# ABSTRACT

## CHANNEL ESTIMATION AND SIGNAL ENHANCEMENT FOR DS-CDMA SYSTEMS

by
Kun Wang

This dissertation focuses on topics of Bayesian-based multiuser detection, space-time (S-T) transceiver design, and S-T channel parameter estimation for direct-sequence code-division multiple-access (DS-CDMA) systems.

Using the Bayesian framework, various linear and simplified nonlinear multiuser detectors are proposed, and their performances are analyzed. The simplified nonlinear Bayesian solutions can bridge the performance gap between sub-optimal linear multiuser detectors and the optimum multiuser detector.

To further improve the system capacity and performance, S-T transceiver design approaches with complexity constraint are investigated. Novel S-T receivers of low-complexity that jointly use the temporal code-signature and the spatial signature are proposed. Our solutions, which lead to generalized near-far resistant S-T RAKE receivers, achieve better interference suppression than the existing S-T RAKE receivers.

From transmitter side, we also proposed a transmit diversity (TD) technique in combination with differential detection for the DS-CDMA systems. It is shown that the proposed S-T TD scheme in combination with minimum variance distortionless response transceiver (STTD+MVDR) is near-far resistant and outperforms the conventional STTD and matched filter based (STTD+MF) transceiver scheme.

Obtaining channel state information (CSI) is instrumental to optimum S-T transceiver design in wireless systems. Another major focus of this dissertation is to estimate the S-T channel parameters. We proposed an asymptotic, joint maximum likelihood (ML) method of estimating multipath channel parameters for DS-CDMA

systems. An iterative estimator is proposed to further simplify the computation. Analytical and simulation results show that the iterative estimation scheme is near-far resistant for both time delays and DOAs. And it reaches the corresponding CRBs after a few iterations.

# CHANNEL ESTIMATION AND SIGNAL ENHANCEMENT FOR DS-CDMA SYSTEMS

by
Kun Wang

A Dissertation
Submitted to the Faculty of
New Jersey Institute of Technology
in Partial Fulfillment of the Requirements for the Degree of
Doctor of Philosophy in Electrical Engineering

Department of Electrical and Computer Engineering

May 2001

## APPROVAL PAGE

## CHANNEL ESTIMATION AND SIGNAL ENHANCEMENT FOR DS-CDMA SYSTEMS

**Kun Wang**

---

Dr. Hongya Ge, Dissertation Advisor — Date
Assistant Professor, Department of Electrical and Computer Engineering, NJIT

---

Dr. Yeheskel Bar-Ness, Committee Member — Date
Distinguished Professor, Department of Electrical and Computer Engineering, NJIT

---

Dr. Nirwan Ansari, Committee Member — Date
Professor, Department of Electrical and Computer Engineering, NJIT

---

Dr. Alexander M. Haimovich, Committee Member — Date
Associate Professor, Department of Electrical and Computer Engineering, NJIT

---

Dr. Jack H. Winters, Committee Member — Date
Department Head, AT&T Labs Research, Middletown, NJ

## BIOGRAPHICAL SKETCH

**Author:** Kun Wang

**Degree:** Doctor of Philosophy

**Date:** May 2001

### Undergraduate and Graduate Education:

- Doctor of Philosophy in Electrical Engineering, May 2001
  New Jersey Institute of Technology, Newark, NJ, U.S.A.
- Master of Science in Electrical Engineering, March 1995
  Northwestern Polytechnic University, Xi'an, China.
- Bachelor of Science in Electrical Engineering, July 1993
  Northwestern Polytechnic University, Xi'an, China.

**Major:** Electrical Engineering

### Publications and Presentations:

K. Wang and H. Ge, "Joint Channel Parameter Estimation for DS-CDMA System over Multipath Rayleigh Fading Channels," submitted to *IEEE Transactions on Vehicular Technology.*

K. Wang and H. Ge, "Differential Transceiver Design for DS-CDMA System with Transmit Diversity," accepted by *IEEE Vehicular Technology Conference*, (Atlantic City, NJ), 2001.

K. Wang and H. Ge, "Differential Detection Scheme for DS-CDMA System with Transmit Diversity," accepted by *IEEE MILCOM Conference*, (McLean, VA), 2001.

K. Wang and H. Ge, "New Space-Time Receivers for DS-CDMA Systems," submitted to *IEEE Communication Letters.*

K. Wang and H. Ge, "Joint Estimation of Time Delays and DOA's for DS-CDMA System over Multipath Rayleigh Fading Channels," *Proceedings of IEEE International Conference on Communications*, (Helsinki, Finland), June 2001.

K. Wang, H. Ge and Y. Ding, "Adaptive Parametric Schemes for Analysis and Synthesis of Musical Signals," *Journal of Audio Engineering Society*, May 2001.

K. Wang and H. Ge, "Estimating Temporal and Spatial Channel Parameters for DS-CDMA System over Multipath Rayleigh Fading Channels," *IEEE International Conference on Acoustics, Speech, and Signal Processing*, (Salt Lake City, UT, U.S.A.), vol. 4, SPCOM-P2.2, May 2001.

K. Wang and H. Ge, "Joint Space-Time Channel Parameter Estimation for DS-CDMA System in Multipath Rayleigh Fading Channels," *IEE Electronics Letters*, vol. 37, pp. 458-460, March 29th 2001.

K. Wang and H. Ge, "A Space-Time Receiver for Asynchronous DS-CDMA Systems Based on Kalman Filter," *Proceedings of the 34th IEEE Asilomar Conference on Signals, Systems, and Computers*, (Pacific Grove, CA, U.S.A.), pp. 547-551, October 2000.

K. C. Hong, H. Ge and K. Wang, "Iterative Propagation Delay Estimation for Asynchronous Direct-Sequence Code Division Multiple Access Communication Systems," *Proceedings IEEE Sixth International Symposium on Spread Spectrum Techniques and Applications*, (Whippany, NJ, U.S.A.), pp. 292-295, September 2000.

K. Wang, X. Cai and H. Ge, "A Novel Space-Time Rake Receiver for DS-CDMA Systems", *Proceedings of 34th Conference on Information Science and Systems, vol. II*, pp. FA3-12-FA3-16, (Princeton, NJ, U.S.A.), March 2000.

H. Ge, K. Wang and K. C. Hong, "Fast Delay estimation for Asynchronous CDMA Communications Systems," *Proceedings of the 33rd IEEE Asilomar Conference on Signals, Systems, and Computers*, (Pacific Grove, CA, U.S.A.), pp. 1589-1593, October 1999.

H. Ge and K. Wang, "Bayesian Based Linear and Non-Linear Detectors for CDMA Communications," *Proceedings of the IEEE Signal Processing Workshop on Higher-Order Statistics*, (Ceasarea, Israel), pp. 135-139, June 1999.

H. Ge and K. Wang, "Efficient Method for Carrier Offset Correction in OFDM system," *Proceedings of IEEE International Conference on Acoustics, Speech, and Signal Processing, vol. V*, (Phoenix,AZ, U.S.A.), pp. 2467-2470, March 1999.

K. Wang, H. Ge and Y. Ding, "Analysis and Synthesis of Musical Tone Signals," *Proceedings of the 33rd Conference on Information Science and Systems*, (Baltimore, MD, U.S.A.), pp. 540-545, March 1999.

To my parents

## ACKNOWLEDGMENT

I would like to express my sincere gratitude to my advisor, Dr. Hongya Ge. Her constant support, detailed guidance and frequent encouragement have been invaluable during my time at Center for Communications and Signal Processing Research. She has greatly contributed to my life as a graduate student both on a professional and on a personal level.

I would also like to express my grateful appreciation to the distinguished members of the dissertation committee: Dr. Nirwan Ansari, Dr. Yeheskel Bar-Ness, Dr. Alex Haimovich, and Dr. Jack Winters. Their valuable discussions and insightful comments have improved the quality of this dissertation.

Many thanks are due to the professors of the ECE department for making my graduate experience intellectually rewarding and for providing me with a strong background in communications and signal processing.

I would also like to thank my friends at the CCSPR for their kindly assistance.

I sincerely thank my parents for their wisdom advice, constant support, and conditionless love in all my life.

Finally, my sincere gratitude goes to my husband, Lingang Li, who has provided me endless love and encouragement during the period of this work.

## TABLE OF CONTENTS

**Chapter** **Page**

## TABLE OF CONTENTS
## (Continued)

**Chapter** **Page**

## TABLE OF CONTENTS
## (Continued)

**Chapter** **Page**

## LIST OF FIGURES

**Figure** **Page**

## LIST OF FIGURES
## (Continued)

**Figure** **Page**

## LIST OF FIGURES
## (Continued)

**Figure** **Page**

## LIST OF FIGURES
## (Continued)

**Figure** **Page**

# CHAPTER 1

# INTRODUCTION

The area of detection and estimation theory represents a combination of the classical techniques of statistical inference and the random process characterization of communications, radar, sonar and other modern data processing systems. In the detection case, one observes an output that has a random character and decide which of two possible causes produced it. In the estimation case, the output is related to the value of some parameter of interest, and one tries to estimate the value of this parameter. The aim of the signal processing technique is to extract the signal from the noisy data, to estimate the values of a group of parameters and to make the decision of the interested information. This work focuses on topics of Bayesian-based multiuser detection (MUD), space-time (S-T) transceiver design, and S-T channel estimation for direct-sequence code-division multiple-access (DS-CDMA) systems.

## 1.1 Multiple Access Techniques

Cellular radio systems rely on an intelligent allocation and reuse of channels throughout a coverage region. Multiple access schemes are used to allow many mobile users to simultaneously share a finite amount of a radio spectrum. There are three major multiple access techniques, namely, frequency-division multiple-access (FDMA), time-division multiple-access (TDMA) and code-division multiple-access (CDMA), used to share the available bandwidth in a wireless communication system. FDMA assigns individual frequency channels to individual users. TDMA systems transform the radio spectrum into time slots, and in each time slot only one user is allowed to either transmit or receive. In DS-CDMA systems, all the users operate in the same frequency and time channels. Each user is assigned a unique pseudo-

random codeword which is approximately orthogonal to all other codewords [1]. This dissertation concentrates on the DS-CDMA system.

## 1.2 Direct-Sequence Code-Division Multiple-Access

In DS-CDMA system, users access the channel in a random manner. Hence, the signal transmissions among multiple users completely overlap both in time and in frequency. Each user has a unique spreading code. This code operates at a chip rate that is $N$ times greater than the information data rate. The spreading code is designed to be orthogonal or quasi-orthogonal. If orthogonal codes are used and there is no multipath, code orthogonality can be maintained, thus users do not interfere with each other and signal detection performance is only noise limited. If we use quasi-orthogonal codes or orthogonal codes in multipath environments, the users interfere with each other and the detection becomes interference limited. The multiple-access interference (MAI) that arises from other users is reduced by the processing gain $N$ [1, 2].

The demodulation and separation of DS-CDMA signals at the receiver is facilitated by the fact that each signal is spread in frequency by its own pseudo-random code sequence (known to both the transmitter and the receiver) which is approximately orthogonal to all other code sequences. The conventional matched filter (MF) receiver performs a time correlation operation to detect the message of the desired user. This receiver is optimal under the conditions that: (a) the codes are orthogonal; (b) perfect symbol synchronization is achieved; (c) no multipath is present and (d) the additive noise is white and Gaussian. However, in practice, these conditions cannot be all met, and hence the MF receiver will not be optimal due to the presence of MAI [2]. The MAI is one of the major limitations to the performance and capacity of conventional receivers in DS-CDMA systems.

In DS-CDMA system, multipath has both a positive and a negative effect. On one hand, the independent fading paths can be a valuable source of diversity. On the other hand, the multipath introduces interpath interference. RAKE combiner is used to match the channel that exhibits multipath with delay spread larger than one chip period. The RAKE receiver uses multiple correlators, one for each path, and the outputs of the correlators (called fingers) are then combined into a single output to maximize the signal to noise ratio (SNR) [3, 2].

### 1.2.1 Multiuser Detection

Compensating for the near-far effect is critical for satisfactory performance of DS-CDMA systems. Commercial digital cellular system based on DS-CDMA uses stringent power control, described in [1], to combat near-far effects. Another approach is MUD. All MUD techniques utilize the temporal spreading code signatures used by users and the structure of the MAI to suppress the MAI and hence enhance the performance and capacity of DS-CDMA systems. The major advantages of using MUD in DS-CDMA are the following: (a) it eliminates the need for stringent power control in alleviating the near-far problem; (b) it also provides substantial system gains in terms of dynamic channel-sharing and allocation, efficient utilization of frequency spectrum and transmission power and other resource management measures. Fundamental investigations by Verdú have demonstrated the huge potential capacity and performance improvements of joint, optimal, maximum-likelihood (ML) decoding structure of all users compared with MF alternatives [4]. However, the complexity of the solution is increased exponentially with the number of users [5]. The promised gains of the MUD have motivated much research for practical schemes with reduced complexity in this area.

Among various suboptimal detectors, the linear class of detectors, the decorrelating detector [6, 7] and the linear minimum mean squared error (LMMSE)

detector [8, 9, 10], need much less computations. The decorrelating detector linearly transforms each vector of MF outputs with a generalized inverse of the signal cross-correlation matrix [6, 7], therefore removes the MAI. The decorrelating detector is not optimal as the premultiplication of the MF output colors the noise. However, it was shown in [6] by Lupas and Verdú that decorrelating detector is optimal near-far resistance. And there are a significant reduction in computational complexity and no need to estimate channel powers for decorrelating receiver. LMMSE detector minimizes the mean square error (MSE) between the transmitted symbol and the received symbol with the linear constraint [8, 9, 10]. It was shown in [8] by Medhow and Honig that LMMSE receiver is also near-far resistant and offers a significant performance improvement over a MF receiver. LMMSE receiver has the important property that a single user can be detected without having to detect all other users and it can be easily structured to be adaptive [8, 11, 12]. In the asymptotic case of background noise going to zero, the LMMSE receiver reduce to the decorrelating receiver. The blind alternative of LMMSE receiver was presented in [9] and this techniques avoids the need for a training sequence that is necessary for the LMMSE receiver, and more importantly, has been shown to converge to an LMMSE receiver.

The performance gap between the LMMSE receivers and the optimal ML receivers can be bridged with the use of interference cancellation (IC) receivers. The IC receivers can provide near-optimal performance with little added complexity [13, 14, 15, 16, 17, 18]. For the multiuser system, the interference does not only originate from past symbols, but also from current symbols of other users. The tentative decisions for the interfering symbols are needed to implement such interference cancellation schemes providing further justification for the use of linear receivers. Both the parallel interference canceler (PIC) [17, 18] and the successive interference canceler (SIC) [13, 14, 15, 16] have a multistage structure. In each stage, PIC simultaneously regenerates and cancels the MAI due to other users based on the

detected bits in the preceding stage. The SIC sequentially removes the MAI due to the stronger users before detecting the weaker one. Generally, the PIC causes much less decision delay than the SIC.

### 1.2.2 Space-Time Receiver for Wireless Communications

All conventional MUD techniques utilize the temporal spreading code signatures used by users to suppress the MAI and hence enhance the performance and capacity of DS-CDMA systems. However, spatial signatures are not utilized in the conventional MUD techniques [4, 5, 19] and thus conventional MUD can not effectively address the problem of co-channel interference (CCI) that arises from the frequency reuse, thereby limiting the quality and capacity of wireless networks. Deploying multiple receive antennas at both the base and remote stations increases the capacity of wireless channels, and information theory provides measures of this increase [20, 21]. The use of multiple antennas adds a new dimension to the DS-CDMA receiver problem, increases the freedom of processing space and allows improved separation of user signals. Therefore, space-time processing can significantly increase the capacity of DS-CDMA systems [2, 22, 23, 24, 25, 26]. A space-time (S-T) receiver operates simultaneously on all the antennas, processing signal samples both in space and time. This extra dimension enables interference cancellation in a way that is not possible with single-antenna-receivers. The desired signal and the interference almost always arrive at the antenna array (even in complex multipath environments) with distinct and often well-separated spatial signatures, thus allowing the receiver to exploit this difference to further reduce interference. In the receiver, the spatial dimension can also be used to enhance array gain, to improve signal to noise ratio, to achieve diversity gain, and even to suppress intersymbol interference.

In order to utilize the additional information inherent in spatial signatures, incorporation of S-T processing in DS-CDMA system was proposed by Naguib and

Paulraj [23]. The decoupled S-T RAKE receiver was a S-T extension of a conventional RAKE receiver. The decoupled S-T RAKE receiver [24, 27] combines the signature MF code processing with disjoint spatial MMSE and temporal RAKE combining. The capacity of this receiver was studied in [28]. The joint S-T RAKE receiver [25, 29, 30] combines the signature MF code processing with jointly optimum MMSE S-T processing. However, spreading codes are not optimally used to maximize the signal to interference and noise ratio (SINR) in the conventional S-T RAKE receivers [24, 25]. As the freedom of the receiving antenna is small compared to the number of active users' multipath components, the ability of the interference suppression for the conventional S-T RAKE receivers is not optimal. Other contributions for applying S-T processing techniques in DS-CDMA system receivers can be found in [31, 32, 33, 34, 35, 36].

### 1.2.3 Transmit Diversity for Wireless Communications

In many systems, however, additional antennas may be expensive or impractical at the remote station. The small size of the mobile receivers limits both the spatial resolution of the array (because of the small number of elements) and the diversity gain (because the elements are close to one another). In these cases multiple transmit antenna array is considered.

One possible approach for antenna array transmit processing is transmit beam-forming [2, 37], which provides array gain at the subscriber unit. In these schemes, the transmitter typically operates in "closed-loop," i.e., it uses channel information that is fed to it by the receiver through the reverse link in order to shape beams in the forward link. The success of transmit beam-forming depends on the quality of the channel estimates, the feedback channel, the mapping between the two links, and the dynamics of the signal and interference. Closed-loop techniques typically suffer from reduced uplink capacity because of the extra channel information that

is transmitted. It is not applicable to situation when the downlink and uplink use different frequency band.

Another approach employs transmit diversity (TD) to provide diversity benefit at a receiver with multiple transmit antennas only. TD is a technique where information is transmitted from multiple antennas in order to mitigate the effects of signal fading. Multiple transmit antennas at the base station will increase the downlink capacity with only minor increase in terminal complexity. TD can be simpler to implement because it can operate in an open-loop, i.e., without channel knowledge at the transmitter. This mode of operation is particularly appealing when the mobile speed is high enough to make channel estimation and tracking too difficult. Moreover, open-loop techniques do not penalize the uplink capacity as closed-loop techniques do. These arguments suggest that multiple antenna open-loop TD is a practical way to improve the performance of current systems.

Recently, some interesting approaches for TD have been suggested. In a delay-transmit diversity (DTD), the base station transmits a delayed version of the original signal, hence creating an artificial multipath distortion [38, 39, 40, 41]. However, due to the degrading orthogonality and increasing the interference level seen at the mobile receiver, DTD has a limited link performance gain over non-TD [42]. Another approach is orthogonal transmit diversity (OTD) introduced in [42], which transmits its signal on multiple antennas each spread by an orthogonal code in base station. OTD was shown to provide large improvements over DTD [42, 43, 44, 45]. Recent work on S-T block codes for TDMA systems, motivated the introduction of space-time transmit diversity (STTD) for DS-CDMA systems [46, 47, 48, 49] . In addressing the issue of decoding complexity, Alamouti discovered a remarkable scheme for transmission using two transmit antennas [46]. This scheme supports an ML detection scheme with only linear processing at the receiver. S-T orthogonal block coding introduced in [49] utilizes the theory of the orthogonal designs. It

generalizes the transmission scheme discovered by Alamouti to an arbitrary number of transmit antennas and is able to achieve the full diversity promised by the transmit and receive antennas. These codes retain the property of having a very simple ML decoding algorithm based only on linear processing at the receiver.

## 1.3 Channel Parameter Estimation

In wireless communication systems, the multipath channel is characterized by both time delays and direction of arrivals (DOA's) of different propagation paths. How to estimate the time delays and the DOA's of a user's multipath signals arriving at a base station antenna array and consequently, utilize the multipath components in the receiver is an issue of great interest in wireless communications. The estimation of the time delay and DOA has been addressed disjointly during the past decades. The estimation of the the time delays while ignoring the spatial characteristics of the multipath channel has been studied in [50, 51, 52, 53, 54], and the estimation of the DOA's while ignoring the time characteristics of the channel has been studied in [55, 56, 57, 58, 59, 54]. However, these disjoint estimation algorithm are definitely not optimal for S-T receiver.

To improve the channel characterization and lead to a better equalization approach, the optimal estimation techniques that exploit both the temporal and the spatial characteristics of the channel should be used. Due to its importance in practice, much research has been done to jointly estimate the time delays and the DOA's of a user's multipath signals arriving at a base station antenna array, and consequently, utilize the multipath components in the receiver [60, 61, 62, 63, 64, 65]. An algorithm for estimating the time delays and the DOA's of multiple reflections of a known transmitted signal is proposed from signal processing perspective in [60]. In [61], a subspace based approach to estimate the time delays and the DOA's of multipath signals is presented for TDMA system. In [62], the existing DOA

estimation methods were extended to the joint time delay and DOA estimation. Compared with disjoint techniques which first estimate delays and subsequently the angle corresponding to each delay, joint estimation has an advantage of increasing the estimation accuracy, especially in cases where multiple rays have approximately equal delays (or angles). In [63, 65, 64], joint ML channel parameter estimation algorithm was developed for DS-CDMA system assuming the knowledge of the signatures and the pilot signals of all $K$ active users.

## 1.4 Dissertation Overview

In this introductory chapter, the background have been laid for the subject materials of this dissertation. In chapter 2, the MUD problem of DS-CDMA systems is solved using the framework of Bayesian approach [66]. Various simplified Bayesian based multiuser detectors, including both linear and non-linear detectors, are presented and analysed for DS-CDMA communication systems. The simplified linear solutions of Bayesian approach are LMMSE detector under quadratic cost function and marginal maximum a posteriori (MAP) detector under hit-or-miss cost function, respectively. Non-linear multi-stage and iterative optimization multiuser detectors based on simplified linear Bayesian detectors are investigated to obtain improved detection performance. Firstly, the performance of the iterative LMMSE estimator with the LMMSE estimator of multiple access users' information as tentative and/or initial statistics for multi-stage iteration is investigated. Secondly, the performance of the multistage MAP detector with marginal MAP estimation as the tentative statistics for the initial stage is investigated. The performances of both non-linear detectors are close to that of the optimum detector after one iteration.

Chapter 3 develops low-complexity S-T receivers that jointly use the signal code signature and the spatial signature to achieve better interference suppression than the existing S-T RAKE receivers [67, 68]. At each antenna elements output,

the minimum variance distortionless response (MVDR) filter instead of MF is used in time domain to preserve the signal of the desired user and to suppress the MAI and noise at the same time. The decision statistics are then obtained by optimally combining the finger outputs across space and time disjointly for MVDR decoupled S-T receiver, and jointly for MVDR joint S-T RAKE receiver, respectively. The proposed S-T receivers with differential encoding/decoding or with training sequence are also investigated to avoid the phase ambiguity problem.

Chapter 4 proposes and evaluates the performance of the differential detection scheme with STTD for DS-CDMA systems [69, 70]. At the transmitter, the STTD scheme, which provides the TD, is combined with the proposed generalized differential encoding scheme; at the receiver, the differential decoding technique is combined with the MVDR receiver, which suppresses the MAI. The performance of the proposed scheme is compared with that of the OTD combining with conventional differential encoding and MVDR receiver. Both transceiver schemes provide full spatial diversity, outperform the non-TD system, and require no channel state information at both the transmitter and the receiver. It is also shown that the performance of the proposed OTD+MVDR and STTD+MVDR receivers are much better than those conventionally used OTD+MF and STTD+MF receivers, and the STTD+MVDR scheme has a much better performance than OTD+MVDR scheme at the price of the higher complexity receiver.

Chapter 5 develops a joint ML estimation method for temporal and spatial channel in DS-CDMA systems [71, 72, 73, 74]. After modeling the known training sequence of a desired user as the desired signal, the MAI-plus-AWGN as an unknown colored Gaussian noise uncorrelated with the desired signal, and exploiting the knowledge of the desired user's spreading signature, a joint ML time delay and the DOA estimator is developed for DS-CDMA system over multipath Rayleigh fading channels. In order to reduce the computational complexity of the multidi-

mensional numerical search associated with the ML estimator, an efficient iterative ML estimation scheme that transforms the multi-dimensional maximization problem into two simple 1-dimensional (1-D) maximization problems is proposed. Analytical and simulation results show that the proposed estimator is near-far resistant for both time delay and DOA estimation, and it can reach the corresponding Cramer-Rao bounds (CRBs) after a few iterations. The CRBs are derived in Appendix A. Chapter 6 concludes the work in this dissertation.

# CHAPTER 2

# BAYESIAN BASED LINEAR AND NON-LINEAR DETECTORS FOR DS-CDMA SYSTEMS

In this chapter, the MUD problem is solved using Bayesian approach [75, 76, 66]. Various simplified Bayesian-based multiuser detectors, including both linear and non-linear detectors, are presented for DS-CDMA communication systems. Due to the non-Gaussian nature of the problem, the Bayesian solutions are generally non-linear. Bayes solution under quadratic and hit-or-miss cost function leads to MMSE and MAP solutions respectively. These two detectors are associated with the highly non-linear multi-dimensional integrations. To reduce the computational complexity, under linear constraint, the MMSE solution leads to the LMMSE detector; the MAP solution leads to the marginal MAP detector. To bridge the performance gap between the linear Bayesian detectors and the optimum detector, the non-linear multi-stage and iterative optimization approaches are investigated. The LMMSE (marginal MAP) estimates of MAI users' information are used as tentative and/or initial statistics for multi-stage iteration. The simulation results show that only one iteration will be enough to reach detection performance close to that of the optimum detector.

## 2.1 Problem Formulation

Consider a synchronous DS-CDMA system with $K$ users transmitting sequences of BPSK symbols over Gaussian channel. The baseband DS-CDMA signal due to the $k$th user is denoted as

$$s_k(t) = \sum_i b_k(i) c_k(t - iT), \quad k = 1, \cdots, K, \tag{2.1}$$

where $T$ is the symbol interval, $b_k(i)$ is the $i$th symbol by the $k$th user, $c_k(t) = \sum_{j=0}^{N-1} c_k(j)\psi(t - jT_c)$ its normalized spreading signature, $0 \leq t \leq T$, $N$ is the

processing gain, $\mathbf{c}_k = [\, c_k(0) \cdots c_k(N-1) \,]^T$ is a signature sequence assigned to the $k$th user, and $\psi(t)$ is a rectangular chip waveform of duration $T_c = T/N$.

The received baseband signal $y(t)$ including all $K$ users and noise is given by

$$y(t) = \sum_i \sum_{k=1}^{K} \sqrt{A_k}\, b_k(i)\, c_k(t - iT) + n(t)\,, \tag{2.2}$$

where $A_k$ is the bit energy of the $k$th user and $n(t)$ is a white Gaussian process with an average power of $\sigma^2$.

At symbol rate, the chip-rate matched filtered and sampled data of (2.2) can be written in matrix form as,

$$\mathbf{y}(n) = \mathbf{S} \cdot \mathbf{A} \cdot \mathbf{b}(n) + \mathbf{n}(n)\,, \tag{2.3}$$

where $(N \times K)$ matrix $\mathbf{S} = [\mathbf{c}_1\, \mathbf{c}_2 \cdots \mathbf{c}_K]$ consists of signatures of MAI, $(K \times K)$ matrix $\mathbf{A} = \mathrm{diag}\{\sqrt{A_1}, \sqrt{A_2}, \cdots, \sqrt{A_K}\}$, and vector $\mathbf{b}(n) = [\, b_1(n)\; b_2(n) \cdots b_K(n) \,]^T$, and $\mathbf{n}(n) \sim \mathcal{N}(\mathbf{0}, \sigma^2\, \mathbf{I})$.

Stacking outputs of a bank of signature matched filters into a vector $\mathbf{x}$, we have,

$$\begin{aligned} \mathbf{x}(n) &= \mathbf{S}^T \cdot \mathbf{y}(n) \\ &= \mathbf{P} \cdot \mathbf{A} \cdot \mathbf{b}(n) + \mathbf{n}_1(n) \\ &= \mathbf{P} \cdot \boldsymbol{\theta}(n) + \mathbf{n}_1(n)\,, \end{aligned} \tag{2.4}$$

where $\mathbf{n}_1(n) \sim \mathcal{N}(\mathbf{0}, \sigma^2\, \mathbf{P})$ being the *colored* Gaussian noise due to matched filtering. The matrix $\mathbf{P}$ is simply the cross-correlation matrix of the signature waveforms, $\mathbf{P} = \mathbf{S}^T\, \mathbf{S}$, which is not an identity matrix due to the non-orthonormal signatures used.

The non-diagonal nature of the $\mathbf{P}$ matrix will cause the MAI, which generates the near-far problem encountered in the conventional MF based detector/receiver. In order to combat the near-far problem, various multiuser detectors have been proposed. This work is mainly concentrated on the multi-stage and iterative non-linear Bayesian approaches to MUD in DS-CDMA system [75, 76, 66].

## 2.2 Optimal Multiuser Detector

The optimum multiuser detector takes into consideration of the existence of MAI and makes the optimal decision by maximizing the following *constrained* likelihood function:

$$\begin{aligned}\hat{\mathbf{b}}(n) &= \arg \max_{\mathbf{b}(n)\in\{-1,+1\}^K} p(y(t)\,|\,\mathbf{b}(n))\,, \quad 0 < t \leq T \\ &= \arg \max_{\mathbf{b}(n)\in\{-1,+1\}^K} p(\mathbf{x}(n)\,|\,\mathbf{b}(n))\,, \\ &= \arg \max_{\mathbf{b}(n)} J(\,\mathbf{b}(n); \mathbf{A}, \mathbf{P}\,)\,, \end{aligned} \tag{2.5}$$

where $J(\,\mathbf{b}(n); \mathbf{A}, \mathbf{P}\,) = 2\,\mathbf{x}(n)^T\,\mathbf{A}\,\mathbf{b}(n) - \mathbf{b}^T(n)\,\mathbf{A}\,\mathbf{P}\,\mathbf{A}\,\mathbf{b}(n)$ is a non-linear function over *discrete* symbol vector $\mathbf{b}(n)$, given the knowledge of matrices of $\mathbf{A}$ and $\mathbf{P}$.

In order to obtain the optimum solution, one needs to test $2^K$ different hypotheses, which is quite computationally demanding for large values of $K$.

## 2.3 Bayesian Approach Based Multiuser Detectors

For notation simplicity, the time index $n$ is omitted from now on knowing that this can cause no confusion. Note that the vector $\boldsymbol{\theta}$ in (2.4) is a random vector. The randomness of $\boldsymbol{\theta}$ is induced by the BPSK information bit vector $\mathbf{b}$. In addition, uncertainty about the transmission power of MAI or matrix $\mathbf{A}$ will also contribute to randomness of the vector $\boldsymbol{\theta}$.

The original probability density function (PDF) of $p(\mathbf{y}|\boldsymbol{\theta})$ can be factored as

$$\begin{aligned} p(\mathbf{y}|\boldsymbol{\theta}) &= p(\boldsymbol{\theta}|\mathbf{y})p(\mathbf{y}) \\ &= p(\boldsymbol{\theta}|\mathbf{x})p(\mathbf{y}). \end{aligned} \tag{2.6}$$

Hence, $\mathbf{x}$ is a sufficient statistic for $\boldsymbol{\theta}$. Let $\epsilon = \boldsymbol{\theta} - \hat{\boldsymbol{\theta}}(\mathbf{x})$ denote the error of the estimator for a particular realization of $\mathbf{x}$ and $\boldsymbol{\theta}$.

Let the deterministic function of $L(\epsilon)$, shown in Figure 2.1, be termed the cost function. It is noted that the large errors are particularly costly. Also, the average

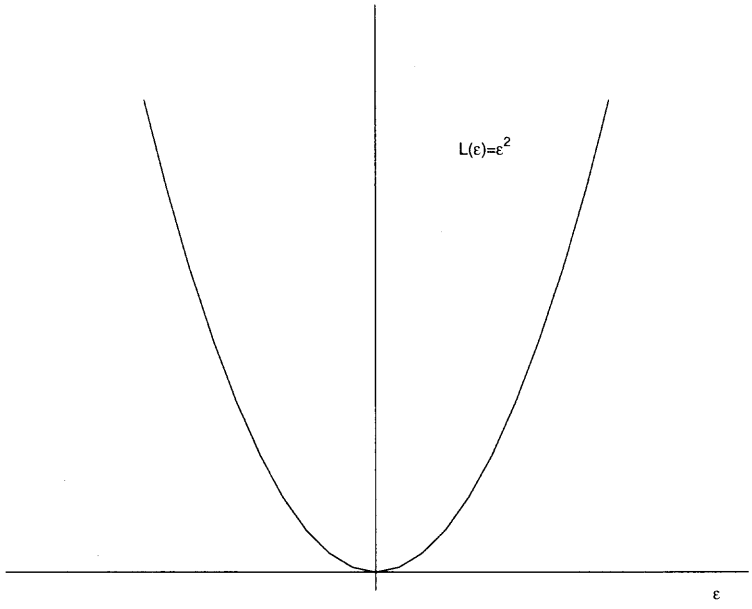


(a) Quadratic error

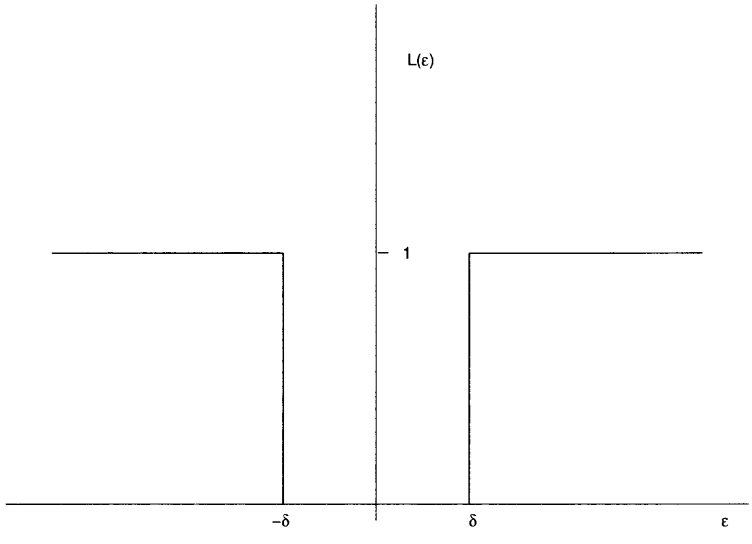


(b) Hit-or-miss error

**Figure 2.1** Examples of cost function

cost or $E[L(\epsilon)]$ is termed the *Bayes risk* $\mathcal{R}$ or

$$\mathcal{R} = E[L(\epsilon)], \tag{2.7}$$

and measures the performance of a given estimator [77]. Now determine the optimal estimators by minimizing the Bayes risk

$$\begin{aligned} \mathcal{R} &= E[L(\epsilon)] \\ &= \int_{\boldsymbol{\theta}} \int_{\mathbf{x}} L\left(\boldsymbol{\theta} - \hat{\boldsymbol{\theta}}(\mathbf{x})\right) p(\mathbf{x}, \boldsymbol{\theta})\, d\mathbf{x} d\boldsymbol{\theta} \\ &= \int_{\mathbf{x}} \left[\int_{\boldsymbol{\theta}} L\left(\boldsymbol{\theta} - \hat{\boldsymbol{\theta}}(\mathbf{x})\right) p(\boldsymbol{\theta}|\mathbf{x})\, d\boldsymbol{\theta}\right] p(\mathbf{x}) d\mathbf{x}. \end{aligned} \tag{2.8}$$

Now since $p(\mathbf{x}) > 0$ for all $\mathbf{x}$, if the integral in brackets can be minimized for each $\mathbf{x}$, then the Bayes risk will be minimized.

### 2.3.1 MMSE Estimator

If $L(\epsilon) = \epsilon^2$, then the cost function is quadratic, see figure 2.1 (a), and the Bayes risk is just the MSE. The optimal Bayes estimator results in the MMSE estimate, or

$$\hat{\boldsymbol{\theta}}(\mathbf{x})_{MMSE} = \arg\min_{\hat{\boldsymbol{\theta}}(\mathbf{x})} \int_{\boldsymbol{\theta}} \left\| \boldsymbol{\theta} - \hat{\boldsymbol{\theta}}(\mathbf{x}) \right\|^2 p(\boldsymbol{\theta}|\mathbf{x})\, d\boldsymbol{\theta}. \tag{2.9}$$

Hence, it results in

$$\begin{aligned} \frac{\partial}{\partial \boldsymbol{\theta}} \int \left\|\boldsymbol{\theta} - \hat{\boldsymbol{\theta}}(\mathbf{x})\right\|^2 p(\boldsymbol{\theta}|\mathbf{x}) d\boldsymbol{\theta} &= \int \frac{\partial}{\partial \boldsymbol{\theta}} \left\|\boldsymbol{\theta} - \hat{\boldsymbol{\theta}}(\mathbf{x})\right\|^2 p(\boldsymbol{\theta}|\mathbf{x}) d\boldsymbol{\theta} \\ &= \int -2\left(\boldsymbol{\theta} - \hat{\boldsymbol{\theta}}(\mathbf{x})\right) p(\boldsymbol{\theta}|\mathbf{x}) d\boldsymbol{\theta} \\ &= -2\int \boldsymbol{\theta} p(\boldsymbol{\theta}|\mathbf{x}) d\mathbf{x} + 2\hat{\boldsymbol{\theta}}(\mathbf{x}) \int p(\boldsymbol{\theta}|\mathbf{x}) d\boldsymbol{\theta} \end{aligned} \tag{2.10}$$

which when set equal to zero results in

$$\begin{aligned} \hat{\boldsymbol{\theta}}(\mathbf{x})_{MMSE} &= \int \boldsymbol{\theta} p(\boldsymbol{\theta}|\mathbf{x}) d\boldsymbol{\theta} \\ &= \mathcal{E}\{\boldsymbol{\theta}|\mathbf{x}\} \\ &= \frac{\int_{\boldsymbol{\theta}} \boldsymbol{\theta}\, p(\mathbf{x}|\boldsymbol{\theta})\; p(\boldsymbol{\theta})\; d\boldsymbol{\theta}}{\int_{\boldsymbol{\theta}} p(\mathbf{x}|\boldsymbol{\theta})\; p(\boldsymbol{\theta})\; d\boldsymbol{\theta}}, \end{aligned} \tag{2.11}$$

as $\int p(\boldsymbol{\theta}|\mathbf{x}) = 1$. The information bits of $K$ users are then obtained based on the decision rule,

$$\hat{\mathbf{b}} = \text{sgn}\left\{ \hat{\boldsymbol{\theta}}(\mathbf{x})_{MMSE} \right\} . \tag{2.12}$$

Due to the non-Gaussian nature of the problem, the MMSE estimator in (2.11) is quite non-linear in data vector $\mathbf{x}$. Only under the very special case of Gaussian a priori $p(\boldsymbol{\theta})$ and Gaussian conditional $p(\mathbf{x}|\boldsymbol{\theta})$, that results in a Gaussian posterior $p(\boldsymbol{\theta}|\mathbf{x})$ in (2.11), the MMSE solution reduces into a linear form. In general, computationally demanding multi-dimensional integrations are needed to be evaluated in order to get the exact form of MMSE estimator in (2.11), on which a decision rule in (2.12) can be applied.

To simplify the above solution one can restrict the estimator to be linear in data $\mathbf{x}$. The LMMSE can be derived from the idea of minimizing the MSE under linear constraint,

$$E\left\{ \left\| \boldsymbol{\theta} - \hat{\boldsymbol{\theta}}(\mathbf{x}) \right\|^2 \right\}, \qquad \text{with } \hat{\boldsymbol{\theta}}(\mathbf{x}) \text{ linear in } \mathbf{x}, \tag{2.13}$$

where the expectation is with respect to the joint PDF of $\mathbf{x}$ and $\boldsymbol{\theta}$, $p(\boldsymbol{\theta}, \mathbf{x})$.

Minimizing (2.13) results in the LMMSE estimate,

$$\hat{\boldsymbol{\theta}}_{LMMSE}(\mathbf{x}) = \left( \mathbf{P} + \sigma^2 \tilde{\mathbf{A}}^{-2} \right)^{-1} \mathbf{x}, \tag{2.14}$$

$$\hat{\mathbf{b}} = \text{sgn}\left\{ \hat{\boldsymbol{\theta}}_{LMMSE}(\mathbf{x}) \right\} . \tag{2.15}$$

where $\tilde{\mathbf{A}}^2 = \mathbf{A}_0^2 + \sigma_A^2 \mathbf{I}$, with $\mathcal{E}(\mathbf{A}) = \mathbf{A}_0$ and $\text{cov}(\mathbf{A}) = \sigma_A^2 \mathbf{I}$ being assumed. For the well-known case when $\mathbf{A}$ is deterministic and known, $\sigma_A^2 = 0$ and $\tilde{\mathbf{A}} = \mathbf{A}_0$. The LMMSE estimate based detector then makes its decision based on the estimate $\hat{\boldsymbol{\theta}}_{MMSE}(\mathbf{x})$ in (2.14). When the interferences of other users are very small compared to the noise level, $(\mathbf{P} + \sigma^2 \mathbf{A}_0^{-2})^{-1} \approx (\mathbf{I} + \sigma^{-2} \mathbf{A}_0^{-2})^{-1}$. In this case, LMMSE detector has the same performance as that of the single user detector, which is the BPSK limit. When the interference levels are very large compared to the noise level, then

$(\mathbf{P}+\sigma^2\mathbf{A}_0^{-2})^{-1} \approx \mathbf{P}^{-1}$. LMMSE detector's performance is comparable to that of the decorrelating detector. Therefore, the overall performance of LMMSE detector is better than that of the decorrelating detector [11]. It should be pointed out that the LMMSE multiuser detector provides the best detection performance among *linear* class of detectors, including the decorrelating detector and other candidates,

However, compared to the performance of the optimum detector in (2.5), there is still a performance loss coming along with the LMMSE, especially when the MAI is strong.

In this work, a one-step iterative optimization approach to *refine* the LMMSE estimator is proposed to improve the detection performance.

Specifically, use the LMMSE estimator of (2.14) and (2.15) as the initial starting point, then evaluate the objective function $J(\mathbf{b};\ \mathbf{A},\mathbf{P})$ at the initial point as well as an *alternative point* $\tilde{\mathbf{b}}$. The alternative point $\tilde{\mathbf{b}}$ resembles the initial point $\hat{\mathbf{b}}$ except that the sign of *the desired user*'s information bit $\hat{b}_k$ is *alternated* in getting $\tilde{\mathbf{b}}$. The estimated symbol of $b_k$ is the one that is corresponding to a larger value of objective function, i.e.,

$$\hat{b}_k = \arg \max_{b_k \in \{-1,+1\}} J\left(b_k;\ \hat{\boldsymbol{\theta}}_{LMMSE}(\mathbf{x})\right), \tag{2.16}$$

It is easily to see that this one-step LMMSE-based iterative multiuser detector have the similar performance as the LMMSE based PIC. In a later simulation section, the improved performance of the one-step LMMSE-based iterative multiuser detector is demonstrated for various near-far situations. The reason for the success of this approach can be explained as follows. Substituting the estimation MAI back to (2.5) is equivalent to remove the estimated MAI from the received data. When the MAI is weaker compared to the desired user, the desired user signal dominates the received data. The the LMMSE detector itself provides detection performance comparable to the optimum detector, therefore, with high probability the one-step up-hill iteration in (2.16) will not change the initial estimate. When the MAI is

stronger than the desired user, the LMMSE detector performs as good as the decorrelating detector, but not as good as the optimum detector. In this case, there exists a gap between the performance of the LMMSE detector and that of the optimum one. Alternating the sign of the *desired user*'s information allows us to seek margin for potential performance improvement by removing the effect of the MAI. The one-step up-hill search in (2.16) provides the chance to improve detection performance at minimum additional computation. Since under strong MAI situation, the *desired user*'s LMMSE estimate is less reliable than the interfering users', one only needs to alternate its sign to realize possible gain in the one-step up-hill search of (2.16).

### 2.3.2 MAP Estimator

On the other hand, the Bayesian solution under "hit-or-miss" cost function, shown in figure 2.1 (b), minimizing

$$\begin{aligned} g(\hat{\boldsymbol{\theta}}(\mathbf{x})) &= \int \left|\boldsymbol{\theta} - \hat{\boldsymbol{\theta}}(\mathbf{x})\right| p(\boldsymbol{\theta}|\mathbf{x}) d\boldsymbol{\theta} \\ &= \int_{-\infty}^{\hat{\boldsymbol{\theta}}(\mathbf{x})-\delta} (\hat{\boldsymbol{\theta}}(\mathbf{x}) - \boldsymbol{\theta}) p(\boldsymbol{\theta}|\mathbf{x}) d\boldsymbol{\theta} + \int_{\hat{\boldsymbol{\theta}}(\mathbf{x})+\delta}^{\infty} (\boldsymbol{\theta} - \hat{\boldsymbol{\theta}}(\mathbf{x})) p(\boldsymbol{\theta}|\mathbf{x}) d\boldsymbol{\theta} \\ &= \int_{-\infty}^{\hat{\boldsymbol{\theta}}(\mathbf{x})-\delta} 1 \cdot p(\boldsymbol{\theta}|\mathbf{x}) d\boldsymbol{\theta} + \int_{\hat{\boldsymbol{\theta}}(\mathbf{x})+\delta}^{\infty} 1 \cdot p(\boldsymbol{\theta}|\mathbf{x}) d\boldsymbol{\theta}. \end{aligned} \tag{2.17}$$

But

$$\int_{-\infty}^{\infty} p(\boldsymbol{\theta}|\mathbf{x}) d\boldsymbol{\theta} = 1, \tag{2.18}$$

yielding

$$g(\hat{\boldsymbol{\theta}}(\mathbf{x})) = 1 - \int_{\hat{\boldsymbol{\theta}}(\mathbf{x})-\delta}^{\hat{\boldsymbol{\theta}}(\mathbf{x})+\delta} p(\boldsymbol{\theta}|\mathbf{x}) d\boldsymbol{\theta}. \tag{2.19}$$

This is minimized by maximizing

$$\int_{\hat{\boldsymbol{\theta}}(\mathbf{x})-\delta}^{\hat{\boldsymbol{\theta}}(\mathbf{x})+\delta} p(\boldsymbol{\theta}|\mathbf{x}) d\boldsymbol{\theta}, \tag{2.20}$$

for $\delta$ arbitrarily small this is maximized by choosing $\hat{\boldsymbol{\theta}}$ to correspond to the location of the *maximum* of $p(\boldsymbol{\theta}|\mathbf{x})$. The estimator that minimizes the Bayes risk for the "hit-or-miss" cost function is therefore the MAP estimator, which results in the following

MAP estimator for $\theta_k$,

$$\begin{aligned}\hat{\theta}_k(\mathbf{x}) &= \arg\max_{\theta_k} p\left(\theta_k|\mathbf{x}\right) \\ &= \arg\max_{\theta_k} \int_{\underline{\boldsymbol{\theta}}_k} p\left(x_k|\boldsymbol{\theta}\right)\ p\left(\underline{\mathbf{x}}_k|x_k,\ \boldsymbol{\theta}\right)\ p\left(\boldsymbol{\theta}\right)\ d\underline{\boldsymbol{\theta}}_k \\ &= \arg\max_{\theta_k} p\left(\theta_k\right) p\left(x_k|\theta_k\right) \int_{\underline{\boldsymbol{\theta}}_k} p\left(\underline{\mathbf{x}}_k|x_k,\boldsymbol{\theta}\right) p\left(\underline{\boldsymbol{\theta}}_k\right) d\underline{\boldsymbol{\theta}}_k \\ & \qquad\qquad\qquad\qquad\qquad\qquad\qquad\qquad k = 1, 2, \cdots, K. \end{aligned} \tag{2.21}$$

The $\underline{\mathbf{x}}_k$ and $\underline{\boldsymbol{\theta}}_k$ are constructed after removing the $k$th user's contribution. Note that the first two terms in the last line of (2.21) give us the *marginal* MAP estimate,

$$\check{\theta}_k\left(\mathbf{x}\right) = \arg\max_{\theta_k} p\left(\theta_k\right)\ p\left(x_k|\theta_k\right)\ ,\ \ k = 1,\ 2,\ \ldots,\ K\,. \tag{2.22}$$

The effect of the last term in (2.21) is to weight the marginal MAP estimate in (2.22) by taking the noise correlation structure into consideration.

To get the exact Bayesian estimate for the "hit-or-miss" cost function, one also needs to evaluate the multi-dimensional integration in (2.21) prior to searching for the maximum. In order to avoid the multi-dimensional integration involved in (2.21), a multi-stage approach based on the marginal MAP estimator is purposed to estimate the multiuser information bit is proposed.

The marginal Bayesian estimate $\check{\boldsymbol{\theta}}$ is calculated from (2.22). The users' information bits is decoded as

$$\hat{\mathbf{b}} = \mathrm{sgn}\left\{\mathbf{x} - \mathbf{P}_0\hat{\boldsymbol{\theta}}\right\}, \tag{2.23}$$

with $\mathbf{P}_0 = \mathbf{P} - \mathbf{I}$.

1. Due to the use of power control in DS-CDMA system, one at least has some approximate knowledge about the range of each user's energy level. In this case, one can make a conservative uniform assumption on a priori PDFs, assuming that $\sqrt{A_k}$'s are independently distributed as

$$p(\sqrt{A_k}) = \begin{cases} \frac{1}{A_H(k) - A_L(k)}, & A_H(k) \le \sqrt{A_k} \le A_L(k) \\ 0, & \text{otherwise} \end{cases} \tag{2.24}$$

$k = 1, \cdots, K$.

Then the marginal Bayesian estimate from (2.22) can be found as,

$$\check{\theta}_k = \begin{cases} \mathbf{A}_L(k) \cdot \text{sgn}\{z_k\}, & 0 \leq |z_k| < A_L(k) \\ z_k, & A_L(k) \leq |z_k| < A_H(k) \\ \mathbf{A}_H(k) \cdot \text{sgn}\{z_k\}, & A_H(k) \leq |z_k| \end{cases} \tag{2.25}$$

$k = 1, \cdots, K$, with $\mathbf{z} = P^{-1}\mathbf{x}$, $z_k$ is the $k$th element of $\mathbf{z}$.

The estimate $\check{\theta}_k = f(x_k)$ in (2.25) is a non-linear one and the nonlinearity is an odd-symmetric function, which limits the range of the noisy $z_k$ into the known range of amplitude. It should be point out that in obtaining (2.25), we assumed that $b_k$'s are i.i.d. with $b_k \in (-1, +1)$, and $b_k$'s are also independent of $\sqrt{A_k}$'s.

2. In the case of having the perfect knowledge of the transmission power of each user is given, i.e., $A_L(k) = A_H(k) = A(k)$, the a priori PDFs simply become delta functions:

$$p(\sqrt{A_k}) = \delta(\sqrt{A_k} - A(k)), \qquad k = 1, \cdots, K. \tag{2.26}$$

Then the marginal Bayesian estimates become

$$\check{\theta}_k = A(k) \cdot \text{sgn}\{z_k\}, \qquad k = 1, \cdots, K. \tag{2.27}$$

The non-linearity involved in (2.27) simply becomes the hard-limiter.

In the second stage, the interferences from other users is removed by taking the noise correlation structure into consideration, and the refined information bit estimate based on the tentative estimate is obtained as

$$\hat{b}_k = \text{sgn}\left\{ \mathbf{w}_k^T \left( \mathbf{y} - \underline{\mathbf{S}}_k \, \underline{\mathbf{A}}_k \cdot \underline{\check{\mathbf{b}}}_k \right) \right\}, \tag{2.28}$$

where $\check{\mathbf{b}} = \text{sgn}\{\check{\boldsymbol{\theta}}\}$, and $\mathbf{w}_k$ is a filter vector used for the desired $k$th user. The filter can be either a simple matched filter or a decorrelating filter, or a LMMSE filter.

The matrices $\underline{\mathbf{S}}_k$, $\underline{\mathbf{A}}_k$ and vector $\underline{\check{\mathbf{b}}}_k$ are constructed from $\mathbf{S}, \mathbf{A}$ and $\check{\mathbf{b}}$, respectively, after detecting the $k$th user's contribution.

The multi-stage MAP solution in (2.28) and (2.27) is essentially a decorrelating detector based multi-stage detector [18]. The improved performance of this detector is also demonstrated in the simulation part.

## 2.4 Simulation Results

The simulation results are presented in this section to demonstrate the improved detection performance of the proposed one-step iterative LMMSE based optimization approach and marginal MAP based multi-stage approach for DS-CDMA MUD. In the computer experiments, a DS-CDMA system with spreading factor $N = 7$ is considered. The desired user is chosen as the first user. To emphasize the effect of MAI, the sets of Gold-code signature are chosen such that we have the worst cross-correlation matrix $\mathbf{P}$.

Figures 2.2 and 2.3 show the near-far performance of the proposed one-step iterative LMMSE based optimization approach in (2.16) with active users $K = 3$ and $K = 5$ respectively, where initial point is given by the LMMSE estimate of (2.14) and (2.15). Also shown in the figures (for reference purpose) are the results of BPSK limit, the LMMSE detector, the decorrelating detector, the conventional MF detector, the optimum detector, and the LMMSE based PIC. It can easily be seen that one-step up-hill iteration from the LMMSE result will be able to bring the performance of LMMSE detector close to that of the optimum one. There is almost no difference being observed between the proposed one-step up-hill iteration LMMSE detector and the LMMSE based PIC.

Figures 2.4 and 2.5 show other aspects of detection performance of the proposed one-step iterative LMMSE based optimization approach in (2.16) with active users $K = 3$ and $K = 5$ respectively. In this case, the detection performance of the

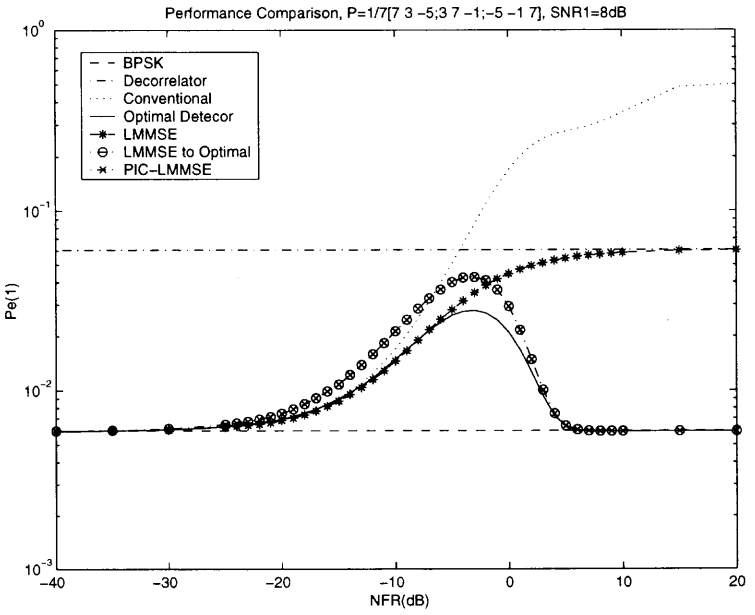


**Figure 2.2** Near-far performance comparison of proposed one-step *non-linear* iterative LMMSE based detector and other linear and non-linear multiuser detectors and the BPSK limit. $K = 3$, medium capacity.

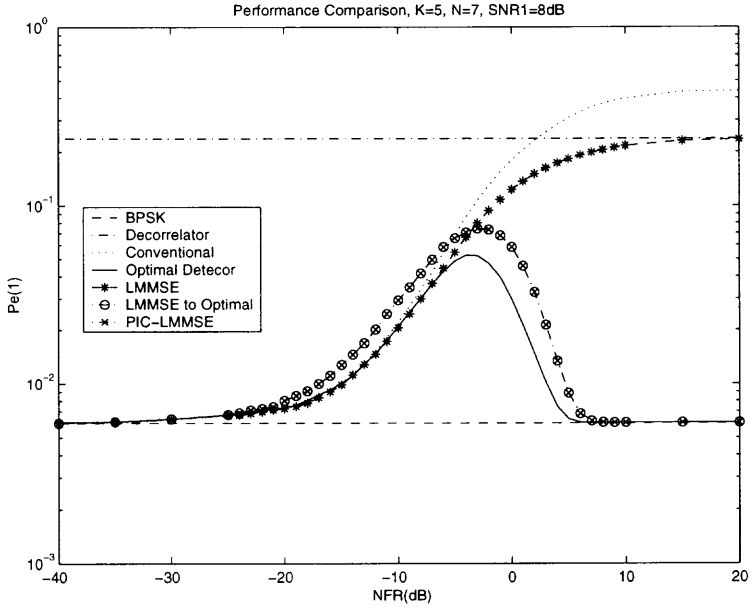


**Figure 2.3** Near-far performance comparison of proposed one-step *non-linear* iterative LMMSE based detector and other *linear* and non-linear multiuser detectors and the BPSK limit. $K = 5$, high capacity.

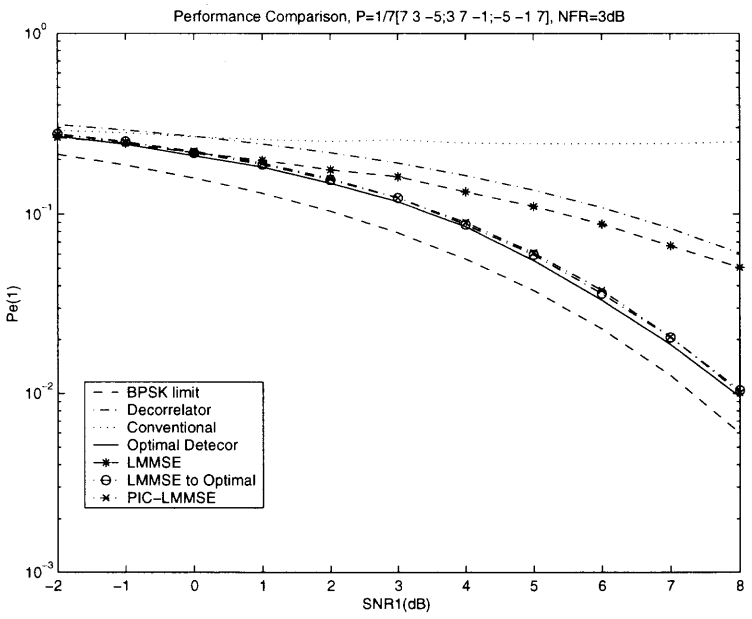


**Figure 2.4** Performance comparison of proposed one-step *non-linear* iterative LMMSE based detector and other *linear* and non-linear multiuser detectors and the BPSK limit. NFR = 3dB, $K = 3$, medium capacity.

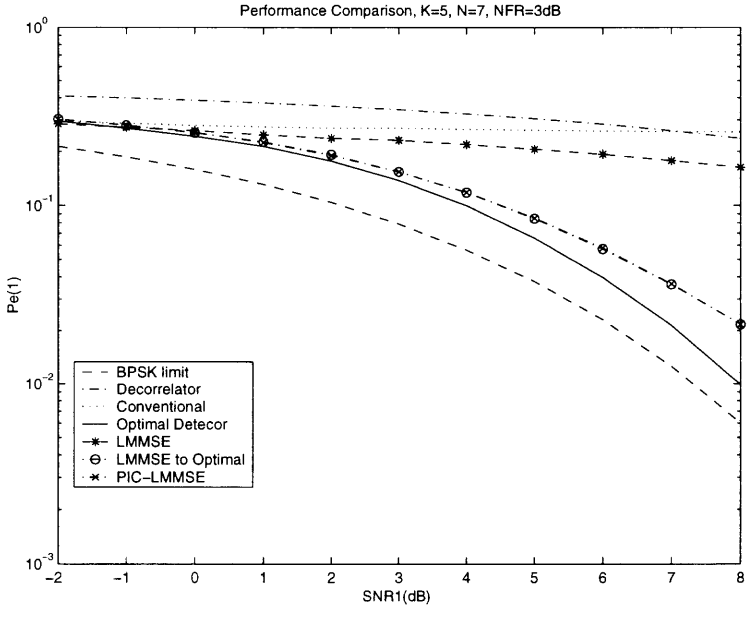


**Figure 2.5** Performance comparison of proposed one-step *non-linear* iterative LMMSE based detector and other *linear* and non-linear multiuser detectors and the BPSK limit. NFR = 3dB, $K = 5$, high capacity.

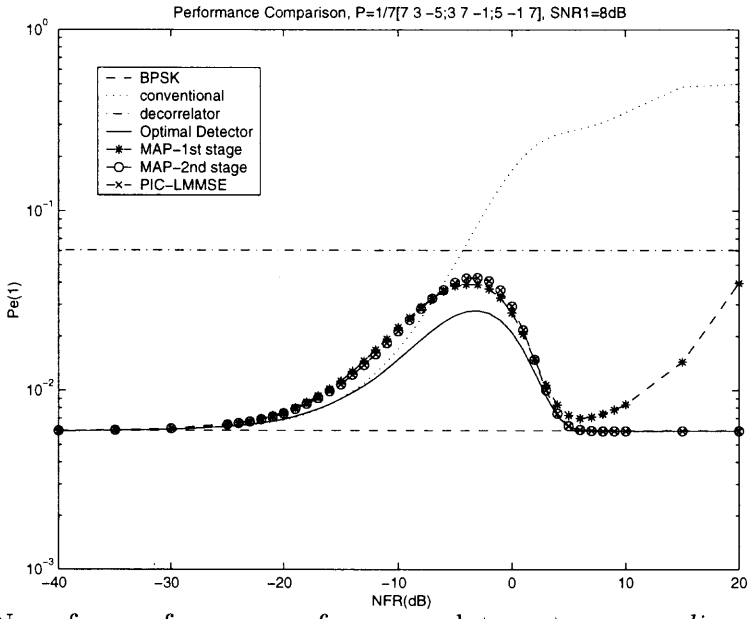


**Figure 2.6** Near-far performance of proposed two-stage *non-linear* the marginal MAP based multiuser in comparison with other linear and non-linear multiuser detectors and the BPSK limit. $K = 3$, medium capacity.

desired user as function of its SNR are plotted, while the near-far ratio (NFR) is fixed at 3dB. That is, the desired user always has a SNR 3dB less than the SNRs of interfering users. One can see the remarkable performance improvement of the proposed *non-linear* one-step iterative LMMSE based optimization approach over the existing *linear* detectors over a wide range of SNR, when NFR = 3dB.

Figures 2.6 and 2.7 show the near-far performance of the proposed two-stage non-linear MAP multiuser detectors in (2.28) with active user $K = 3$ and $K = 5$ respectively, where the first stage is based on the marginal MAP estimate and the second stage is working on the residual data after MAI cancellation. For reference purpose, the results of BPSK limit, the decorrelating detector, the conventional MF detector, the optimum detector, and the LMMSE based PIC are also shown in the figures. One can see that the marginal MAP detector is not near-far resistant when NFR is high. However, one can bring the detection performance on the MAI cancelled data close to that of the optimum detector using the marginal MAP estimate as the

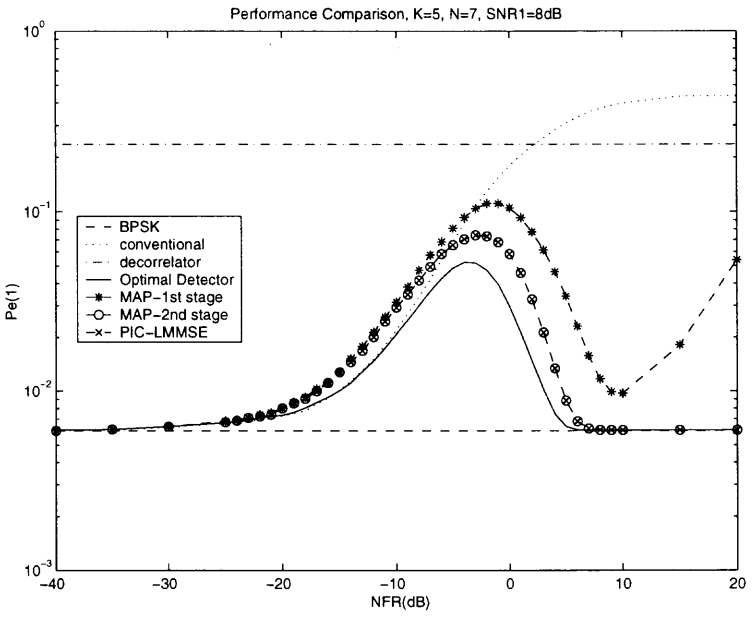


**Figure 2.7** Near-far performance of proposed two-stage *non-linear* the marginal MAP based multiuser in comparison with other linear and non-linear multiuser detectors and the BPSK limit. $K = 5$, high capacity.

tentative estimate. Almost no difference is observed between the proposed two stage MAP detector and the LMMSE based PIC.

Figures 2.8 and 2.9 show other aspects of detection performance of the proposed two-stage non-linear MAP multiuser detectors in (2.28) with active user $K = 3$ and $K = 5$ respectively. In this case, the detection performance of the desired user as function of its SNR are plotted, while the NFR is fixed at 3dB. One can see the remarkable performance improvement of the proposed *non-linear* two stage approaches over the existing *linear* detectors over a wide range of SNR, when NFR = 3dB.

Figures 2.10 and 2.11, we show the performance of different kinds of two-stage non-linear multiuser detectors with active user $K = 3$ and $K = 5$ respectively, where each stage is sorely based on either a simple matched filter or a decorrelator, or a LMMSE estimator. One can see that there exists a performance gap between the

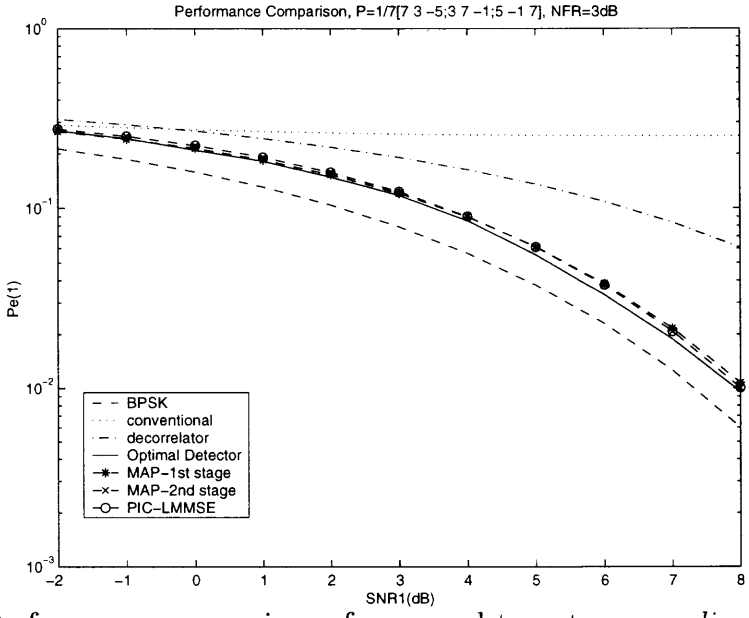


**Figure 2.8** Performance comparison of proposed two-stage *non-linear* the marginal MAP based multiuser in comparison with linear and non-linear multiuser detectors and the BPSK limit. $K = 3$, medium capacity.

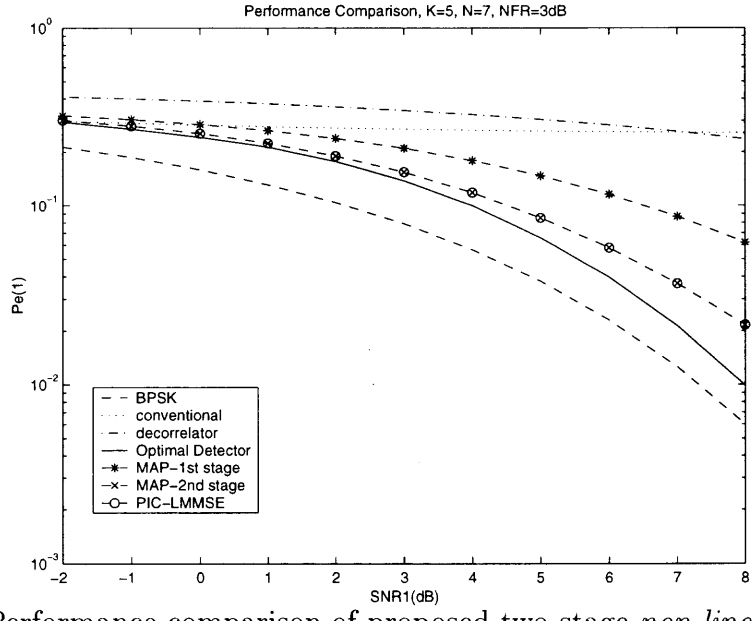


**Figure 2.9** Performance comparison of proposed two-stage *non-linear* the marginal MAP based multiuser in comparison with linear and non-linear multiuser detectors and the BPSK limit. $K = 5$, high capacity.

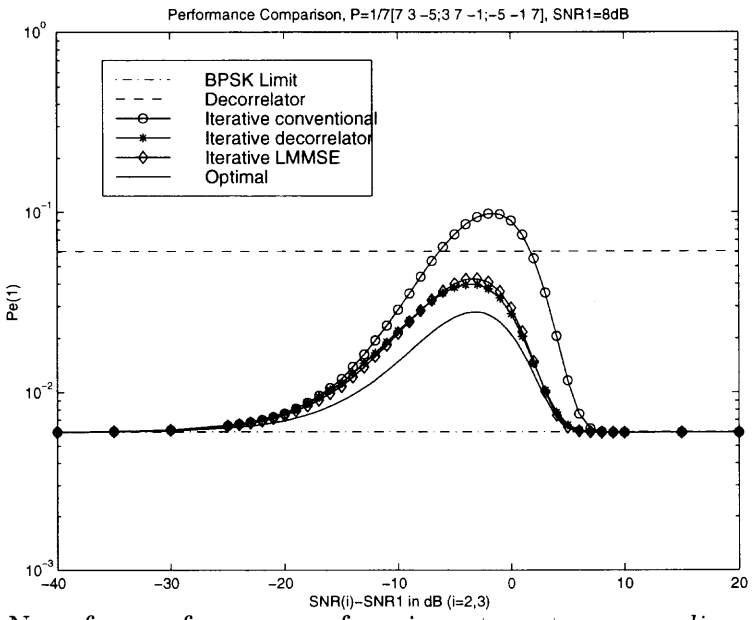


**Figure 2.10** Near-far performance of various two-stage *non-linear* multiuser in comparison with linear and non-linear multiuser detectors and the BPSK limit. $K = 3$, medium capacity.

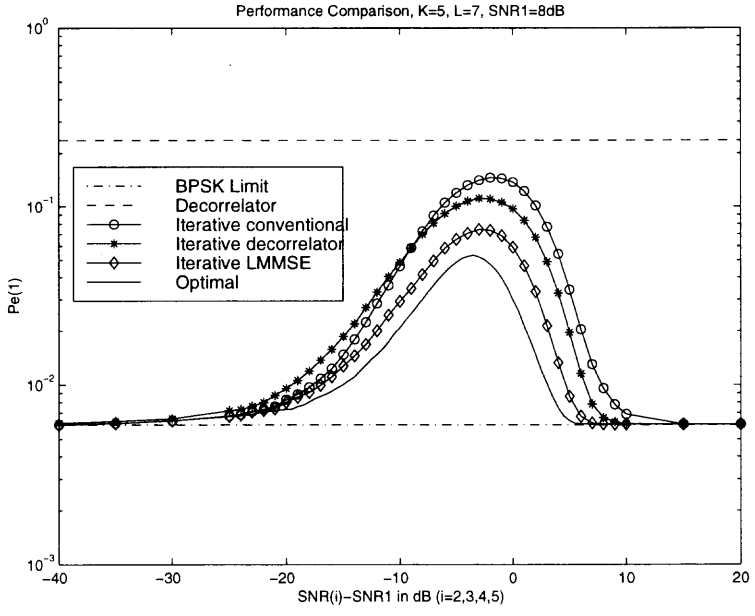


**Figure 2.11** Near-far performance of various two-stage *non-linear* multiuser in comparison with linear and non-linear multiuser detectors and the BPSK limit. $K = 5$, high capacity.

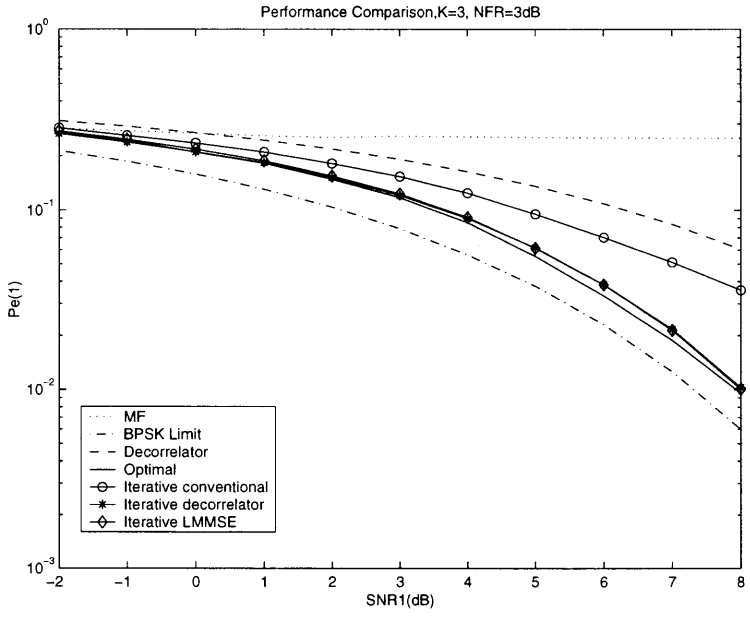


**Figure 2.12** Performance comparison of various two-stage *non-linear* multiuser in comparison with linear and non-linear multiuser detectors and the BPSK limit. $K = 3$, medium capacity.

MF based two-stage approach and decorrelator or LMMSE based approach. The latter has a detector performance closer to that of the optimum detector.

Figures 2.12 and 2.13 show other aspects of detection performance of different kinds of two-stage non-linear multiuser detectors with active user $K = 3$ and $K = 5$ respectively. In this case, the detection performance of the desired user as function of its SNR are plotted, while the NFR is fixed to 3dB. One can see the remarkable performance improvement of the proposed *non-linear* two stage MAP approach over the existing *linear* detectors over a wide range of SNR, when NFR = 3dB.

## 2.5 Conclusions

In this chapter, the MUD problem is solved using Bayesian approach. Due to the non-Gaussian nature of the problem, the Bayesian solutions are generally highly non-linear. Under the quadratic cost function and linear constraint, the

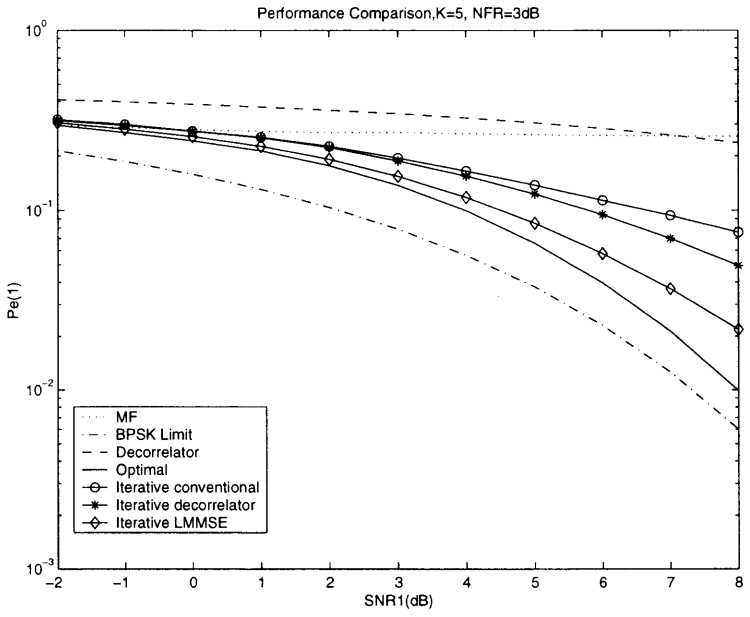


**Figure 2.13** Performance comparison of various two-stage *non-linear* multiuser in comparison with linear and non-linear multiuser detectors and the BPSK limit. $K = 5$, high capacity.

Bayesian solution leads to the LMMSE detector; under hit-or-miss cost function and linear constraint, the Bayesian solution leads to marginal MAP detector. Non-linear iterative optimization approaches and multi-stage approaches are proposed to improve the detection performance and bridge the performance gap between the linear detector and the optimal detector with little computational increase. The simple one-step iterative optimization approach uses LMMSE estimate as a starting point. Multi-stage marginal MAP based MAI cancellation uses the marginal MAP estimate as the initial or tentative statistics. One can obtain a detection performance that is comparable to that of the optimum detector using the multi-stage or iterative optimization approaches.

# CHAPTER 3

# SPACE-TIME RECEIVERS FOR DS-CDMA SYSTEMS

All conventional MUD techniques utilize the temporal spreading code signatures used by active users to suppress the MAI, and hence enhance the performance and capacity of DS-CDMA systems [4, 5, 19]. However, spatial signatures are not utilized in the conventional MUD techniques. When multiple receiving antennas are available, in corporation of S-T processing in DS-CDMA system utilizes the additional information inherent in spatial signatures, adds a new dimension to the DS-CDMA receiver, increases the degree of the freedom for the processing space, and allows improved separation of user signal. Hence, it is possible to obtain better performance of interference suppression. A S-T receiver operates simultaneously on all the antennas, processes signal samples both in space and time [2, 78, 33]. The optimal S-T processor should exploit both the spatial signature that depends on the DOA and the time delay of the desired user to maximize the SINR.

In this chapter, low-complexity S-T receivers that jointly use the signal code signature and the spatial signature are developed to achieve better interference suppression than the existing suboptimal S-T RAKE receivers. The MVDR filter instead of MF is used at each antenna elements output as the MVDR filter outperforms the MF in colored noise caused by the MAI. Further interference and noise suppression is obtained by the spatial beam-former. The decision statistics are then obtained by combining the finger outputs across space and time separately for decoupled S-T receiver, and jointly for joint S-T receiver, respectively.

## 3.1 Signal Model

As in (2.1), for a $K$ users DS-CDMA system, the $k$th user's baseband signal is

$$s_k(t) = \sum_i b_k(i) c_k(t - iT), \quad k = 1, \cdots, K \tag{3.1}$$

Let $s_k(t)$ be transmitted through a chip delay discrete linear channel with a baseband impulse response $g_k(t)$ (including the transmitter and receiver filters) [79, 34]. The received signal at the output of a $M$-element antenna array, $\mathbf{y}_k(n)$, due to user $k$ is

$$\mathbf{y}_k(t) = \sum_{l=0}^{L-1} s_k(t - iT - l - \tau_k) g_k(l) \mathbf{a}(\theta_{kl}), \tag{3.2}$$

where $L$ is the number of paths associated with each user's channel, $g_k(l)$ is the complex gain and delay of the $l$th path of the $k$th user's signal, $0 \leq \tau_k < N$ is the delay of the first path of user $k$ in chip periods, and $\theta_{kl}$ is the DOA of $l$th path of $k$th user, $\mathbf{a}(\theta_{kl})$ is the steering vector corresponding to the signal of the $l$th path of the $k$th user, and the $m$th element of $\mathbf{a}(\theta_{kl})$ has the form $\mathbf{a}^m(\theta_{kl}) = e^{j2\pi/\lambda(x_m \sin\theta_{kl} + y_m \cos\theta_{kl})}$, with $(x_m, y_m)$ being the sensor locations, for $m = 1, \cdots, M$.

The total received signal at the receiver is then the superposition of the signals from the $K$ users plus the additive ambient noise given by

$$\mathbf{y}(t) = \sum_{k=1}^{K} \sum_{l=0}^{L-1} s_k(t - iT - l - \tau_k) g_k(l) \mathbf{a}(\theta_{kl}) + v(t), \tag{3.3}$$

where $v(t)$ is the spatially and temporally i.i.d complex AWGN with variance $2\sigma_v^2$.

Denoting $\mathbf{h}_k(n) = \sum_{l=1}^{L} c_k(n-l) g_k(l) \mathbf{a}(\theta_{kl})$, and define $\mathbf{T}_L$ and $\mathbf{T}_R$ as the acyclic left shift operator and the acyclic right shift operator on vectors of length $Q = N + L - 1$ [19], i.e. for a vector $\mathbf{x} = [x_1 \cdots x_Q]^T$, $\mathbf{T}_L \mathbf{x} = [x_2 \cdots x_Q \, 0]^T$ and $\mathbf{T}_R \mathbf{x} = [0 \, x_1 \cdots x_{Q-1}]^T$; for a matrix $\mathbf{X} = [\mathbf{x}_1 \cdots \mathbf{x}_Q]$, $\mathbf{T}_L\{\mathbf{X}\} = \mathbf{X} \cdot \mathbf{T}_L = [\mathbf{x}_2 \cdots \mathbf{x}_Q \, 0]$ and $\mathbf{T}_R\{\mathbf{X}\} = \mathbf{X} \cdot \mathbf{T}_R = [0 \, \mathbf{x}_1 \cdots \mathbf{x}_{Q-1}]$. Let $\mathbf{H}_k(n) = [\mathbf{h}_k(nN) \cdots \mathbf{h}_k(nN + Q - 1)]$, then $\mathbf{H}_k^{(0)}(n) = \left(\mathbf{T}_R^{\nu_k} \mathbf{H}_k^T(n)\right)^T$, $\mathbf{H}_k^{(-1)}(n) = \left(\mathbf{T}_L^{N-\nu_k} \mathbf{H}_k^T(n)\right)^T$, and $\mathbf{H}_k^{(+1)}(n) = \left(\mathbf{T}_R^{N+\nu_k} \mathbf{H}_k^T(n)\right)^T$ with $\nu_k = \lfloor \frac{\tau_k}{T_C} \rfloor$, where $\lfloor x \rfloor$ denotes the integer portion of $x$. Note that $\mathbf{H}_k^{(+1)}(n) = 0$ when $\tau_k$ is larger than the maximum delay spread $\tau_{max}$.

Define the $M \times 3KQ$ matrix $\mathcal{H}(n) \triangleq \left[\mathbf{H}_1^{(-1)}(n) \, \mathbf{H}_1^{(0)}(n) \, \mathbf{H}_1^{(+1)}(n) \cdots \mathbf{H}_K^{(-1)}(n) \, \mathbf{H}_K^{(0)}(n) \, \mathbf{H}_K^{(+1)}(n)\right]^T$, $3KQ \times Q$ matrix $\mathcal{B}(n) \triangleq \mathbf{B}(n) \otimes \mathbf{I}_Q$, where $\otimes$ stands for Kronecker product, $\mathbf{I}_Q$ is the $Q \times Q$ identity matrix, and $\mathbf{B}(n) = [b_1(n-1) \, b_1(n) \, b_1(n+$

$1)\cdots b_K(n-1)\ b_K(n)\ b_K(n+1)\,]^T$ is a $3K\times 1$ vector contains $K$ users' transmission information. Collecting $Q$ snapshots into an $M\times Q$ data matrix, the total received data is then given by

$$\begin{aligned}\mathcal{Y}(n) &\triangleq [\mathbf{y}(nN)\cdots\mathbf{y}(nN+Q-1)]\\ &= \mathcal{B}(n)\,\mathcal{H}(n)+\mathcal{V}(n)\\ &= \underbrace{\left[\mathbf{H}_1^{(-1)}(n)\ \mathbf{H}_1^{(0)}(n)\ \mathbf{H}_1^{(+1)}(n)\right]\left(\begin{bmatrix} b_1(n-1)\\ b_1(n)\\ b_1(n+1)\end{bmatrix}\otimes\mathbf{I}_Q\right)}_{\text{Desired signal}}\\ &+ \underbrace{\sum_{k=2}^{K}\left[\mathbf{H}_k^{(-1)}(n),\mathbf{H}_k^{(0)}(n),\mathbf{H}_k^{(+1)}(n)\right]\left(\begin{bmatrix} b_k(n-1)\\ b_k(n)\\ b_k(n+1)\end{bmatrix}\otimes\mathbf{I}_Q\right)}_{MAI}+\mathcal{V}(n),\end{aligned}\tag{3.4}$$

where $\mathcal{V}(n)=[\mathbf{v}(nN)\ \cdots\ \mathbf{v}(nN+Q-1)]$, with $\mathbf{v}(n)$ spatially and temporally i.i.d complex AWGN with variance $2\sigma_v^2$. Without loss of generality, the user 1 is assumed to be the desired user in the sequel. The two existing conventional S-T RAKE receivers are first reviewed in the following section.

## 3.2 Conventional Space Time RAKE Receiver

### 3.2.1 Conventional Decoupled Space Time RAKE Receiver

The beam-former RAKE receiver originally proposed in [24], shown in figure 3.1, can be interpreted as a decoupled S-T RAKE receiver. The output of the correlator $\mathbf{w}_{m,l}$ passes the spatial beam-former $\mathbf{w}_s(l)$, followed by a temporal RAKE combiner. At the output of the $m$th sensor, the delayed version of the code signature of the desired user is chosen as the correlator for the $l$th RAKE finger, i.e. $\mathbf{w}_{m,l}=[\mathbf{0}_{l,1};\ \mathbf{s}_1;\ \mathbf{0}_{L-l-1,1}]$. The $N_f=\lfloor\frac{N+L-1}{L}\rfloor$ correlator outputs at $m$th at time $n$ are then given by

$$z_l(m,n,i) = \mathbf{w}_{m,l}^H\mathcal{Y}_m(n,i)\qquad \text{for } i=1,\cdots,N_f,\tag{3.5}$$

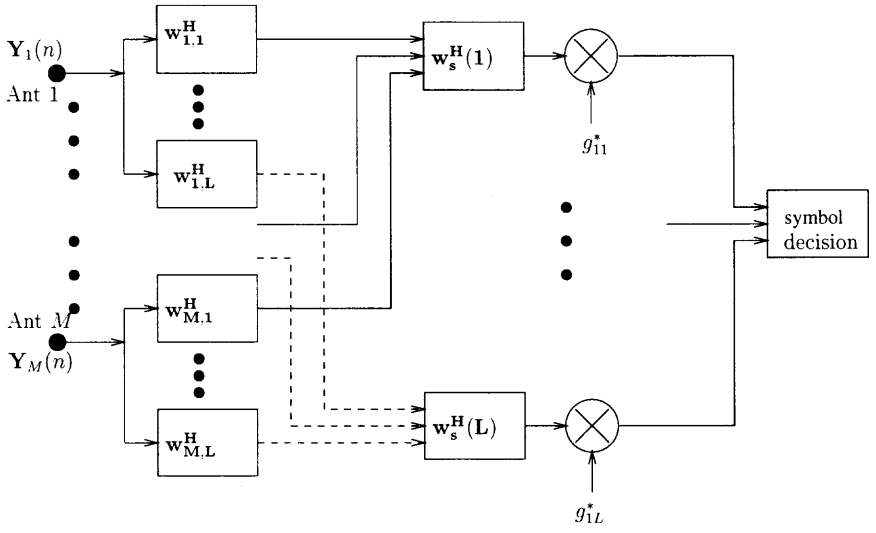


**Figure 3.1** Structure of the decoupled S-T receiver.

where $\mathcal{Y}_m(n)$ is the $m$th row of $\mathcal{Y}(n)$, and $\mathcal{Y}_m(n,i) = [\mathcal{Y}_m(n)[iL+l : Q]\ \mathcal{Y}_m(n+1)[1 : iL+l-1]]^T$. At the $l$th $(1 \le l \le L)$ RAKE finger position, the spatial covariance matrix of signal-plus-interference-plus-noise, $\hat{\mathbf{R}}_S^{(l)}$, is estimated using the sampled covariance matrix during the portion of the bit interval where the fingers of RAKE occurs [25, 80]

$$\hat{\mathbf{R}}_S^{(l)} = \frac{1}{J}\sum_{n=1}^{J} \mathbf{z}_l(n,1)\mathbf{z}_l^H(n,1), \tag{3.6}$$

where $\mathbf{z}_l(n,i) = [z_l(1,n,i)\ \cdots\ z_l(M,n,i)]^T$, and $J$ is the number of available symbols. The spatial covariance matrix of interference-plus-noise only, $\hat{\mathbf{R}}_{IN}$, is estimated using sampled covariance during the portion of bit interval away from the fingers (multiple "away from fingers" space-time snapshots per bit) [25, 80]. The $\hat{\mathbf{R}}_{IN}$ of the $l$th finger is calculated as

$$\hat{\mathbf{R}}_{IN}^{(l)} = \frac{1}{J(N_f-1)}\sum_{n=1}^{J}\sum_{i=2}^{N_f} \mathbf{z}_l(n,i)\mathbf{z}_l^H(n,i). \tag{3.7}$$

The spatial weight $\mathbf{w}_s(l)$ $(1 \le l \le L)$ yielding the optimum signal to interference plus noise ratio for bits decisions is the generalized eigenvector corresponding to the largest generalized eigenvalue $\lambda_l$ of the matrix pencil $\left\{\hat{\mathbf{R}}_S, \hat{\mathbf{R}}_{IN}\right\}$. And the value of $\lambda_l - 1$ is also a good estimate of the corresponding average path strength. The output

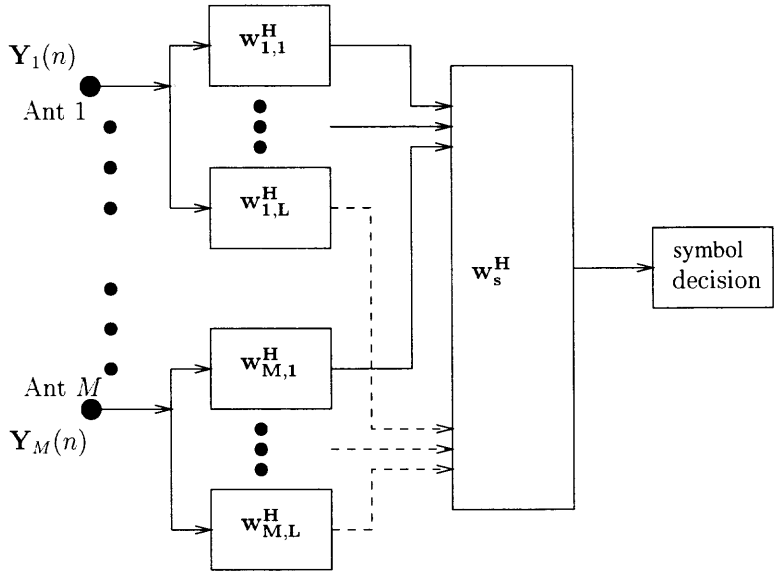


**Figure 3.2** Structure of the joint S-T receiver.

$SINR(l)$ at $l$th path is given by

$$SINR(l) = \frac{\mathbf{w}_s^H(l)\hat{\mathbf{R}}_S^{(l)}\mathbf{w}_s(l)}{\mathbf{w}_s^H(l)\hat{\mathbf{R}}_{IN}^{(l)}\mathbf{w}_s(l)} - 1 = \lambda_l - 1 \tag{3.8}$$

After the spatial filters, the $L$ outputs are combined to get the decision statistic for bit decision.

The decoupled S-T RAKE receiver separately process in the space and time domains. And the degree of freedom of such receiver is only $M + L$ rather than $ML$ which results in the information loss during the processing. To overcome this shortcoming, the joint S-T RAKE receiver was proposed in [25, 35].

### 3.2.2 Conventional Joint S-T RAKE Receiver

The joint S-T RAKE receiver, shown in figure 3.2, jointly processes the outputs of $ML$ MFs in space and time. Let $\underline{\mathbf{z}}(n,i) = vec(\mathbf{Z}(n,i))$ with $\mathbf{Z}(n,i) = [\mathbf{z}_1(n,i), \cdots, \mathbf{z}_L(n,i)]$ . The $vec(\cdot)$ operator transforms $M \times L$ matrix into an $ML$-dimensional column vector. The space-time covariance matrix of the signal plus interference and noise, $\hat{\mathbf{R}}_S^{st}$, is estimated using sampled covariance matrix during

the portion of the bit interval where the fingers of the RAKEs occur (one space-time snapshot per bit with "fingers") [25]

$$\hat{\mathbf{R}}_S^{st} = \frac{1}{J}\sum_{n=1}^{J} \underline{\mathbf{z}}(n,1)\underline{\mathbf{z}}^H(n,1). \tag{3.9}$$

The space-time covariance matrix of interference-plus-noise only, $\hat{\mathbf{R}}_{IN}^{st}$, is estimated using sampled covariance matrix during the portion of bit interval away from the fingers ( multiple "away from fingers" space-time snapshots per bit)

$$\hat{\mathbf{R}}_{IN}^{st} = \frac{1}{J(N_f-1)}\sum_{n=1}^{J}\sum_{i=2}^{N_f} \underline{\mathbf{z}}(n,i)\underline{\mathbf{z}}^H(n,i). \tag{3.10}$$

The optimum weight vector $\mathbf{w}_s$ yielding the maximum SINR for bit decisions is the generalized eigenvector of the matrix pencil $\left\{\hat{\mathbf{R}}_S^{st}, \hat{\mathbf{R}}_{IN}^{st}\right\}$ that corresponding to the largest generalized eigenvalue $\lambda$ of $\left\{\hat{\mathbf{R}}_S^{st}, \hat{\mathbf{R}}_{IN}^{st}\right\}$, and the output $SINR$ is given by

$$SINR = \frac{\mathbf{w}_s^H \hat{\mathbf{R}}_S \mathbf{w}_s}{\mathbf{w}_s^H \hat{\mathbf{R}}_{IN} \mathbf{w}_s} - 1 = \lambda - 1 \tag{3.11}$$

Although the joint S-T RAKE receiver has the better perform than the decoupled S-T RAKE receiver, the interference suppression capability of this joint S-T RAKE receiver is limited by the spatial processing freedom $M$ as no knowledge of the signal code signatures is exploited. As $M$ is much smaller than $KL$ in practice, the joint S-T RAKE receiver can not provide enough interference suppression for DS-CDMA system, and it is still suffering from the near-far problem. In order to utilize the signal code signatures and to increase the processing freedom, the MVDR S-T receiver is presented as follows.

## 3.3 The Minimum Variance Distortionless Response Space Time Receivers

### 3.3.1 The MVDR Decoupled S-T Receiver

At the output of the $m$th sensor, shown in figure 3.1, instead of using the MF for the $l$th path of the desired user, the MVDR decoupled S-T receiver selects the MVDR

filter $\mathbf{w}_{m,l}$ for the $l$th path. The MVDR decoupled S-T receiver exploits both the temporal code signature and the spatial signature for interference suppression, and hence improves the system's output SINR.

In certain array applications, constraints on the beam-former weights are often utilized to control its response to the desired signal. Usually the constraints are designed to prevent signal distortion and/or cancellation. When both the desired signal and the desired signal direction are known, the popular beam-forming approach is to minimize the array output noise variance while constraining the response of the array to the desired user to a constant [81, 82]. The MVDR beam-former minimize the output mean energy with the unbiased output of the desired signal. In this way, the MVDR filter suppresses interfering users without impeding the signal of interest. The constraints that have the response of the array to the desired user to a constant is to avoid the trivial minimization with the all zero weights filter. It is shown that there is only a scalar difference between the LMMSE receiver and the MVDR receiver. Hence, the MVDR and LMMSE receivers are expected to exhibit identical performance with respect to output SINR [81].

Such constrained optimization ideas can also be applied to DS-CDMA systems [9, 79, 83]. Here, the signature of each contributing symbol is corresponding to the column of the matrix $\mathbf{C}$, where $\mathbf{C}$ is given by

$$\mathbf{C} = \begin{bmatrix} c_1(0) & & \mathbf{0} \\ c_1(1) & \ddots & c_1(0) \\ \vdots & \ddots & c_1(1) \\ c_1(N-1) & & \vdots \\ \mathbf{0} & \dots & c_1(N-1) \end{bmatrix}_{Q \times L}, \tag{3.12}$$

whose columns specify the constraints. A special weight vectors $\mathbf{w}_{m,l}$ is then constructed to extract the desired signal along individual code vectors while suppressing all interference. That is, the MVDR principle would translate into

the following optimization problem

$$\begin{aligned} &\min \mathbf{w}_{m,l}^H \mathbf{R}_{y_m} \mathbf{w}_{m,l} \\ &\text{subject to} \quad \mathbf{C}^H \mathbf{w}_{m,l} = \mathbf{f}_l, \end{aligned} \tag{3.13}$$

where $\mathbf{R}_{y_m} = E\left\{\mathcal{Y}_m^H(n)\mathcal{Y}_m(n)\right\}$ is the covariance matrix of data $\mathcal{Y}_m(n)$ from the $m$th sensor. $\mathbf{f}_l$ is the constraint vector with all elements 0's except 1 at the $l$th position [79]. The optimal solution to this problem is [82]

$$\mathbf{w}_{m,l} = \mathbf{R}_{y_m}^{-1}\mathbf{C}(\mathbf{C}^H\mathbf{R}_{y_m}^{-1}\mathbf{C})^{-1}\mathbf{f}_l. \tag{3.14}$$

The reason for choosing MVDR filter instead of the well known LMMSE receiver is that MVDR only requires the time delay information to decode. However, LMMSE receiver need the training sequence in order to find the desired weight besides the time delay information. The output of the MVDR filter in the absence of noise is

$$\mathbf{w}_{m,l}^H \mathbf{H}_{1,m}^{(0)T}(n) = g_1(l)\mathbf{a}^m(\theta_{1l}), \tag{3.15}$$

which is exactly the signal of the desired user, where $\mathbf{H}_{1,m}^{(0)}(n)$ is the $m$th row of $\mathbf{H}_1^{(0)}(n)$. Thus, by minimizing the output power, the MVDR filter suppresses interfering users without impeding the signal of interest. Denote the output of the MVDR filter for the $l$th path at the $m$th sensor as

$$z_l(m,n) = \mathbf{w}_{m,l}^H \mathcal{Y}_m^T(n) = g_1(l)\mathbf{a}^m(\theta_{1l})b_1(n) + e(m,l), \tag{3.16}$$

where $e(m,l)$ is the residual part of the interference and noise. Let $\mathbf{z}_l(n) = [z_l(1,n) \ \cdots \ z_l(M,n)]^T$. The spatial covariance matrix of the desired signal at the $l$th path can be estimated using sample data covariance matrix with $J$ available $\mathbf{z}_l(n)$ as

$$\hat{\mathbf{R}}_S^{(l)} = \sum_{n=1}^{J} \mathbf{z}_l(n)\mathbf{z}_l^H(n). \tag{3.17}$$

Because of the interference and the noise suppression by the MVDR filters, the signal power in $\mathbf{z}_l(n)$ is much higher than that of residual of the interference and the

noise. This enables us to estimate the steering vector of the $l$th path $\mathbf{a}(\theta_{1l})$ directly from $\hat{\mathbf{R}}_S^{(l)}$ [84, 85]. The solution estimator is the eigenvector corresponding to the largest eigenvalue $\lambda$ of $\hat{\mathbf{R}}_S^{(l)}$. The largest eigenvalue is also a good estimate of the corresponding average path strength. It is shown in [86] that the noise at the output of the MVDR filters is approximately white, in which case a delay-sum beam-former (i.e. $\mathbf{w}_s(l) = \mathbf{a}(\theta_{1l})$) is optimal for source extraction. The output $SINR$ for the $l$th path is given by

$$SINR(l) = \frac{|g_1(l)\mathbf{w}_s^H(l)\mathbf{a}(\theta_{1l})|^2}{\mathbf{w}_s^H(l)\hat{\mathbf{R}}_S^{(l)}\mathbf{w}_s(l) - |g_1(l)\mathbf{w}_s^H(l)\mathbf{a}(\theta_{1l})|^2} \tag{3.18}$$

When the residual interference is very low, the steering vector itself is an approximately an optimal beam-former. If the residual interference is not negligible at the output of the MVDR filter, we still use the steering vector is still used as the beam-former. Although it is no longer optimal, it still exploits the spatial signature to further suppress the interference. After the spatial beam-former, the $L$ fingers' outputs are combined to get the decision statistic for bit decision.

As the proposed MVDR decoupled S-T receiver exploits not only the spatial signature but also the temporal code signature to suppress the interference, it can overcome the near-far problem existing in the conventional S-T RAKE receiver. The output SINR is greatly improved when NFR is high and hence the capacity of the CDMA system is increased. This has been demonstrated through the simulation results shown in figure 3.7. It is also shown that the proposed MVDR decoupled S-T RAKE receiver has the better performance than the conventional joint S-T RAKE receiver in figures 3.7 and 3.8. However, there is some performance loss due to the separately processing of the outputs from $M$ antenna sensors for MVDR decoupled S-T receiver. To further improve the output SINR, the new joint S-T receiver is presented in the following section.

### 3.3.2 The MVDR Joint S-T Receiver

In joint S-T receiver, shown in figure 3.2, the outputs of $ML$ MVDR filters are jointly processed. Let $\underline{\mathbf{z}}(n) = vec(\mathbf{Z}(n))$ with $\mathbf{Z}(n) = [\mathbf{z}_1(n), \cdots, \mathbf{z}_L(n)]$. Then the space-time covariance matrix of the desired signal is estimated during the portion of the bit interval where the fingers of the RAKEs occur (one space-time snapshot per bit with "fingers")

$$\hat{\mathbf{R}}_S^{st} = \sum_{n=1}^{J} \underline{\mathbf{z}}(n)\, \underline{\mathbf{z}}^H(n). \tag{3.19}$$

Because of the interference suppression ability of the MVDR, the total signal power in $\underline{\mathbf{z}}(n)$ is much higher than that of the interference and the noise. This enables us to estimate the space-time signature of the desired user directly from $\hat{\mathbf{R}}_S^{st}$, which is the eigenvector corresponding to the largest eigenvalue of $\hat{\mathbf{R}}_S^{st}$. And the eigenvector can be used as the weight vector $\mathbf{w}_s$ to extract the source information. This beam-former achieves a spatial-temporal blind equalization in an $ML$ dimensional space. The output $SINR$ is then given by

$$SINR = \frac{|\mathbf{w}_s^H \mathbf{s}|^2}{\mathbf{w}_s^H \hat{\mathbf{R}}_S^{st} \mathbf{w}_s - |\mathbf{w}_s^H \mathbf{s}|^2}, \tag{3.20}$$

with $\mathbf{s} = vec(g_1(1)\mathbf{a}(\theta_{11}) \cdots g_1(L)\mathbf{a}(\theta_{1L}))$.

The proposed MVDR joint S-T RAKE receiver not only exploits the signal code signature to suppress the MAI and noise, it also processes the $ML$ outputs from the $M$ sensors together and makes the jointly optimum beam-former in the $ML$ space and time processing space. From the simulation, it is shown that MVDR joint S-T receiver has better performance than those of both the conventional joint S-T RAKE receiver and the proposed MVDR decoupled S-T receiver.

## 3.4 The MVDR S-T Receivers with Differential Encoding

The MVDR S-T receivers presented in previous section have the phase ambiguity problem if there is no channel information available at the receiver antenna array.

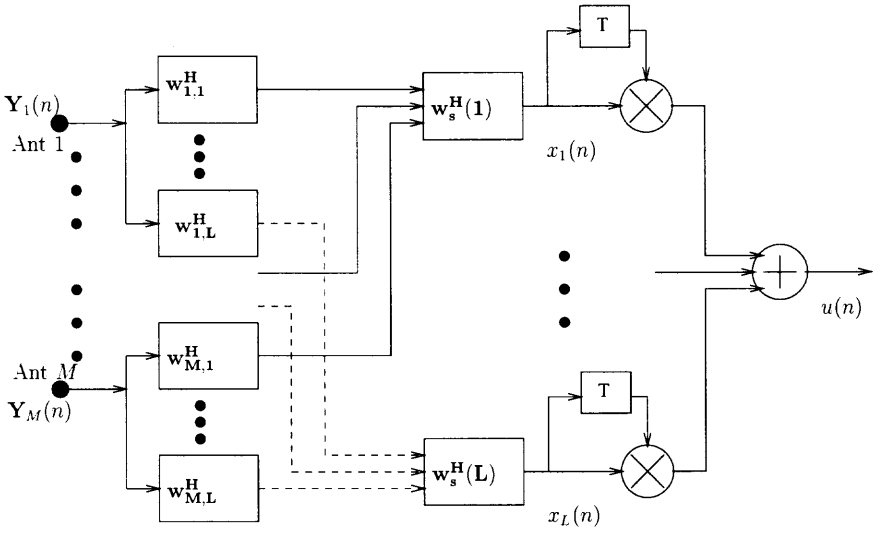


**Figure 3.3** Structure of the decoupled S-T receiver with differential encoding.

To solve this problem, the differential encoding/decoding is implemented in the modulation/receiver to achieve the blind detection without phase ambiguity problem.

### 3.4.1 The Minimum Variance Decoupled S-T Receiver with Differential Encoding

The MVDR decoupled S-T receiver with the users' information bits differentially encoded is shown in figure 3.3. After the spatial beam-former, we get the vector $\mathbf{x}(n) = [x_1(n), \cdots, x_L(n)]^T$ with

$$x_l(n) = \mathbf{w}_s^H(l)\mathbf{z}_l(n). \tag{3.21}$$

According to [86], the decision variable $u(n)$ is given by the equal gain combiner as

$$u(n) = \mathbf{x}^H(n-1)\mathbf{x}(n). \tag{3.22}$$

Compared to the coherent MVDR decoupled S-T receiver, there is a performance loss around 3dB. However, there is no channel information needed in the receiver.

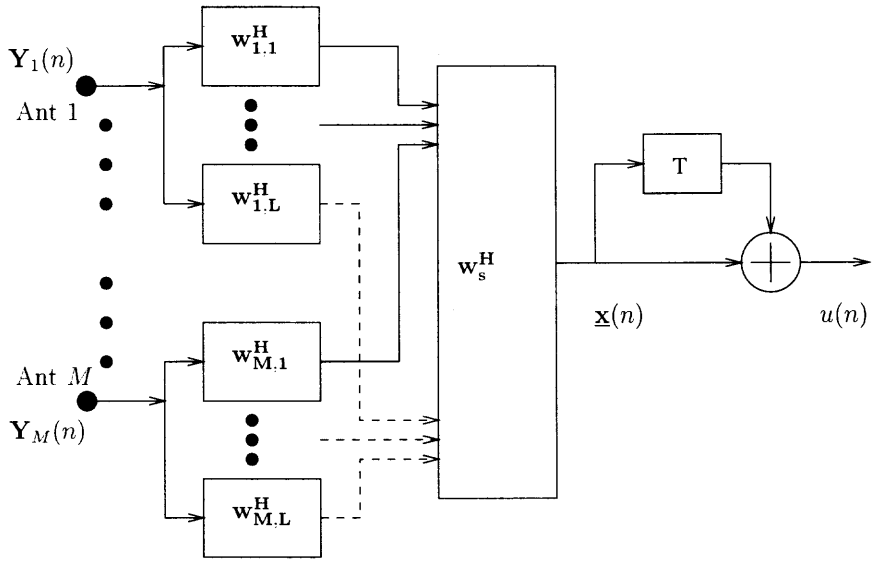


**Figure 3.4** Structure of the joint S-T receiver with differential encoding.

### 3.4.2 The Minimum Variance Joint S-T Receiver with Differential Encoding

In the MVDR joint S-T receiver with the users' information bit differentially encoded, shown in figure 3.4, the outputs of $M\,L$ MVDR filters are jointly processed. The decision statistic for the desired user is

$$u(n) = \underline{\mathbf{x}}^H(n-1)\underline{\mathbf{x}}(n), \tag{3.23}$$

with $\underline{\mathbf{x}}(n) = \mathbf{w}_s^H \underline{\mathbf{z}}(n)$.

As the receiver is non-coherent, the output SINR is almost $3dB$ poorer than the coherent receiver assuming the channel information known. However, the receiver does not need the channel information.

## 3.5 The Minimum Variance S-T Receivers with Training Sequence

The channel information can be estimated If the training sequence is available. The information of the desired user is then coherently detected without the SINR

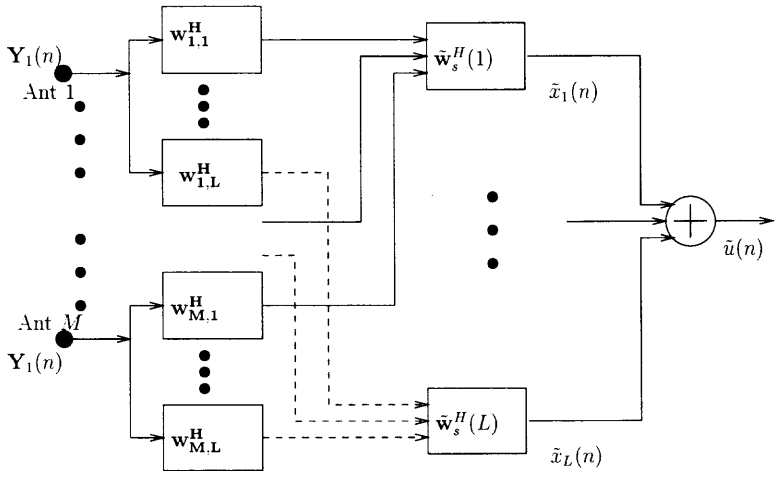


**Figure 3.5** Structure of the decoupled S-T receiver with training sequence.

loss associated with the differential MVDR S-T receivers and avoiding the phase ambiguity at the same time.

### 3.5.1 The Minimum Variance Decoupled S-T Receiver with Training Sequence

The block diagram for the MVDR decoupled S-T receiver for the users' information bit using BPSK with training sequence is shown in figure 3.5. The MVDR decoupled S-T receiver utilizes the pilot signal to estimate the channel information, and combines the maximum ratio multiplication with the spatial beam-former for each path, and then makes the equal gain combining for $l$ paths' signals before make the decision.

With the training sequence, the estimation of $g_1(l)\mathbf{a}(\theta_{1l})(m)$ of $l$th path of the desired user can be easily found from

$$\mathbf{V}_l(n) = [\mathbf{z}_l(n), \cdots, \mathbf{z}_l(n+J-1)] \tag{3.24}$$

as

$$\tilde{\mathbf{w}}_s(l) = g_1(l)\mathbf{a}(\theta_{1l}) = \mathbf{V}_l(n)\mathbf{b}_1^{\dagger}(n), \tag{3.25}$$

where $\mathbf{b}_1(n) = [b_1(n), \cdots, b_1(n+J-1)]$ with $\dagger$ stands for the pseudo inverse. The reason that we could use $\tilde{\mathbf{w}}_s(l)$ as the spatial beam-former for the $l$th path of the desired user is that the residual of the interference and noise after the MVDR filter is nearly white, and hence the $\tilde{\mathbf{w}}_s(l)$ is nearly optimal space beam-former in this situation. The output of the $l$th space beam-former is $\tilde{x}_l(n) = \tilde{\mathbf{w}}_s^H(l)\mathbf{z}_l(n)$, and the decision statistic $\tilde{u}(n)$ is just the summation of the $L$ space beam-former outputs as

$$\tilde{u}(n) = \sum_{l=1}^{L} \tilde{x}_l(n). \tag{3.26}$$

The near-far performance is shown in the figure 3.15. By estimating channel phase information with the training sequence and combine the information of each paths coherently, the $SINR$ loss introduced by differential decoding is compensated at the price of some bandwidth loss by transmitting the training sequence.

### 3.5.2 The Minimum Variance Joint S-T Receiver with Training Sequence

The MVDR joint S-T receiver with training sequence, shown in figure 3.6, is investigated with the users' information bit using BPSK modulation

Similar to the decoupled one, the space time beam-former $\tilde{\mathbf{w}}_s$ can be estimated as

$$\tilde{\mathbf{w}}_s = \underline{\mathbf{V}}(n)\mathbf{b}_1^{\dagger}(n), \tag{3.27}$$

with $\underline{\mathbf{V}}(n) = [\underline{\mathbf{z}}(n), \cdots, \underline{\mathbf{z}}(n+J-1)]$. And the decision statistic for the desired user is

$$\tilde{u}(n) = \tilde{\mathbf{w}}_s^H \underline{\mathbf{z}}(n). \tag{3.28}$$

It is easy to see the $SINR$ improvement compared with the one with the differential decoding in the simulation results shown in next section.

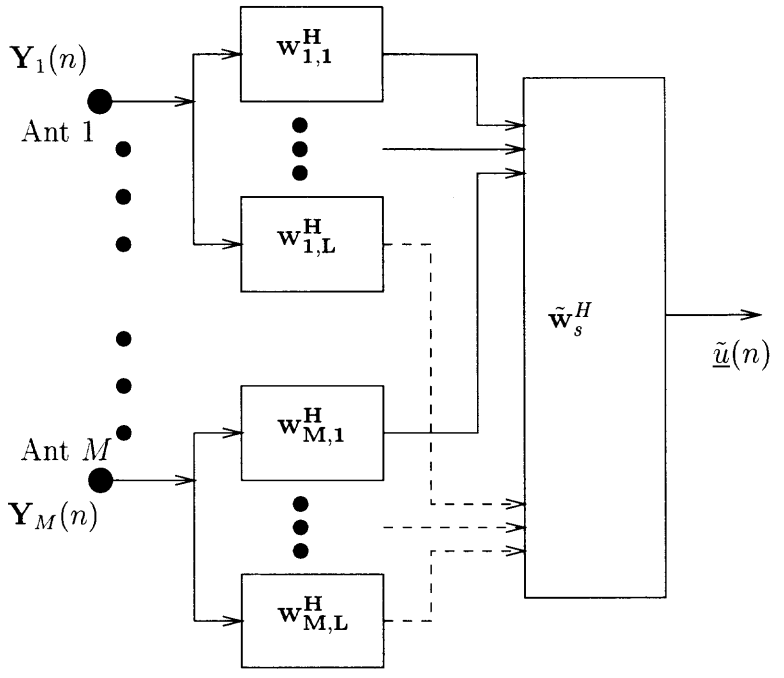


**Figure 3.6** Structure of the joint S-T receiver with training sequence.

## 3.6 Simulation Results

Simulation results are presented to demonstrate the performance of the proposed MVDR S-T receivers. The averaged output SINR is used as the performance measure. The Gold sequences of length $N = 31$ are used as spreading sequences. The number of user is $K = 8$ and each user's propagation channel has $L = 3$ paths. The receivers employ a linear antenna array with $M = 4$ elements with half-wavelength spacing. Let the DOA of the $k$th user's signal along the $l$th path with respect to the antenna array be $\theta_{kl}$, the array response is given by $\mathbf{a}^m(\theta_{kl}) = \exp[j(m-1)\pi \sin(\theta_{kl})]$. $R_S$ and $R_{IN}$ are estimated with $J = 500$ except in figures 3.11 and 3.12 where the performance vs. $J$ is illustrated.

Figure 3.7 shows the output SINR vs. NFR for the MVDR decoupled S-T receiver in comparison with conventional one. The input SNR of the desired user is 10dB. It is shown that the proposed MVDR decoupled S-T receiver outperforms the

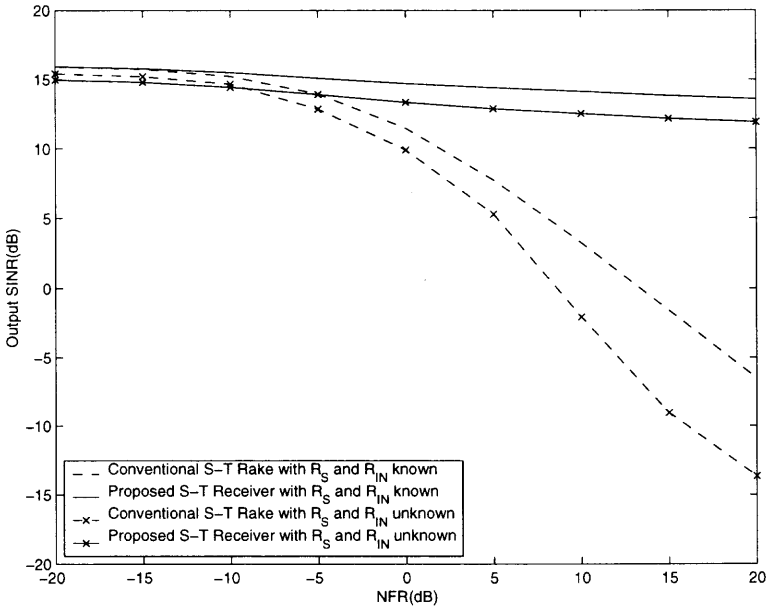


**Figure 3.7** Output SINR vs. NFR for decoupled S-T receiver. $N = 31, K = 8, SNR = 10dB, L = 3, M = 4$.

conventional decoupled S-T RAKE receiver in both situations when $R_S$ and $R_{IN}$ are known or estimated from the received data. The performance gain introduced from the MVDR is obvious when the NFR is high. When NFR= 10dB, the output SINR improvement is about 11dB and 14.5dB for $R_S$ and $R_{IN}$ known or estimated cases, respectively.

Figure 3.8 is the output SINR vs. NFR for the MVDR joint S-T receiver in comparison with conventional one. The input SNR of the desired user is $10dB$. It is shown that the proposed MVDR joint S-T receiver is much better than the conventional S-T RAKE no matter $R_S$ and $R_{IN}$ are known or estimated. When NFR= 10dB, the output SINR improvement is about 5.5dB and 12.5dB for $R_S$ and $R_{IN}$ known or estimated cases, respectively. Comparing figure 3.7 with figure 3.8, it is shown that even the proposed decoupled S-T RAKE receiver has the better performance than the conventional joint S-T RAKE receiver. When NFR= 10dB, the output SINR improvement is about 5.3dB and 12.2dB for $R_S$ and $R_{IN}$ known or

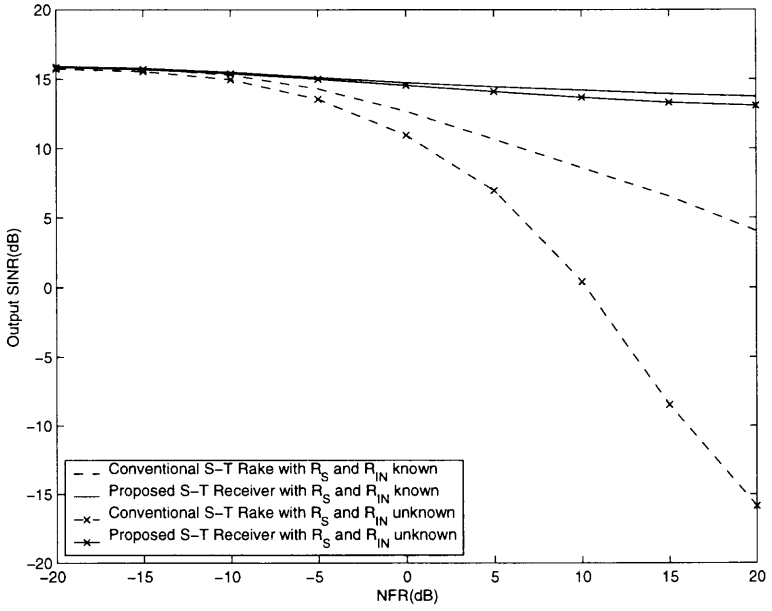


**Figure 3.8** Output SINR vs. NFR for joint S-T receiver. $N = 31, K = 8, SNR = 10dB, L = 3, M = 4$.

estimated cases, respectively. The utilization of the signal code structure brings us the high performance with relatively low increasing of the processing complexity.

Figure 3.9 is the output SINR vs. input SNR of the desired user for the decoupled S-T receivers. The NFR is fixed at 0dB. It is shown that the performance gain of the proposed MVDR decoupled S-T receiver over the conventional S-T RAKE receiver is larger with increased SNR. When SNR= 10dB, the output SINR improvement is about 5dB for both $R_S$ and $R_{IN}$ known or estimated cases.

Figure 3.10 is the output SINR vs. input SNR of the desired user for the joint S-T receivers. When SNR= 10dB, the SNR improvement is about 5dB both $R_S$ and $R_{IN}$ known or estimated cases. The NFR is fixed at 0dB. It is observed that even the proposed decoupled receiver is better than the conventional joint S-T receiver. The reason is that the degree of freedom for the interference cancellation for the MVDR decoupled S-T receiver is $Q + M$, which is much higher than that of

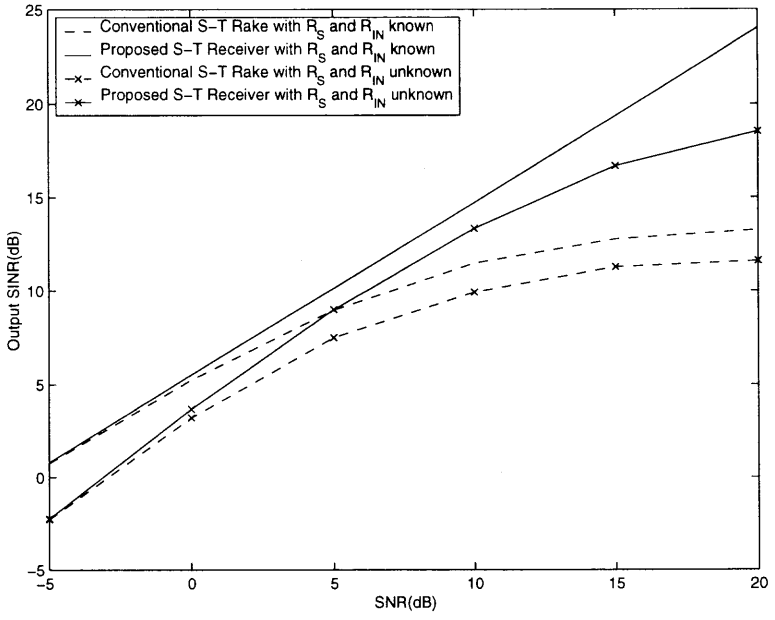


**Figure 3.9** Output SINR vs. input SNR of desired user for decoupled S-T receiver. $N = 31, K = 8, NFR = 0dB, L = 3, M = 4$.

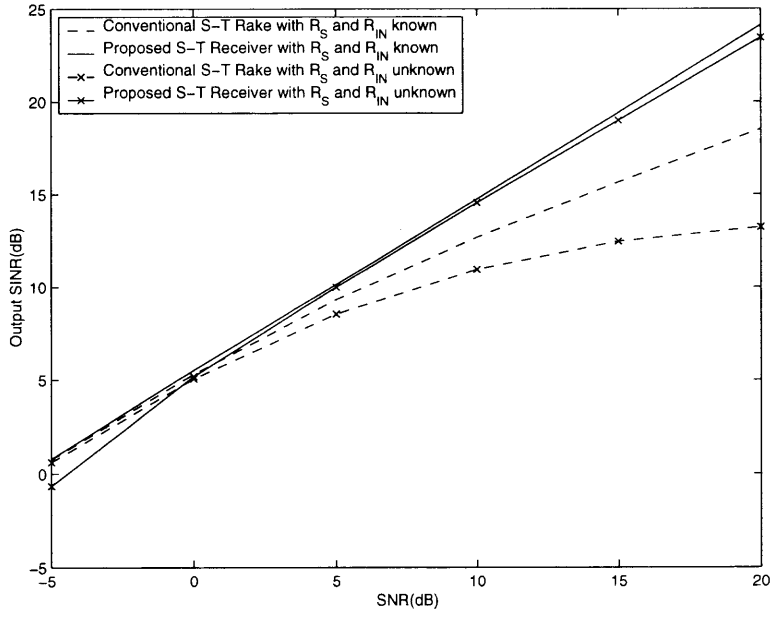


**Figure 3.10** Output SINR vs. input SNR of desired user for joint S-T receiver. $N = 31, K = 8, NFR = 0dB, L = 3, M = 4$.

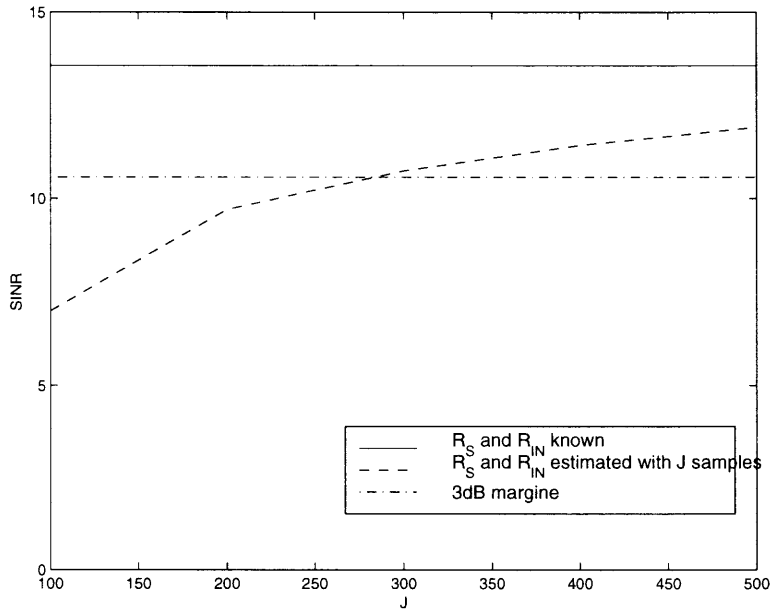


**Figure 3.11** Output SINR vs. $J$ for MVDR decoupled S-T receiver. $N = 31, K = 8, SNR = 10dB, NFR = 20dB, L = 3, M = 4$.

conventional decoupled S-T RAKE receiver, which is only $M$. Hence, the MVDR decoupled S-T receiver has a better interference suppression ability. Figures 3.11 and 3.12 show the receivers SINR vs. different $J$, with $J$ ranging from 100 to 500. The SNR of the desired user is equal to $10dB$ and $NFR = 20dB$. It shows that with more $J$ available, the output SINR increases. The reason is that the estimations of $R_S$ and $R_{IN}$ are more accurate with more data available. Figure 3.13 shows the output SINR vs. NFR for the MVDR decoupled S-T receiver with differential decoding in comparison with conventional one. The input SNR of the desired user is $10dB$. It is shown that the proposed MVDR decoupled S-T receiver outperforms the conventional decoupled S-T RAKE receiver. When NFR= 10dB, the output SINR improvement is about 20dB. The performance gain from the MVDR is obvious when the NFR is high. Figure 3.14 is the output SINR vs. NFR for the MVDR joint S-T receiver with differential decoding in comparison with conventional one. The input SNR of the desired user is $10dB$. It is obvious that the proposed MVDR

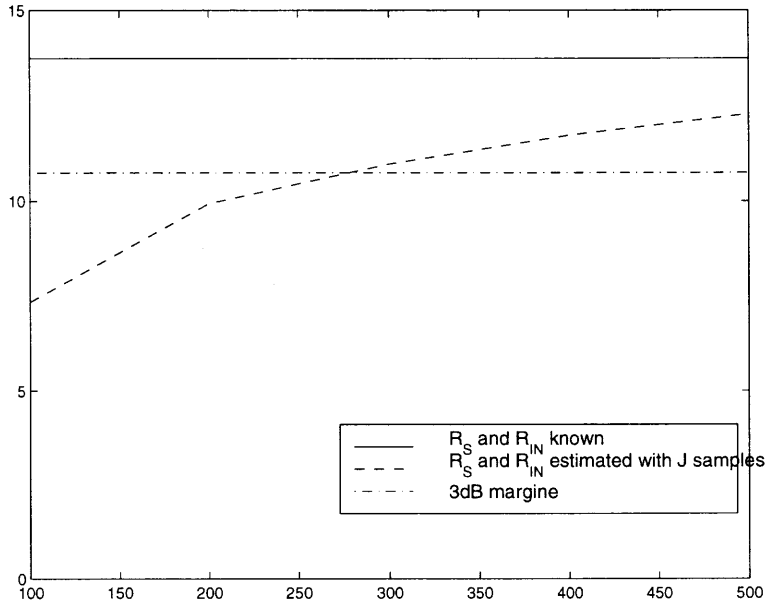


**Figure 3.12** Output SINR vs. $J$ for MVDR joint S-T receiver. $N = 31, K = 8, SNR = 10dB, NFR = 20dB, L = 3, M = 4$.

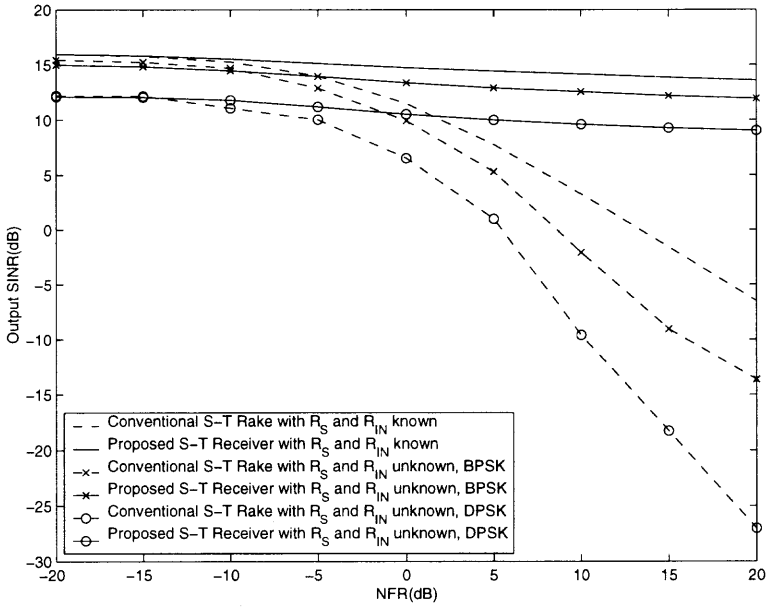


**Figure 3.13** Output SINR vs. NFR for decoupled S-T receiver with differential encoding. $N = 31, K = 8, SNR = 10dB, L = 3, M = 4$.

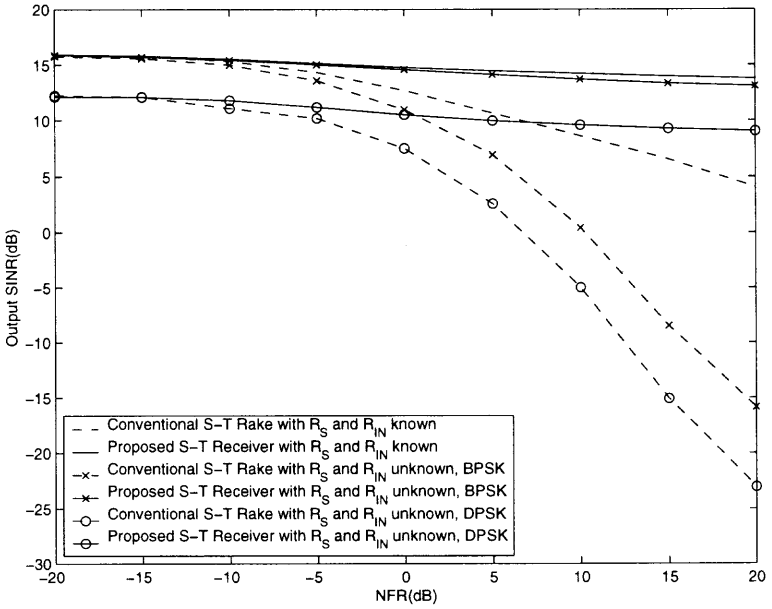


**Figure 3.14** Output SINR vs. NFR for joint S-T receiver with differential encoding. $N = 31, K = 8, SNR = 10dB, L = 3, M = 4$.

joint S-T receiver is much better than the conventional S-T RAKE receivers. When NFR= 10dB, the output SINR improvement is about 10dB. However, compared with the coherent receiver using the channel phase information, there exists around $3dB$ loss in the output SINR. Figure 3.15 and 3.16 are the output SINR vs. NFR for the MVDR decoupled and joint S-T receivers. It is shown that with the training sequence available, the receiver can implement the estimated channel information for the coherent detection. With the coherent detection using estimated phase information, the output SINR is increased around $1.5dB$ compared with that of the non-coherent ones.

## 3.7 Conclusions

New MVDR decoupled and joint S-T receivers are presented in this chapter. The new S-T receivers combine the MUD technique and the S-T processing to achieve better the MAI suppression. The proposed receivers overcome the near-far problem

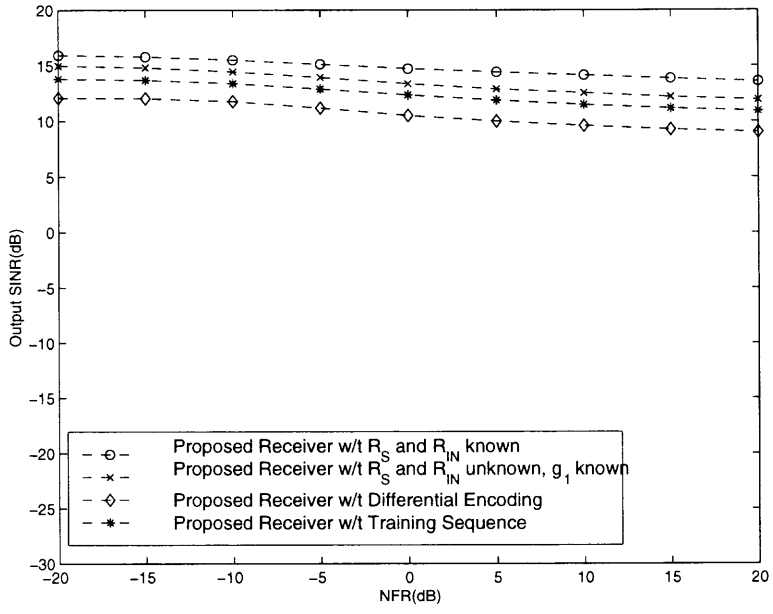


**Figure 3.15** Output SINR vs. NFR comparison for various MVDR decoupled S-T receivers. $N = 31, K = 8, SNR = 10dB, L = 3, M = 4$.

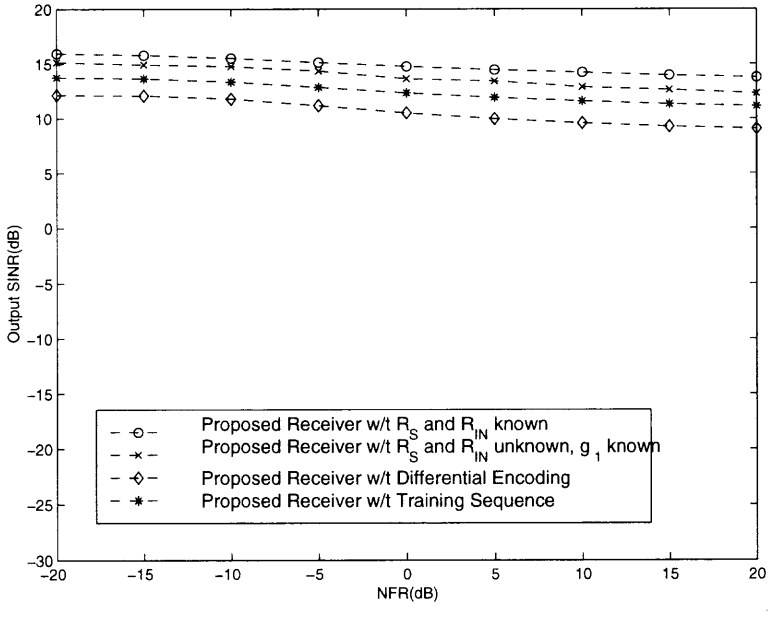


**Figure 3.16** Output SINR vs. NFR comparison for various MVDR joint S-T receivers. $N = 31, K = 8, SNR = 10dB, L = 3, M = 4$.

existing in the conventional S-T RAKE receivers. The simulation results show that the proposed MVDR S-T receivers significantly outperform the existing ones without significant increase in complexity. The phase ambiguity problem in channel estimation is solved in two ways. With the differential code, it is able to detect the information of the desired user blindly using the non-coherent receiver without the phase information. However, there exists $3dB$ output SINR gap between it and the coherent receiver using the phase information. With the training sequence, it is possible to estimate the channel phase information and detect the information of the desired user coherently and the output SINR is increased around $1.5dB$. Simulation results show that both solutions work well even with high NFR and obviously outperform the conventional S-T RAKE receivers when NFR is high.

# CHAPTER 4

# DIFFERENTIAL DETECTION SCHEME FOR DS-CDMA SYSTEMS WITH TRANSMIT DIVERSITY

In many systems, additional antennas may be expensive or impractical at the remote station. In these cases TD can be used to provide diversity benefit of reducing the effect of multipath fading with multiple transmit antenna array. The link performance of TD technique for the DS-CDMA systems with differential detection scheme is evaluated in this chapter [70, 69]. At the transmitter, the STTD scheme, which provide the TD, is combined with the presented generalized differential encoding scheme; at the receiver, the differential decoding technique is combined with the MVDR receiver. The performance of the proposed scheme is compared with that of the OTD combining with conventional differential encoding. Both transmission schemes provide full spatial diversity, outperform the non-TD system, and require no channel state side information at both the transmitter and the receiver. It is also shown that the performance of the proposed OTD+MVDR and STTD+MVDR receivers are much better than those conventionally used OTD+MF and STTD+MF receivers, and the STTD+MVDR has a much better performance than OTD+MVDR at the price of the higher complexity receiver.

## 4.1 Differential Detection Scheme with Orthogonal Transmit Diversity

### 4.1.1 Orthogonal Transmit Diversity

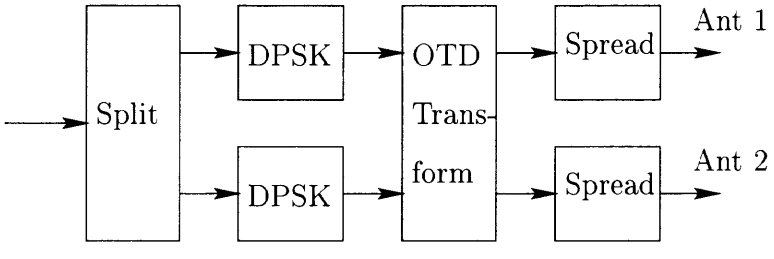


**Figure 4.1** Base station transmitter using OTD transmit diversity.

One open-loop approach that offers some diversity gains without requiring extra resources is the OTD scheme. Figure 4.1 shows the block diagram of the transmission system that OTD is used. According to OTD technique, each user's data stream $b_k(n)$ is first split into two independent data streams, namely its odd and even substreams $b_{k1}(n)$ and $b_{k2}(n)$, respectively. In OTD, the first antenna transmits the spread odd substream of the user's data $b_{k1}(n)$ during odd symbol periods and repeats the transmission of the spread odd substream of the user's data $b_{k1}(n)$ during even symbol periods. The second antenna transmits the spread even substream of the user's data $b_{k2}(n)$ during odd symbol periods and transmits the the spread even substream of the user's data $-b_{k2}(n)$ during even symbol periods. The transmitted signal constellation of the $k$th user may be described as the matrix shown below

$$\begin{bmatrix} b_{k1}(n)\mathbf{c}_k & b_{k2}(n)\mathbf{c}_k \\ b_{k1}(n)\mathbf{c}_k & -b_{k2}(n)\mathbf{c}_k \end{bmatrix} \tag{4.1}$$

where $\mathbf{c}_k$ is the spreading code of length $N$ assigned to the $k$th user, and 1st and 2nd columns of the matrix in (4.1) are corresponding to the signals that are transmitted at the first and second antenna, respectively. Note that since each symbol is repeated twice, the total code length used on each antenna is $2N$, i.e., the odd symbol is spread with the spreading code $\mathbf{c}_{1,k} = \left[\mathbf{c}_k^T \ \mathbf{c}_k^T\right]^T$, the even symbol is spread with the spreading code $\mathbf{c}_{2,k} = \left[\mathbf{c}_k^T \ -\mathbf{c}_k^T\right]^T$. Hence, two $2N$ chip codes are assigned to a single user.

Suppose that $K$ users are transmitted simultaneously from the base station, and $b_k(n)$ is the differential encoded symbol for the $k$th user, in the case of an $L$-ray channel, the received data is given by

$$\mathbf{y}(n) = \sum_{k=1}^{K}\sum_{l=1}^{L}\left(\frac{1}{\sqrt{2}}g_{k1}(l)b_{k1}(n)\mathbf{c}_{1,k}(n-l) + \frac{1}{\sqrt{2}}g_{k2}(l)b_{k2}(n)\mathbf{c}_{2,k}(n-l)\right) + \mathbf{v}(n), \tag{4.2}$$

where $g_{k1}(l)$ and $g_{k2}(l)$ are the complex-valued fading coefficients on the two transmit antennas of the $k$th user's $l$th path's signal, $\mathbf{c}_{1,k}$ and $\mathbf{c}_{2,k}$ represent the $2N$ spreading codes assigned to $k$th user, and $\mathbf{v}(n)$ denotes the spatial and temporal AWGN.

### 4.1.2 The MVDR Receiver

As in chapter 3, we choose the MVDR filter $\mathbf{w}_{1,l}$ to extract the desired signal transmitted from first antenna and suppress the interference including the other users' signal transmitted from first antenna and all signals transmitted from second antenna by minimizing the output power subject to a set of constraints:

$$\min \mathbf{w}_{1,l}^H \mathbf{R}_y \mathbf{w}_{1,l} \quad \text{subject to} \quad \mathbf{C}^H \mathbf{w}_{1,l} = \mathbf{f}_l, \tag{4.3}$$

where $\mathbf{R}_y = E\left\{\mathbf{y}(n)\mathbf{y}^H(n)\right\}$ is the data covariance matrix, and the $(2N+L-1)\times L$ matrix $\mathbf{C}_1$, whose columns specify the constraints, is shown to be

$$\mathbf{C}_1 = \begin{bmatrix} c_1(0) & & \mathbf{0} \\ c_1(1) & \ddots & c_1(0) \\ \vdots & \ddots & c_1(1) \\ c_1(2N) & & \vdots \\ \mathbf{0} & \cdots & c_1(2N) \end{bmatrix}_{(2N+L-1)\times L}. \tag{4.4}$$

The optimal solution to this problem is given by

$$\mathbf{w}_{1,l} = \mathbf{R}_y^{-1}\mathbf{C}_1(\mathbf{C}_1^H\mathbf{R}_y^{-1}\mathbf{C}_1)^{-1}\mathbf{f}_l. \tag{4.5}$$

Similarly, we can obtain the $\mathbf{w}_{2,l}$ to extract the desired signal transmitted from the second antenna as

$$\mathbf{w}_{2,l} = \mathbf{R}_y^{-1}\mathbf{C}_2(\mathbf{C}_2^H\mathbf{R}_y^{-1}\mathbf{C}_2)^{-1}\mathbf{f}_l, \tag{4.6}$$

with constraint matrix $\mathbf{C}_2$ as

$$\mathbf{C}_2 = \begin{bmatrix} c_2(0) & & \mathbf{0} \\ c_2(1) & \ddots & c_2(0) \\ \vdots & \ddots & c_2(1) \\ c_2(2N) & & \vdots \\ \mathbf{0} & \cdots & c_2(2N) \end{bmatrix}_{(2N+L-1)\times L}. \tag{4.7}$$

### 4.1.3 Differential Decoding

Arrange the outputs of the MVDR filters to be vectors, then $\mathbf{z}_1(n) = [z_{1,1}(n), \cdots, z_{1,L}(n)]^T$ and $\mathbf{z}_2(n) = [z_{2,1}(n), \cdots, z_{2,L}(n)]^T$ with

$$\begin{aligned} z_{1,l}(n) &= \mathbf{w}_{1,l}^H \mathbf{y}(n) \\ &= \frac{1}{\sqrt{2}} g_{11}(l) b_{11}(n) + \mathbf{n}_1(n), \\ z_{2,l}(n) &= \mathbf{w}_{2,l}^H \mathbf{y}(n) \\ &= \frac{1}{\sqrt{2}} g_{12}(l) b_{12}(n) + \mathbf{n}_2(n), \end{aligned}$$

where

$$\mathbf{n}_{1l}(n) = \mathbf{w}_{1,l}^H \left\{ \sum_{k=2}^{K} \sum_{l=1}^{L} \left( \frac{1}{\sqrt{2}} g_{k1}(l) b_{k1}(n) \mathbf{c}_{1,k}(n-l) + \frac{1}{\sqrt{2}} g_{k2}(l) b_{k2}(n) \mathbf{c}_{2,k}(n-l) \right) + \mathbf{v}(n) \right\}, \tag{4.8}$$

and

$$\mathbf{n}_{2l}(n) = \mathbf{w}_{2,l}^H \left\{ \sum_{k=2}^{K} \sum_{l=1}^{L} \left( \frac{1}{\sqrt{2}} g_{k1}(l) b_{k1}(n) \mathbf{c}_{1,k}(n-l) + \frac{1}{\sqrt{2}} g_{k2}(l) b_{k2}(n) \mathbf{c}_{2,k}(n-l) \right) + \mathbf{v}(n) \right\}. \tag{4.9}$$

According to [86], the decision variable $u_1(n)$ and $u_2(n)$ are given by the equal gain combiner as

$$u_1(n) = \mathbf{z}_1(n-1)^H \mathbf{z}_1(n), \tag{4.10}$$

and

$$u_2(n) = \mathbf{z}_2(n-1)^H \mathbf{z}_2(n). \tag{4.11}$$

It is easy to obtain the transmitted information by differential decoding after having $u_1(n)$ and $u_2(n)$.

And the output SINRs for the signal that transmitted from the first and second antenna are

$$SINR_1 = \frac{(\sum_{l=1}^{L} |g_{11}(l)|^2)^2}{Q_1} \tag{4.12}$$

$$\begin{aligned} Q_1 &= 2 \sum_{l'=1}^{L} |g_{11}(l')|^2 \mathbf{w}_{1,l'}^H \Big( \sum_{k=2}^{K} \sum_{l_1=1}^{L} \sum_{l_2=1}^{L} g_{k1}^*(l_1) g_{k1}(l_2) \mathbf{c}_{1,k}(n-l_1) \mathbf{c}_{1,k}^T(n-l_2) \\ &+ g_{k2}^*(l_1) g_{k2}(l_2) \mathbf{c}_{2,k}(n-l_1) \mathbf{c}_{2,k}^T(n-l_2) + 2\sigma^2 \mathbf{I} \Big) \mathbf{w}_{1,l'} \end{aligned} \tag{4.13}$$

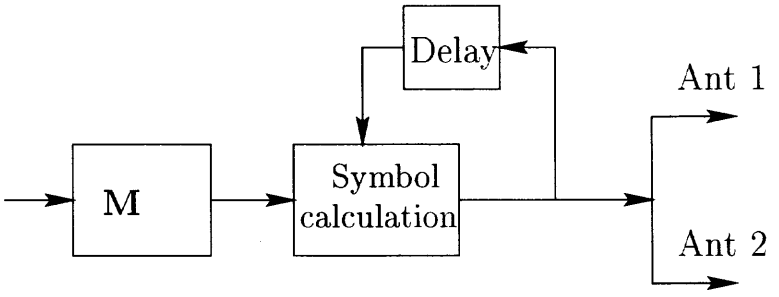


**Figure 4.2** Base station transmitter using STTD transmit diversity.

and

$$SINR_2 = \frac{(\sum_{l=1}^{L} |g_{12}(l)|^2)^2}{Q_2} \tag{4.14}$$

$$\begin{aligned} Q_2 &= 2\sum_{l'=1}^{L} |g_{12}(l')|^2 \mathbf{w}_{1,l'}^H (\sum_{k=2}^{K} \sum_{l_1=1}^{L} \sum_{l_2=1}^{L} g_{k1}^*(l_1) g_{k1}(l_2) \mathbf{c}_{1,k}(n-l_1) \mathbf{c}_{1,k}^T(n-l_2) \\ &+ g_{k2}^*(l_1) g_{k2}(l_2) \mathbf{c}_{2,k}(n-l_1) \mathbf{c}_{2,k}^T(n-l_2) + 2\sigma^2 \mathbf{I}) \mathbf{w}_{1,l'}. \end{aligned} \tag{4.15}$$

Essentially, OTD sends half of the coded bits from one antenna and the other half of the coded bits from the other antenna. The diversity is achieved at the channel coding level since half of the coded bits fade independently from the other half. The space-time mapping does not provide any diversity advantage.

Although the case of two transmit antennas is considered, the scheme can be readily applied to any number of transmit antenna. Any $M \times M$ unitary transformation can map $M$ symbols into an $M \times M$ orthogonal code matrix.

## 4.2 Differential Detection Scheme with Space-Time Transmit Diversity

### 4.2.1 Space-Time Transmit Diversity

STTD employs a space-time block coding. Using the same notation as in the previous section, i.e., splitting the user's data into its even and odd substreams, the Alamouti's space-time block code for two antenna system [46] can be extended to DS-CDMA system with processing gain $N$. For a specific user $k$, it maps two symbols into a

$2N \times 2$ code matrix according to the symbol transmission matrix

$$\begin{bmatrix} b_{k1}(n)\mathbf{c}_k & b_{k2}(n)\mathbf{c}_k \\ -b_{k2}^*(n)\mathbf{c}_k & b_{k1}^*(n)\mathbf{c}_k \end{bmatrix} = \begin{bmatrix} b_k(2n-1)\mathbf{c}_k & b_k(2n)\mathbf{c}_k \\ -b_k^*(2n)\mathbf{c}_k & b_k^*(2n-1)\mathbf{c}_k \end{bmatrix}. \tag{4.16}$$

In STTD, the first antenna transmits the spread odd substream of the user's data $b_{k1}(n)$ during odd symbol periods and the spread even substream of the user's data $-b_{k2}^*(n)$ during even symbol periods. The second antenna transmits the spread even substream of the user's data $b_{k2}(n)$ during odd symbol periods and transmits the the spread odd substream of the user's data $b_{k1}^*(n)$ during even symbol periods. Instead of using code length $2N$ as in OTD, only code length $N$ is used in this case. For a downlink DS-CDMA system, the chip-rate matched filtered and sampled $N$ snapshot of data at $2n-1$ and $2n$ are

$$\begin{aligned} \mathbf{y}(2n-1) &= \sum_{k=1}^{K}\sum_{l=1}^{L}\left(\frac{1}{\sqrt{2}}g_{k1}(l)b_k(2n-1)\mathbf{c}_k(n-l)\right. \\ &\quad \left. + \frac{1}{\sqrt{2}}g_{k2}(l)b_k(2n)\mathbf{c}_k(n-l)\right) + \mathbf{v}(2n-1), \end{aligned} \tag{4.17}$$

$$\begin{aligned} \mathbf{y}(2n) &= \sum_{k=1}^{K}\sum_{l=1}^{L}\left(-\frac{1}{\sqrt{2}}g_{k1}(l)b_k^*(2n)\mathbf{c}_k(n-l)\right. \\ &\quad \left. + \frac{1}{\sqrt{2}}g_{k2}(l)b_k^*(2n-1)\mathbf{c}_k(n-l)\right) + \mathbf{v}(2n). \end{aligned} \tag{4.18}$$

The symbols are orthogonal across antennas.

### 4.2.2 The Coherent Detection Algorithm

Assuming coherent detection, ML decoding can be achieved based only on linear processing at the receiver. The $2n-1$th and $2n$th symbols of the 1st user is recovered as follows

$$\begin{aligned} x_1(2n-1) &= \sum_{l=1}^{L}\mathbf{y}(2n-1)\mathbf{c}_1^T(n-l)g_{11}^*(l) + \mathbf{y}^*(2n)\mathbf{c}_1^T(n-l)g_{12}(l) \\ &\quad + g_{11}^*(l)n_1(2n-1) + g_{12}(l)n_1(2n), \end{aligned} \tag{4.19}$$

$$\begin{aligned} x_1(2n) &= \sum_{l=1}^{L}\mathbf{y}(2n-1)\mathbf{c}_1^T(n-l)g_{12}^*(l) - \mathbf{y}^*(2n)\mathbf{c}_1^T(n-l)g_{11}(l) \\ &\quad + g_{12}^*(l)n_1(2n-1) + g_{11}(l)n_1(2n), \end{aligned} \tag{4.20}$$

where $n_1(n)$ denotes the interference from other users plus noise. The conventional ML decoding scheme requires the channel knowledge of $g_{k1}$ and $g_{k1}$ which is not always available.

### 4.2.3 Differential Encoding for Multiple Transmitters

When no knowledge of the channel is available, at neither the transmitter nor at the receiver, the above schemes require the transmission of pilot symbols. Motivated by Tarokh's work in [87], a simple differential space-time encoding algorithm is presented. Given a pair of symbols $x_1$ and $x_2$, it is easily shown that the complex vector $(x_1\ x_2)$ and $(-x_2^*\ x_1^*)$ are orthogonal to each other and have unit lengths. Any two-dimensional vector $\mathcal{X} = (x_3\ x_4)$ can be uniquely represented in the orthonormal basis given by these vectors, i.e., there exists a unique complex vector $P_{\mathcal{X}} = (A_{\mathcal{X}}\ B_{\mathcal{X}})$ such that $A_{\mathcal{X}}$ and $B_{\mathcal{X}}$ satisfy the vector equation

$$(x_3\ x_4) = A_{\mathcal{X}}(x_1\ x_2) + B_{\mathcal{X}}(-x_2^*\ x_1^*). \tag{4.21}$$

The coefficients $A_{\mathcal{X}}$ and $B_{\mathcal{X}}$ are given by

$$A_{\mathcal{X}} = x_3x_1^* + x_4x_2^* \tag{4.22}$$

$$B_{\mathcal{X}} = -x_3x_2 + x_4x_1. \tag{4.23}$$

Mapping $(x_3\ x_4)$ to $(A_{\mathcal{X}}\ B_{\mathcal{X}})$ is just a basis change from the standard basis given by vectors $\{(1\ 0),\ (0\ 1)\}$ to the orthonormal basis given by $\{(x_1\ x_2)\ \ (-x_2^*\ x_1^*)\}$ which preserves the distances between the points of the two-dimensional complex space.

### 4.2.4 The Encoding Algorithm

Figure 4.2 shows the block diagram of the transmission system when STTD is used. For $k$th user, the transmission is begun with sending arbitrary symbols $b_k(1)$ and $b_k(2)$ at time 1 and symbols $-b_k^*(2)$ and $b_k^*(1)$ at time 2 unknown to the receiver. These two transmissions do not convey any information. The rest of the data are

transmitted in the following way. Suppose that $b_k(2n-1)$ and $b_k(2n)$ are transmitted, respectively, from first and second antennas at odd time $2n-1$, and that $-b_k^*(2n)$, $b_k^*(2n-1)$ are transmitted from first and second antennas at even time $2n$. The constellation $\mathcal{A}$ is restricted to $2^d$-PSK, for $d = 1, 2, 3, \cdots$. For the new coming $2d$ bits arriving at the encoder at odd time $2n+1$, the transmitter maps the first $d$ bits into a constellation symbol $s_k(2n+1)$ and the second $d$ bits into a constellation symbol $s_k(2n+2)$ using Grey mapping. Then, the transmitted symbols are computed as

$$\begin{aligned}[b_k(2n+1)\ b_k(2n+2)] &= s_k(2n+1)[b_k(2n-1)\ b_k(2n)] \\ &+ s_k(2n+2)[-b_k^*(2n)\ b_k^*(2n-1)]. \end{aligned} \tag{4.24}$$

At odd time $2n+1$ and even time $2n+2$, the first antenna transmits $b_k(2n+1)$, $b_k(2n+2)$, and the second antenna transmits $-b_k^*(2n+2)$, $b_k^*(2n+1)$, respectively. This process is repeated until the end of the frame (or end of the transmission). The $s_k(2n+1)$ and $s_k(2n+2)$ can be recovered as

$$s_k(2n+1) = b_k(2n+1)b_k^*(2n-1) + b_k(2n+2)b_k^*(2n+1), \tag{4.25}$$

$$s_k(2n+2) = -b_k(2n+1)b_k(2n) + b_k(2n+2)b_k(2n-1). \tag{4.26}$$

### 4.2.5 The MVDR Receiver

As before, the MVDR filter is chosen for each path of the desired user in order to preserve the desired signal's information and to suppress the interference from other users and the noise. $\mathbf{w}_l$ is obtained by minimizing the output power subject to a set of constraints:

$$\min \mathbf{w}_l^H \mathbf{R}_y \mathbf{w}_l \quad \text{subject to} \quad \mathbf{C}^H \mathbf{w}_l = \mathbf{f}_l, \tag{4.27}$$

where $\mathbf{R}_y = E\left\{\mathbf{y}(n)\mathbf{y}^H(n)\right\}$ is the data covariance matrix, $\mathbf{f}_l$ is the constraint vector, and the $(N+L-1) \times L$ matrix $\mathbf{C}$ same as 3.12.

The optimal solution to this problem is obtained as

$$\mathbf{w}_l = \mathbf{R}_y^{-1}\mathbf{C}(\mathbf{C}^H\mathbf{R}_y^{-1}\mathbf{C})^{-1}\mathbf{f}_l. \tag{4.28}$$

### 4.2.6 Differential Decoding

Let us assume that signals $z_l(2n-1)$, $z_l(2n)$, $z_l(2n+1)$and $z_l(2n+2)$ are the outputs of the MVDR filter at time $2n-1$, $2n$, $2n+1$, and $2n+2$, i.e.

$$\begin{aligned} z_l(2n-1) &= \mathbf{w}_l^H\mathbf{y}(2n-1), \\ z_l(2n) &= \mathbf{w}_l^H\mathbf{y}(2n), \\ z_l(2n+1) &= \mathbf{w}_l^H\mathbf{y}(2n+1), \\ z_l(2n+2) &= \mathbf{w}_l^H\mathbf{y}(2n+2). \end{aligned} \tag{4.29}$$

As the MVDR filter preserve the desired signal and suppress the interference by minimizing the output power, it shows that

$$z_l(2n-1) = \frac{1}{\sqrt{2}}g_{11}(l)b_1(2n-1) + \frac{1}{\sqrt{2}}g_{12}(l)b_1(2n) + n(2n-1), \tag{4.30}$$

$$z_l(2n) = -\frac{1}{\sqrt{2}}g_{11}(l)b_1^*(2n) + \frac{1}{\sqrt{2}}g_{12}(l)b_1^*(2n-1) + n(2n), \tag{4.31}$$

where

$$\begin{aligned} n(2n-1) &= \mathbf{w}_l^H(\sum_{l=1}^{L}\sum_{k=2}^{K}(\frac{1}{\sqrt{2}}g_{k1}(l)b_k(2n-1)\mathbf{c}_k(n-l) \\ &+ \frac{1}{\sqrt{2}}g_{k2}(l)b_k(2n)\mathbf{c}_k(n-l)) + \mathbf{v}(2n-1)), \\ n(2n) &= \mathbf{w}_l^H(\sum_{l=1}^{L}\sum_{k=1}^{K}(-\frac{1}{\sqrt{2}}g_1(l)b_k^*(2n)\mathbf{c}_k(n-l) \\ &+ \frac{1}{\sqrt{2}}g_2(l)b_k^*(2n-1)\mathbf{c}_k(n-l)) + \mathbf{v}(2n)). \end{aligned}$$

Let $\mathbf{G}(g_1(l), g_2(l)) = \begin{bmatrix} g_1(l) & g_1(l)^* \\ g_2(l) & -g_1(l)^* \end{bmatrix}$ and $\mathbf{V}_{2n-1} = [n_{2n-1} \quad -n_{2n}^*]$, it is easy to show that

$$z_l(2n+1)z_l(2n-1)^* + z_l(2n+2)^*z_l(2n)$$

$$
\begin{aligned}
&= \frac{E_1}{2}(|g_1(l)|^2 + |g_2(l)|^2)(b_1(2n+1)b_1(2n-1)^* + b_1(2n+2)b_1(2n)^*) \\
&+ \sqrt{\frac{E_1}{2}} \begin{bmatrix} b_1(2n+1) \\ b_1(2n+2) \end{bmatrix}^T \mathbf{G}(g_1(l), g_2(l))\mathbf{V}_{2n-1}^* \\
&+ \sqrt{\frac{E_1}{2}} \mathbf{V}_{2t+1}\mathbf{G}^H(g_1(l), g_2(l)) \begin{bmatrix} b_1(2n-1) \\ b_1(2n) \end{bmatrix}^* + \mathbf{V}_{2n+1}\mathbf{V}_{2n+1}^H, \\
&z_l(2n+1)z_l(2n)^* - z_l(2n+2)^* z_l(2n-1) \\
&= \frac{E_1}{2}(|g_1(l)|^2 + |g_2(l)|^2)(-b_1(2n+1)b_1(2n) + b_1(2n+2)b_1(2n-1)) \\
&+ \sqrt{\frac{E_1}{2}} \begin{bmatrix} b_1(2n+1) \\ b_1(2n+2) \end{bmatrix}^T \mathbf{G}(g_1(l), g_2(l))\mathbf{V}_{2n}^* \\
&+ \sqrt{\frac{E_1}{2}} \mathbf{V}_{2t+1}\mathbf{G}^H(g_1(l), g_2(l)) \begin{bmatrix} -b_1(2n) \\ b_1(2n-1) \end{bmatrix} + \mathbf{V}_{2n+1}\mathbf{V}_{2n}^H,
\end{aligned}
$$

where $\mathbf{V}_{2n} = [n_{2n}\ n_{2n-1}^*]$. For notational simplicity, let

$$
\begin{aligned}
\mathcal{Z}_1 &= \sum_{l=1}^{L} z_l(2n+1)z_l(2n-1)^* + z_l(2n+2)^* z_l(2n), \\
\mathcal{Z}_2 &= \sum_{l=1}^{L} z_l(2n+1)z_l(2n)^* - z_l(2n+2)^* z_l(2n-1), \\
\mathcal{N}_1 &= \sqrt{\frac{E_1}{2}}\Big(\sum_{l=1}^{L} \begin{bmatrix} b_1(2n+1) \\ b_1(2n+2) \end{bmatrix}^T \mathbf{G}(g_1(l), g_2(l))\mathbf{V}_{2n-1}^* \\
&+ \mathbf{V}_{2t+1}\mathbf{G}^H(g_1(l), g_2(l)) \begin{bmatrix} b_1(2n-1) \\ b_1(2n) \end{bmatrix}^*\Big) + \mathbf{V}_{2n+1}\mathbf{V}_{2n+1}^H, \\
\mathcal{N}_2 &= \sqrt{\frac{E_1}{2}}\Big(\sum_{l=1}^{L} \begin{bmatrix} b_1(2n+1) \\ b_1(2n+2) \end{bmatrix}^T \mathbf{G}(g_1(l), g_2(l))\mathbf{V}_{2n}^* \\
&+ \mathbf{V}_{2t+1}\mathbf{G}^H(g_1(l), g_2(l)) \begin{bmatrix} -b_1(2n) \\ b_1(2n-1) \end{bmatrix}\Big) + \mathbf{V}_{2n+1}\mathbf{V}_{2n}^H,
\end{aligned}
$$

Thus, it yields

$$
\begin{aligned}
\mathcal{Z}_1 &= \frac{E_1}{2}\sum_{l=1}^{L}(|g_1(l)|^2 + |g_2(l)|^2)s_1(2n+1) + \mathcal{N}_1, \\
\mathcal{Z}_2 &= \frac{E_1}{2}\sum_{l=1}^{L}(|g_1(l)|^2 + |g_2(l)|^2)s_1(2n+2) + \mathcal{N}_2.
\end{aligned}
$$

It could be written as

$$
\begin{aligned}
(\mathcal{Z}_1\ \mathcal{Z}_2) &= \frac{E_1}{2}\sum_{l=1}^{L}(|g_1(l)|^2 + |g_2(l)|^2)(s_1(2n+1)\ s_1(2n+2)) \\
&+ (\mathcal{N}_1\ \mathcal{N}_2).
\end{aligned} \tag{4.32}
$$

As the elements of $\mathcal{A}$ have equal length, to compute $(s_1(2n+1)\ s_1(2n+2))$, the receiver now computes the closest vector to $(\mathcal{R}_1\ \mathcal{R}_2)$. Once this vector is computed, the inverse mapping of $\mathcal{M}$ is applied and the transmitted bits are recovered.

The diversity gain is obtained by combining the RAKE outputs prior to the decoding. The SINR possesses the optimum two-fold diversity gain with respect to a single transmitter antenna for $M = 2$.

## 4.3 Simulation Results

In this section, some simulation results are presented to demonstrate the performance of the proposed detect scheme. Assume that the system has 2 transmit antennas and 1 receiving antenna. The Gold sequence of length $N = 15$ is used with $K = 4$ active users. The SNR of the desired user in dB is defined as $SNR_1 = 10\log_{10}\frac{E(\|\mathbf{g}_1\|^2)}{2\sigma^2}$, and the NFR in dB is defined as $NFR = 10\log_{10}\frac{E(\|\mathbf{g}_k\|^2)}{E(\|\mathbf{g}_1\|^2)}$. Figures 4.3 to 4.10 show the performance when the transmitted signal are BPSK modulated. Figures 4.11 to 4.18 show the performance when the transmitted signal are QPSK modulated.

Figures 4.3 and 4.4 show the near-far performance comparison of OTD and STTD when $\mathbf{R}_y$ is known for $L = 1$ and $L = 2$, respectively. $SNR_1 = 10$dB. The two receiver schemes combining OTD and STTD with the MVDR receiver provide the near-far resistant performance while those two receivers combining OTD and STTD with the MF do not. The performance enhancement due to STTD over OTD at the cost of the higher complexity receiver is obviously shown in the figures.

Figures 4.5 and 4.6 show the near-far performance comparison of OTD and STTD when $\mathbf{R}_y$ is estimated with $J = 100$, $J = 300$ and $J = 500$ symbols for $L = 1$ and $L = 2$, respectively. Still $SNR_1 = 10$dB. The two receivers combining OTD and STTD with the MVDR receiver. When $J$ is increased, both receivers converge to the the theoretical performance with $R_y$ known .

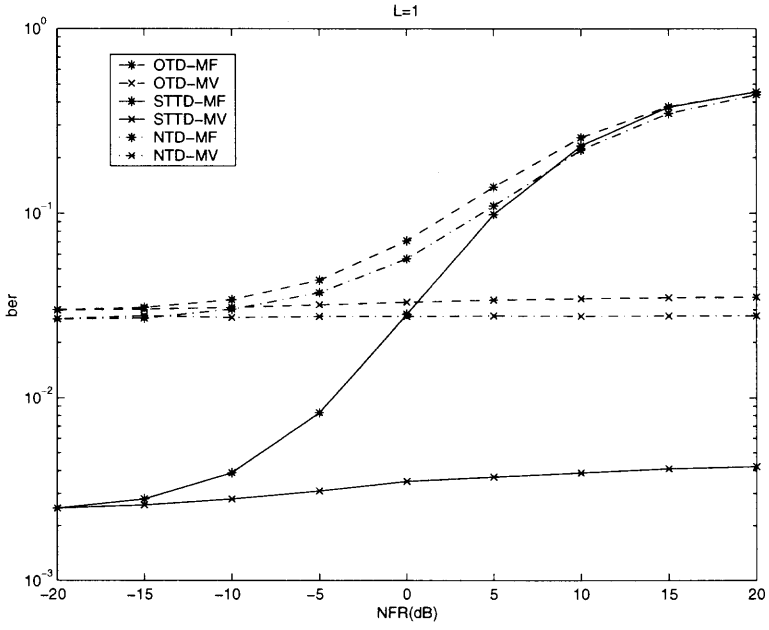


**Figure 4.3** Near-far performance comparison with $\mathbf{R}_y$ known, with $SNR_1 = 10$dB. Parameter used are: $K = 4$, $N = 15$, $L = 1$. BPSK modulation

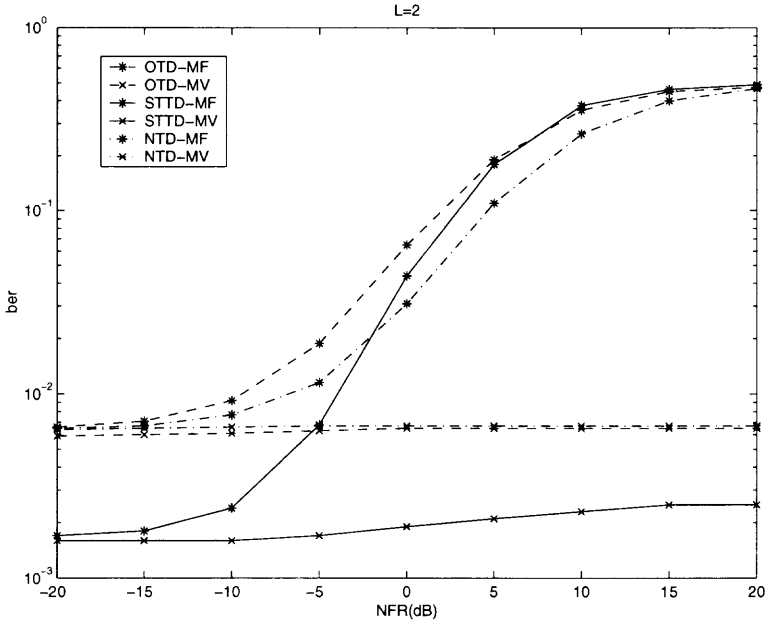


**Figure 4.4** Near-far performance comparison with $\mathbf{R}_y$ known, with $SNR_1 = 10$dB. Parameter used are: $K = 4$, $N = 15$, $L = 2$. BPSK modulation

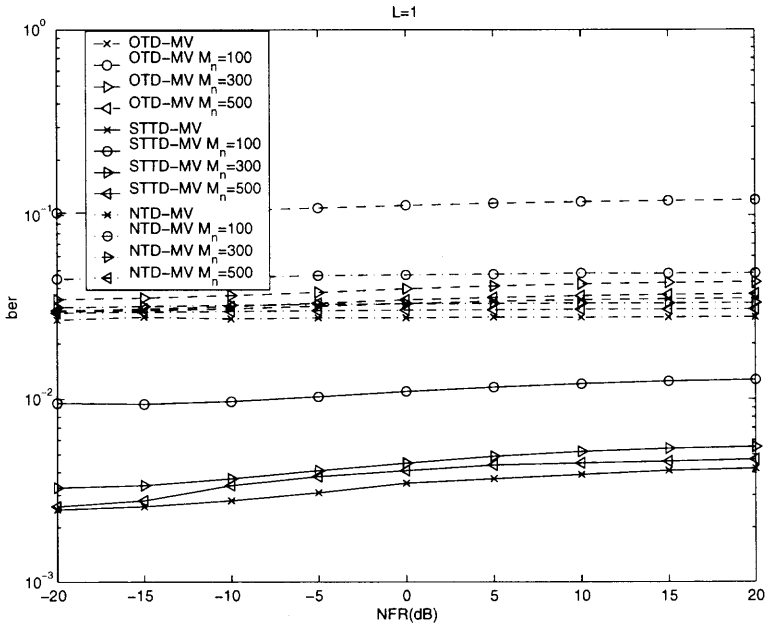


**Figure 4.5** Near-far performance comparison with $\mathbf{R}_y$ estimated, with $SNR_1 =$ 10dB. Parameter used are: $K = 4$, $N = 15$, $L = 1$. BPSK modulation

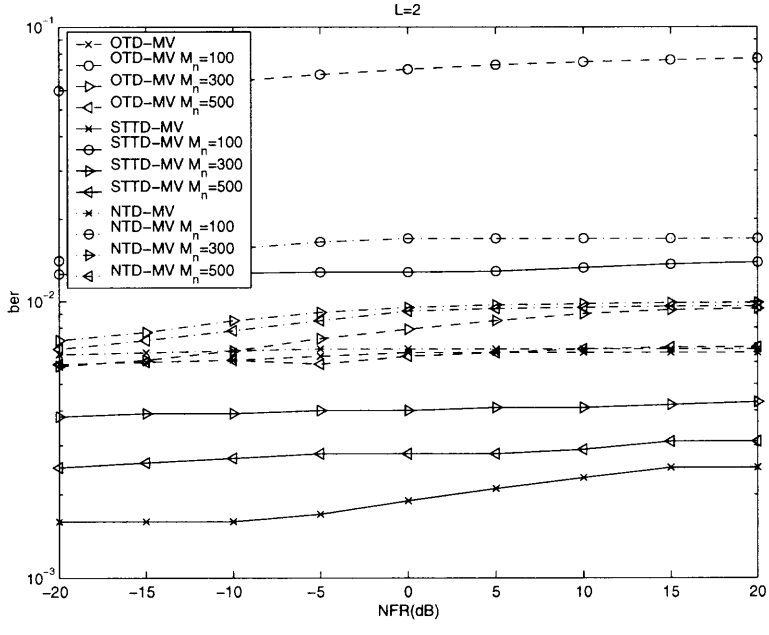


**Figure 4.6** Near-far performance comparison with $\mathbf{R}_y$ estimated, with $SNR_1 =$ 10dB. Parameter used are: $K = 4$, $N = 15$, $L = 2$. BPSK modulation

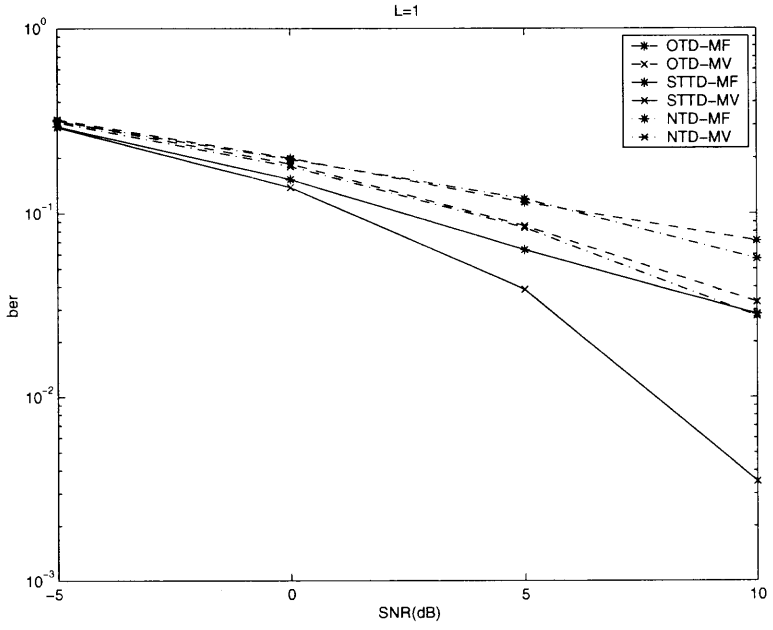


**Figure 4.7** SNR performance comparison with $\mathbf{R}_y$ known, with $SNR_1 = 10$dB. Parameter used are: $K = 4$, $N = 15$, $L = 1$. BPSK modulation

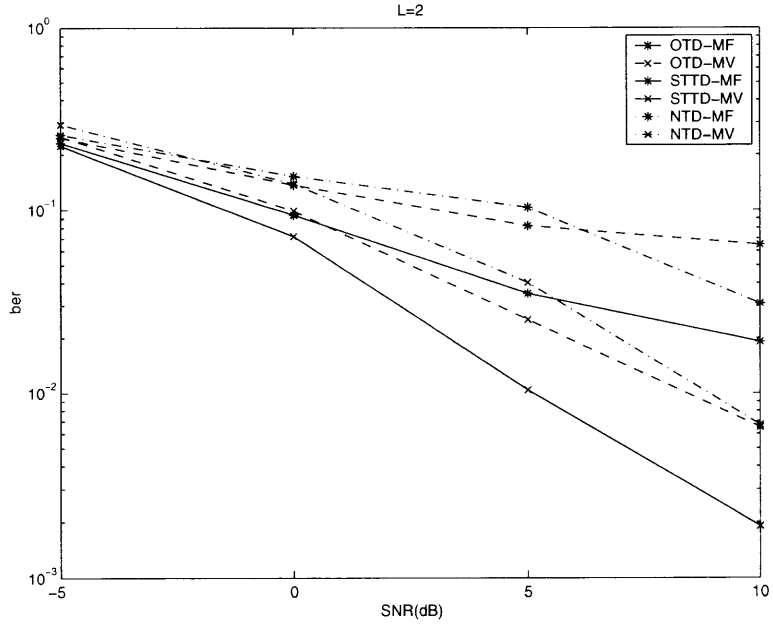


**Figure 4.8** SNR performance comparison with $\mathbf{R}_y$ known, with $SNR_1 = 10$dB. Parameter used are: $K = 4$, $N = 15$, $L = 2$. BPSK modulation

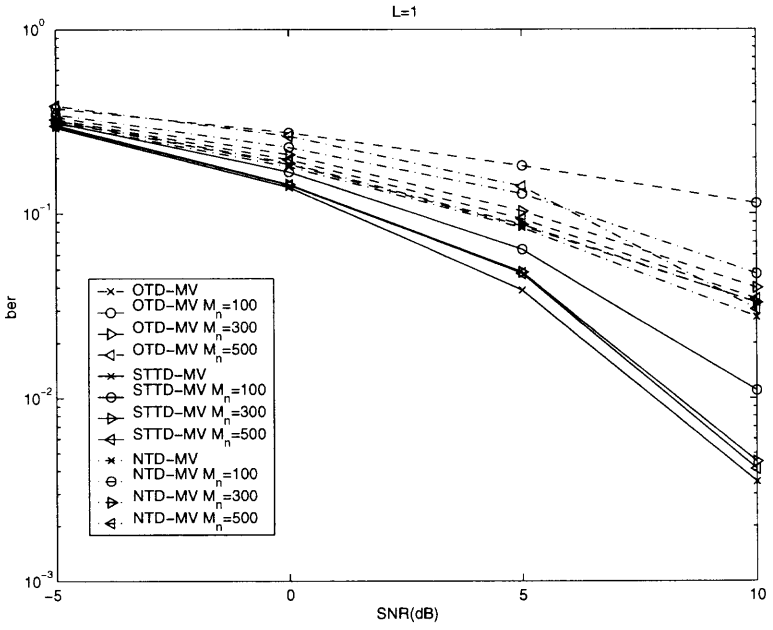


**Figure 4.9** SNR performance comparison with $\mathbf{R}_y$ estimated, with $SNR_1 = 10$dB. Parameter used are: $K = 4$, $N = 15$, $L = 1$. BPSK modulation

Figures 4.7 and 4.8 show another aspect of performance comparison of OTD and STTD when $\mathbf{R}_y$ is known for $L = 1$ and $L = 2$, respectively. The $SNR_1$ ranges from $-5$dB to 10dB, with $NFR = 0$dB. The two receivers combining OTD and STTD with the MVDR receiver provide better performance than those two receivers combining OTD and STTD with the MF do not have this property. The performance enhancement due to STTD over OTD at the price of the higher receiver is also shown in the figures.

Figures 4.9 and 4.10 show the performance comparison of OTD and STTD when $\mathbf{R}_y$ is estimated with $J = 100$, $J = 300$ and $J = 500$ symbols for $L = 1$ and $L = 2$, respectively. The $SNR_1$ ranges from $-5$dB to 10dB, with $NFR = 0$dB. The two receivers combining OTD and STTD with the MVDR receiver. When $J$ is increased, both receivers approach to the the theory performance when $R_y$ is known.

Figures 4.11 to 4.18 are the performance comparison when the transmitted signal are QPSK modulated.

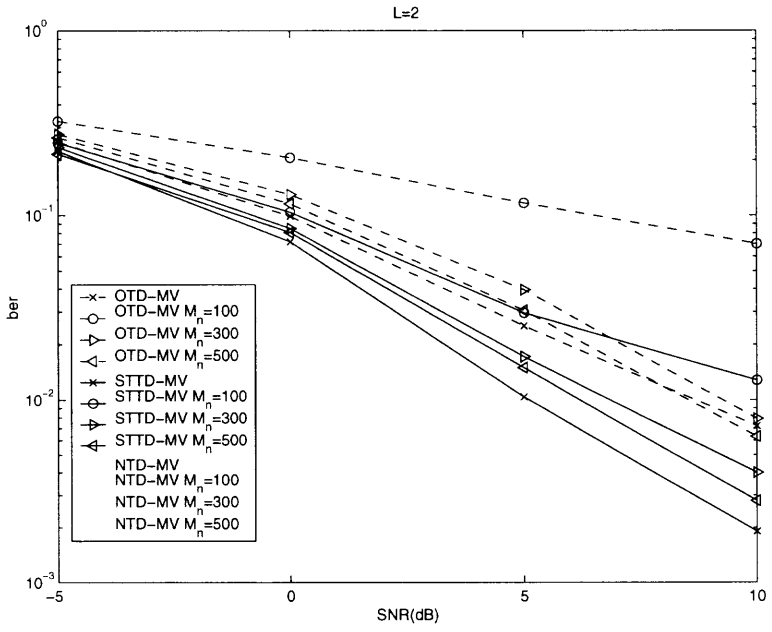


**Figure 4.10** SNR performance comparison with $\mathbf{R}_y$ estimated, with $SNR_1 = 10$dB. Parameter used are: $K = 4$, $N = 15$, $L = 2$. BPSK modulation

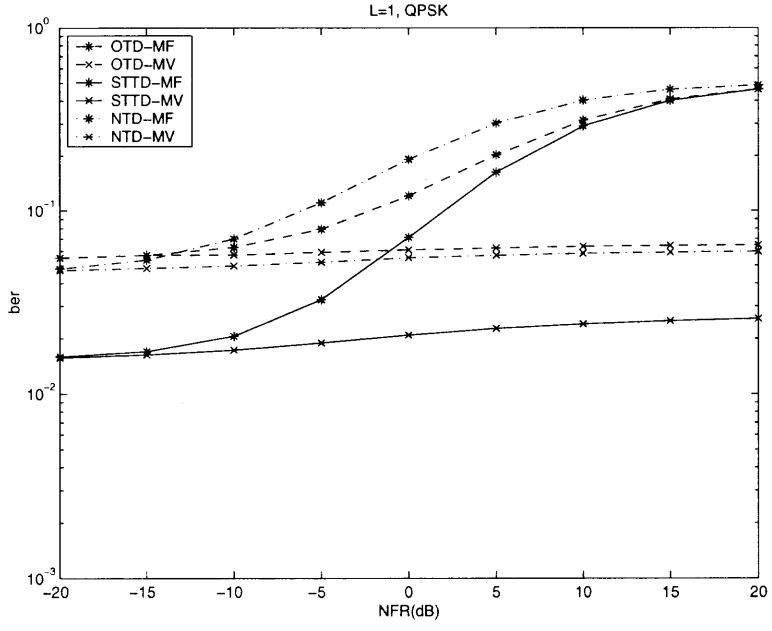


**Figure 4.11** Near-far performance comparison with $\mathbf{R}_y$ known, with $SNR_1 = 10$dB. Parameter used are: $K = 4$, $N = 15$, $L = 1$. QPSK modulation

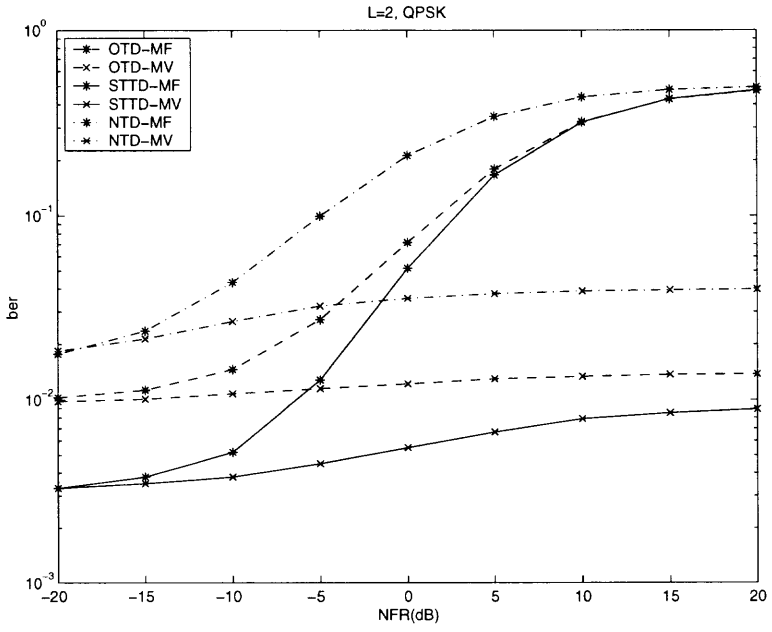


**Figure 4.12** Near-far Performance comparison with $\mathbf{R}_y$ known, with $SNR_1 = 10$dB. Parameter used are: $K = 4$, $N = 15$, $L = 2$. QPSK modulation

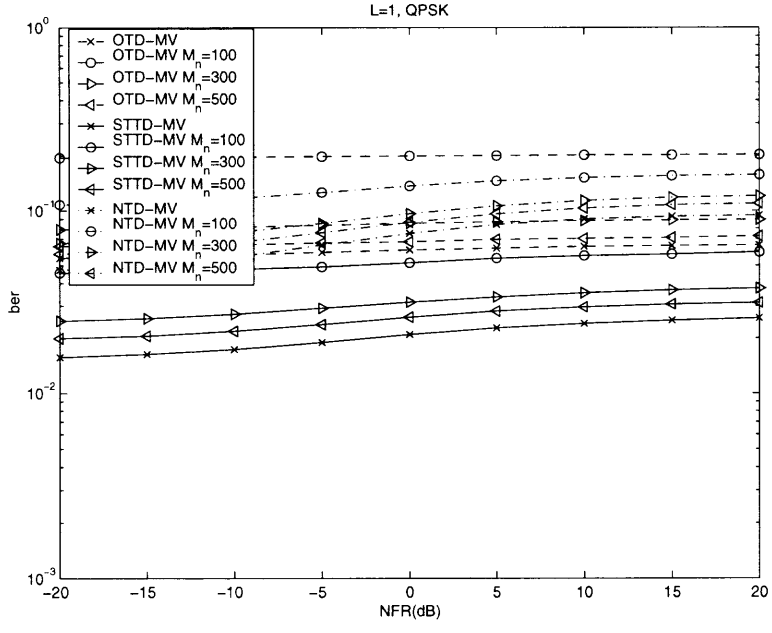


**Figure 4.13** Near-far performance comparison with $\mathbf{R}_y$ estimated, with $SNR_1 = 10$dB. Parameter used are: $K = 4$, $N = 15$, $L = 1$. QPSK modulation

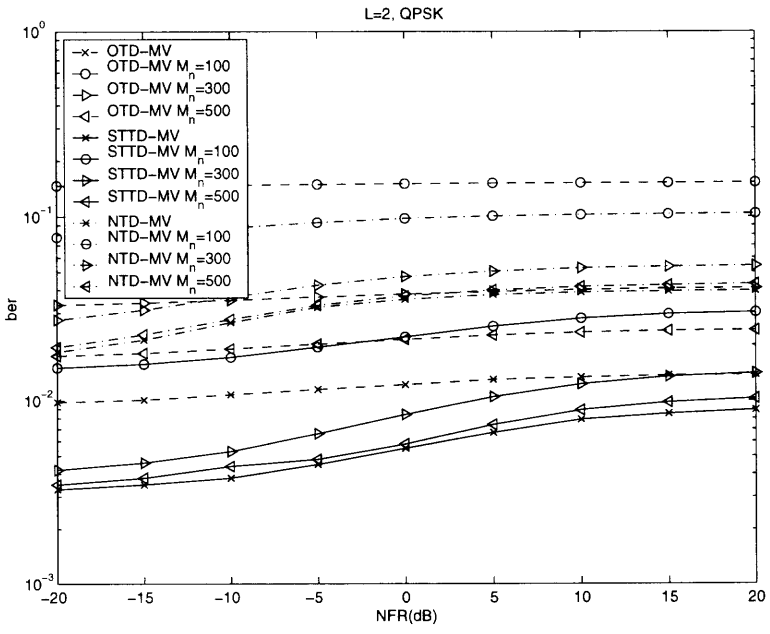


**Figure 4.14** Near-far performance comparison with $\mathbf{R}_y$ estimated, with $SNR_1 = 10$dB. Parameter used are: $K = 4$, $N = 15$, $L = 2$. QPSK modulation

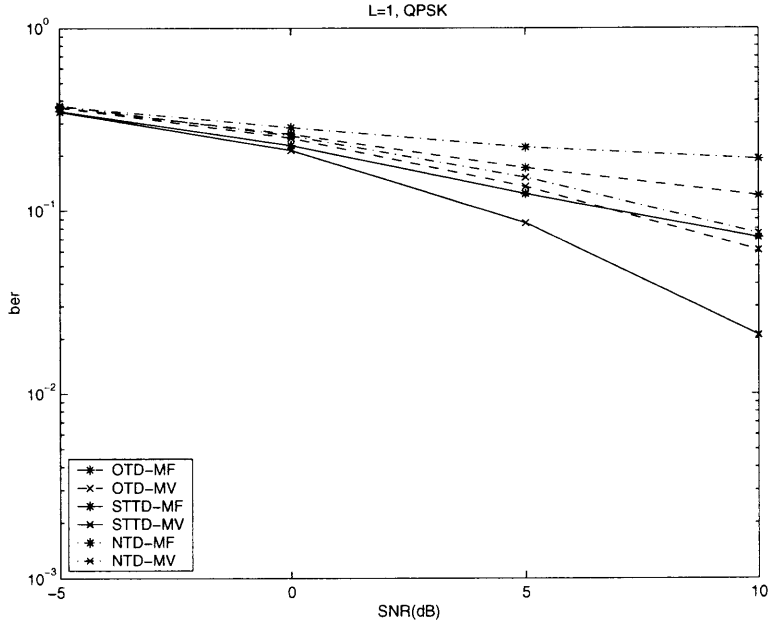


**Figure 4.15** SNR performance comparison with $\mathbf{R}_y$ known, with $SNR_1 = 10$dB. Parameter used are: $K = 4$, $N = 15$, $L = 1$. QPSK modulation

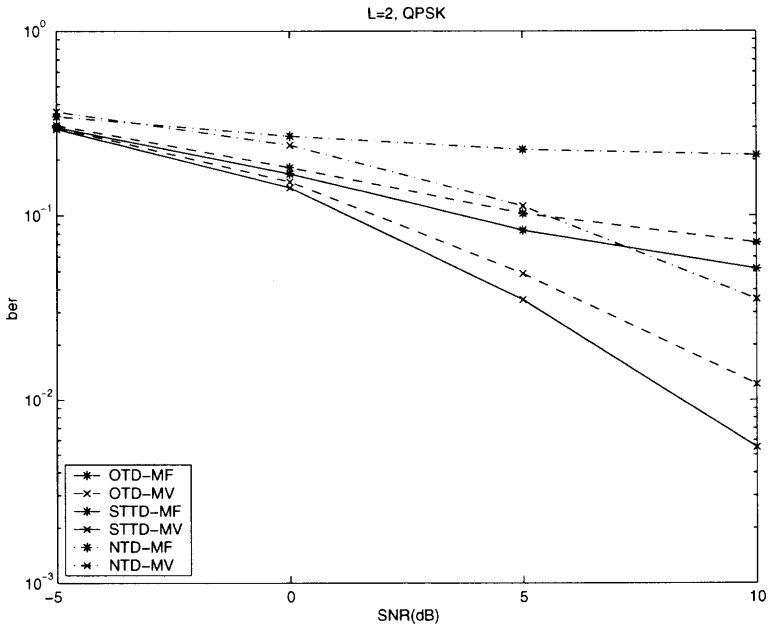


**Figure 4.16** SNR performance comparison with $\mathbf{R}_y$ known, with $SNR_1 = 10$dB. Parameter used are: $K = 4$, $N = 15$, $L = 2$. QPSK modulation

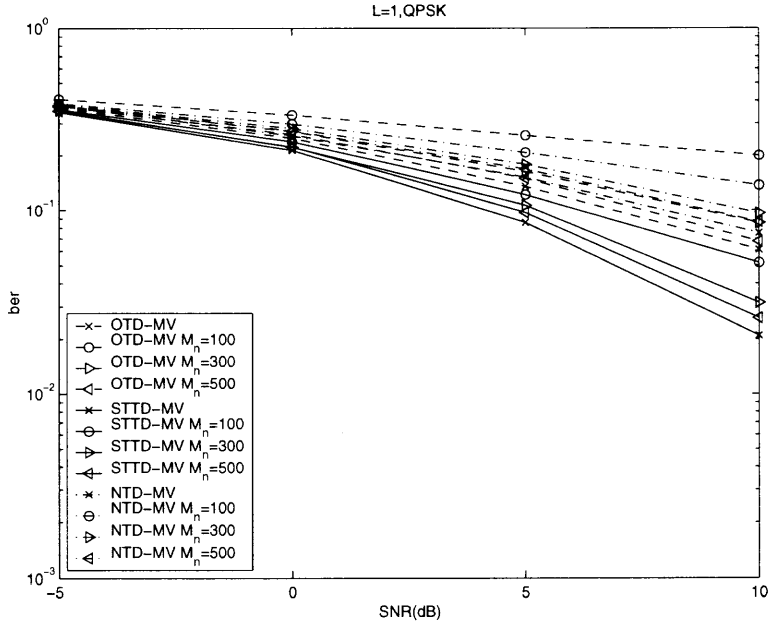


**Figure 4.17** SNR performance comparison with $\mathbf{R}_y$ estimated, with $SNR_1 = 10$dB. Parameter used are: $K = 4$, $N = 15$, $L = 1$. QPSK modulation

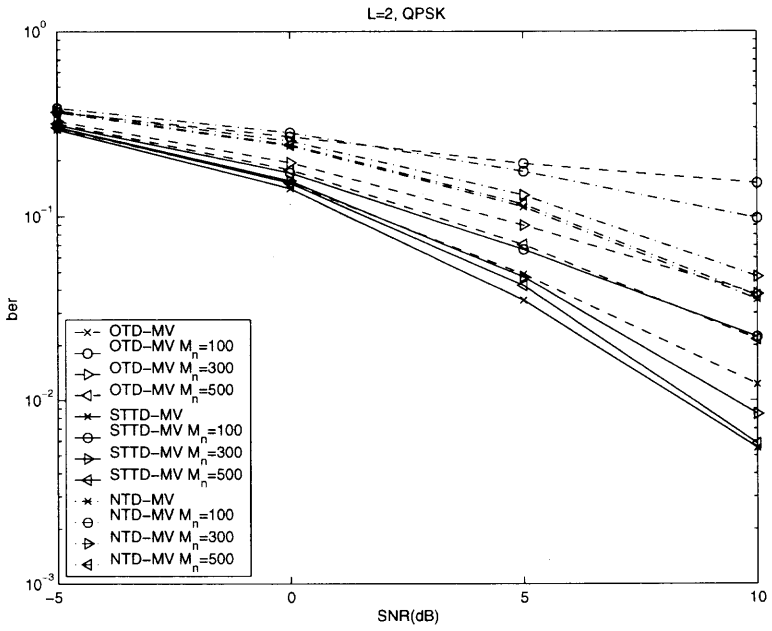


**Figure 4.18** SNR performance comparison with $\mathbf{R}_y$ estimated, with $SNR_1 = 10$dB. Parameter used are: $K = 4$, $N = 15$, $L = 2$. QPSK modulation

## 4.4 Conclusions

A new generalized differential encoder scheme is proposed for transmit system with two transmit antennas. To get the transmit diversity, the STTD is applied to the DS-CDMA systems transmitter. At the receiver, after the MVDR receiver, which suppresses the MAI, the corresponding differential decoder is used to realize the blind detection. The simulation results show that the performance is much better when STTD is combined with MVDR receiver rather than MF receiver. It is also shown that the STTD combined with MVDR receiver has a much better performance than OTD combined with MVDR with little complexity increasing in the receiver.

# CHAPTER 5

# JOINT TEMPORAL AND SPATIAL CHANNEL PARAMETER ESTIMATION FOR DS-CDMA SYSTEMS

In order to estimate the channel characteristics of the multipath wireless communication channel and consequently, to utilize the multipath components in the receiver, the spatial-temporal channel parameter estimation problem is investigated in this chapter. In this chapter, an approximate ML method for joint estimation of time delays and DOA's for the DS-CDMA systems over the multipath Rayleigh fading channels is developed. The proposed estimation scheme is developed by modeling the known training sequence of the desired user as the desired signal and the MAI-plus-AWGN as unknown colored Gaussian noise uncorrelated with the desired signal. An efficient iterative algorithm for estimating channel parameters (the time delays and DOA's of multipath signals) is proposed to reduce computational complexity. The algorithm transforms the multi-dimensional maximization problem into two simple 1-D maximization problems based on the alternating projection concept. Analytical and simulation results are presented to illustrate the performance in comparison with the corresponding CRBs. It is shown that the proposed algorithm is near-far resistant for both time delay and DOA estimation and little performance loss is observed in comparison with the CRBs at reasonable SNRs.

## 5.1 Signal Model

Consider a DS-CDMA system with $K$ users transmitting sequences of BPSK symbols through their respective multipath Rayleigh fading channels. Same as in (2.1), the baseband DS-CDMA signal due to the $k$th user as,

$$s_k(t) = \sum_i b_k(i) c_k(t - iT), \quad k = 1, \cdots, K,$$

The $k$th user's channel is modeled as a multipath channel with $L$ paths, each associated with a complex Gaussian fading coefficient $\{g_k(l)\}_{l=1}^{L}$. For each multipath component, there are different path delay and DOA associated with the signal of the $k$th user. Hence the received baseband signal at the output of an $M$-element antenna array due to the $k$th user is

$$\mathbf{y}_k(t) = \sum_{l=1}^{L} g_k(l)\, s_k(t-\tau_{kl})\mathbf{a}(\theta_{kl}).$$

The total received data in a $K$ users DS-CDMA system is

$$\mathbf{y}(t) = \sum_{k=1}^{K}\sum_{l=1}^{L} g_k(l)\, s_k(t-\tau_{kl})\mathbf{a}(\theta_{kl}) + \mathbf{v}(t), \tag{5.1}$$

where $\mathbf{v}(t)$ is spatially and temporally i.i.d. complex AWGN with zero mean and variance $2\sigma^2$. At the chip rate, the discrete-time version of the received data in equation (5.1) can be formulated as

$$\mathbf{y}(n) = \sum_{k=1}^{K}\sum_{l=1}^{L} g_k(l)\, s_k(n-\tau_{kl})\mathbf{a}(\theta_{kl}) + \mathbf{v}(n), \tag{5.2}$$

Within the $n$th processing interval of length $T$, which is commonly not aligned with the unknown delays, the chip-rate matched filtered and sampled $N$ snapshots of data in equation (5.2) can be collected into a $M \times N$ matrix

$$\begin{aligned}\mathbf{Y}(n) &\triangleq [\mathbf{y}(nN)\cdots\mathbf{y}(nN+N-1)] \\ &= \sum_{k=1}^{K}\sum_{l=1}^{L} g_k(l)\mathbf{a}(\theta_{kl})\left[\mathbf{u}_k^{(r)T}(\tau_{kl})b_k(n-1) + \mathbf{u}_k^{(l)T}(\tau_{kl})b_k(n)\right] + \mathbf{V}(n),\end{aligned}$$

where $M \times N$ matrix $\mathbf{V}(n)$ is spatially and temporally white Gaussian noise given by $\mathbf{V}(n) = [\mathbf{v}(n), \cdots, \mathbf{v}(n+N-1)]$, $(N \times 1)$ vectors $\mathbf{u}_k^{(r)}(\tau_{kl})$ and $\mathbf{u}_k^{(l)}(\tau_{kl})$ are partitioned temporal signature vectors of the $k$th user's $l$th path, parameterized by the time delay $\tau_{kl} = \nu_{kl}\, T_c + \gamma_{kl}$, where $\nu_{kl}$ and $\gamma_{kl}$ are the integer and fractional parts of the delay parameter $\tau_{kl}$ modulo $T_c$ (in the further analyses and simulations, a normalized chip interval is chosen, i.e., $T_c = 1$) as follows

$$\begin{aligned}\mathbf{u}_k^{(r)}(\tau_{kl}) &= (1-\gamma_{kl})\,\mathbf{c}_k^{(r)}(\nu_{kl}) + \gamma_{kl}\,\mathbf{c}_k^{(r)}(\nu_{kl}+1), \\ \mathbf{u}_k^{(l)}(\tau_{kl}) &= (1-\gamma_{kl})\,\mathbf{c}_k^{(l)}(\nu_{kl}) + \gamma_{kl}\,\mathbf{c}_k^{(l)}(\nu_{kl}+1).\end{aligned}$$

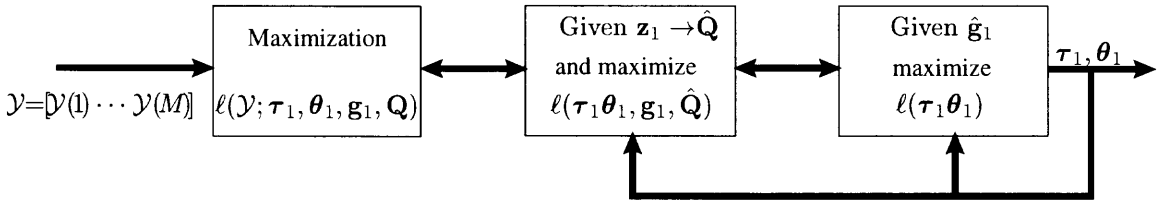


**Figure 5.1** Block diagram of the joint time-delay and DOA estimation scheme.

Vectors $\mathbf{c}_k^{(r)}(\nu_{kl})$ and $\mathbf{c}_k^{(l)}(\nu_{kl})$ are the right and left portion of signature vector $\mathbf{c}_k$ partitioned by integer part of delay $\nu_{kl}$, i.e.,

$$\begin{aligned}\mathbf{c}_k^{(r)}(\nu_{kl}) &= [c_k^{(N-\nu_{kl})}\cdots c_k^{(N-1)}\,0\cdots 0]^T,\\ \mathbf{c}_k^{(l)}(\nu_{kl}) &= [0\cdots 0\,c_k^{(0)}\cdots c_k^{(N-\nu_{kl}-1)}]^T.\end{aligned}$$

Vectorize columns of data matrix $\mathbf{Y}(n)$ into an $MN\times 1$ observation vector $\mathcal{Y}(n)$, then

$$\begin{aligned}\mathcal{Y}\ (n) &= vec(\mathbf{Y}(n))\\ &= \sum_{k=1}^{K}\sum_{l=1}^{L} g_k(l)\left[\mathbf{u}_k^{(r)}(\tau_{kl})b_k(n-1)+\mathbf{u}_k^{(l)}(\tau_{kl})b_k(n)\right]\otimes\mathbf{a}(\theta_{kl})+\mathcal{N}(n)\\ &= \underbrace{\mathbf{H}_1(\boldsymbol{\tau}_1,\boldsymbol{\theta}_1)\mathbf{G}_1(\mathbf{g}_1)\mathbf{z}_1(n)}_{\text{desired signal}}+\underbrace{\sum_{k=2}^{K}\mathbf{H}_k(\boldsymbol{\tau}_k,\boldsymbol{\theta}_k)\mathbf{G}_k(\mathbf{g}_k)\mathbf{z}_k(n)+\mathcal{N}(n)}_{\text{MAI+noise: }\mathcal{N}_I(n)},\end{aligned}\tag{5.3}$$

where $\mathbf{H}_k(\boldsymbol{\tau}_k,\boldsymbol{\theta}_k)=\left[\mathbf{h}_{k1}^{(r)}\,\mathbf{h}_{k1}^{(l)}\cdots\mathbf{h}_{kL}^{(r)}\,\mathbf{h}_{kL}^{(l)}\right]$, with $\mathbf{h}_{kl}^{(r)}=\mathbf{u}_k^{(r)}(\tau_{kl})\otimes\mathbf{a}(\theta_{kl})$, $\mathbf{h}_{kl}^{(l)}=\mathbf{u}_{kl}^{(l)}(\tau_{kl})\otimes\mathbf{a}(\theta_{kl})$, $\boldsymbol{\tau}_k=[\tau_{k1}\cdots\tau_{kL}]^T$, and $\boldsymbol{\theta}_k=[\theta_{k1}\cdots\theta_{kL}]^T$, $\mathbf{G}_k(\mathbf{g}_k)=\mathbf{g}_k\otimes\mathbf{I}_2$, with $\mathbf{g}_k=[g_k(1)\cdots g_k(L)]^T$, $\mathbf{z}_k(n)=[b_k(n-1)\ b_k(n)]^T$, $\mathcal{N}(n)=vec(\mathbf{N}(n))$, and $\mathcal{N}_I(n)=\sum_{k=2}^{K}\mathbf{H}_k(\boldsymbol{\tau}_k,\boldsymbol{\theta}_k)\,\mathbf{G}_k(\mathbf{g}_k)\,\mathbf{z}_k(n)+\mathcal{N}(n)$.

The focus of this work is to estimate channel parameters using the received data $\{\mathcal{Y}(n)\}$.

## 5.2 The Maximum Likelihood Estimators

To set the basis for the iterative solution, the joint ML estimators for the channel parameters (time delays and DOA's) of a desired user (user 1) is first presented. The block diagram is shown in figure 5.1. When the number of active users in combination with number of multipath components is reasonably large, the MAI-plus-AWGN can be modeled as *colored* Gaussian noise. Then the received data $\mathcal{Y}(n)$ is modeled as a complex Gaussian random vector with mean vector parameterized by $\boldsymbol{\tau}_1$, $\boldsymbol{\theta}_1$ and $\mathbf{g}_1$ as

$$E\left[\mathcal{Y}(n)\right] = \mathbf{H}_1(\boldsymbol{\tau}_1, \boldsymbol{\theta}_1)\, \mathbf{G}_1(\mathbf{g}_1)\mathbf{z}_1(n), \tag{5.4}$$

and the second-order statistics summarized in matrices

$$\begin{aligned} E &\left\{\left[\mathcal{Y}(n) - E\left(\mathcal{Y}(n)\right)\right]\left[\mathcal{Y}(m) - E\left(\mathcal{Y}(m)\right)\right]^H\right\} \approx \mathbf{Q}\,\delta_{mn}, \\ E &\left\{\left[\mathcal{Y}(n) - E\left(\mathcal{Y}(n)\right)\right]\left[\mathcal{Y}(m) - E\left(\mathcal{Y}(m)\right)\right]^T\right\} = \mathbf{0}, \end{aligned}$$

where $\delta_{mn}$ is a discrete Kronecker delta function, and

$$\mathbf{Q} = \sum_{k=2}^{K} \mathbf{H}_k(\boldsymbol{\tau}_k, \boldsymbol{\theta}_k)\, \mathbf{G}_k(\mathbf{g}_k)\, \mathbf{G}_k^H(\mathbf{g}_k)\mathbf{H}_k^H(\boldsymbol{\tau}_k, \boldsymbol{\theta}_k) + 2\sigma^2\, \mathbf{I}. \tag{5.5}$$

The likelihood function for a given $\mathcal{Y}(n)$ is given by

$$L(\mathcal{Y}(n); \boldsymbol{\tau}_1, \boldsymbol{\theta}_1, \mathbf{g}_1, \mathbf{Q}) = \frac{1}{\pi^{NM} \mid \mathbf{Q} \mid} \exp\left\{-\mathcal{N}_I^H(n)\, \mathbf{Q}^{-1}\, \mathcal{N}_I(n)\right\},$$

where $\mid \cdot \mid$ stands for the determinant, and $\mathcal{N}_I(n) = \mathcal{Y}(n) - \mathbf{H}_1(\boldsymbol{\tau}_1, \boldsymbol{\theta}_1)\mathbf{G}_1(\mathbf{g}_1)\mathbf{z}_1(n)$. Since $\mathcal{Y}(n)$ and $\mathcal{Y}(m)$ are approximately uncorrelated complex Gaussian vectors for $m \neq n$, the likelihood function based on the observation $\mathcal{Y} = [\,\mathcal{Y}(1)\,\mathcal{Y}(2)\,\cdots\,\mathcal{Y}(J)]$ can be written as

$$\begin{aligned} L(\mathcal{Y}; \boldsymbol{\tau}_1, \boldsymbol{\theta}_1, \mathbf{g}_1, \mathbf{Q}) &= \prod_{n=1}^{J} L(\mathcal{Y}(n); \boldsymbol{\tau}_1, \boldsymbol{\theta}_1, \mathbf{g}_1, \mathbf{Q}) \\ &= \frac{1}{\pi^{JNM} \mid \mathbf{Q} \mid^J} \exp\left\{-\sum_{n=1}^{J} \mathcal{N}_I^H(n)\, \mathbf{Q}^{-1}\, \mathcal{N}_I(n)\right\}. \end{aligned} \tag{5.6}$$

The log-likelihood function is (when ignoring constant terms)

$$\ell(\boldsymbol{\tau}_1, \boldsymbol{\theta}_1, \mathbf{g}_1, \mathbf{Q}) = -J \log \mid \mathbf{Q} \mid \\ -\mathrm{tr}\left\{ \mathbf{Q}^{-1} \sum_{n=1}^{J} \left[\mathcal{Y}(n) - \mathbf{D}\mathbf{z}_1(n)\right] \left[\mathcal{Y}(n) - \mathbf{D}\mathbf{z}_1(n)\right]^H \right\}, \quad (5.7)$$

where $\mathbf{D} = \mathbf{H}_1(\boldsymbol{\tau}_1, \boldsymbol{\theta}_1)\, \mathbf{G}_1(\mathbf{g}_1)$, tr means the trace of the matrix. The ML estimators are therefore given by

$$\left[\hat{\boldsymbol{\tau}}_1, \hat{\boldsymbol{\theta}}_1, \hat{\mathbf{g}}_1, \hat{\mathbf{Q}}\right] = \arg \max_{\boldsymbol{\tau}_1, \boldsymbol{\theta}_1, \mathbf{g}_1, \mathbf{Q}} \left\{ \ell(\boldsymbol{\tau}_1, \boldsymbol{\theta}_1, \mathbf{g}_1, \mathbf{Q}) \right\}. \quad (5.8)$$

Maximizing $\ell(\boldsymbol{\tau}_1, \boldsymbol{\theta}_1, \mathbf{g}_1, \mathbf{Q})$ first with respect to $\mathbf{Q}$ for a fixed $\mathbf{D}$ yields

$$\hat{\mathbf{Q}} = \frac{1}{J} \sum_{n=1}^{J} \left[\mathcal{Y}(n) - \mathbf{D}\, \mathbf{z}_1(n)\right] \left[\mathcal{Y}(n) - \mathbf{D}\, \mathbf{z}_1(n)\right]^H, \quad (5.9)$$

which, when substituted back into equation (5.7), yields the ML estimators of channel parameters,

$$\begin{aligned} \left[\hat{\boldsymbol{\tau}}_1, \hat{\boldsymbol{\theta}}_1, \hat{\mathbf{g}}_1\right] &= \arg \min_{\boldsymbol{\tau}_1, \boldsymbol{\theta}_1, \mathbf{g}_1} \left| \frac{1}{J} \sum_{n=1}^{J} [\mathcal{Y}(n) - \mathbf{D}\mathbf{z}_1(n)][\mathcal{Y}(n) - \mathbf{D}\mathbf{z}_1(n)]^H \right| \\ &= \arg \min_{\boldsymbol{\tau}_1, \boldsymbol{\theta}_1, \mathbf{g}_1} F. \end{aligned} \quad (5.10)$$

Instead of minimizing $F$ directly with respect to $\boldsymbol{\tau}_1$, $\boldsymbol{\theta}_1$ and $\mathbf{g}_1$, we minimize $F$ first with respect to the unstructured matrix $\mathbf{D}$, and $\hat{D}$ is shown as

$$\hat{\mathbf{D}} = \arg \min_{\mathbf{D}} F.$$

The unstructured estimate $\hat{\mathbf{D}}$ of $\mathbf{D}$ is then given by

$$\hat{\mathbf{D}} = \hat{\mathbf{R}}_{yz}\, \hat{\mathbf{R}}_{zz}^{-1},$$

with $\hat{\mathbf{R}}_{zz} = \frac{1}{J} \sum_{n=1}^{J} \mathbf{z}_1(n) \mathbf{z}_1^H(n)$ and $\hat{\mathbf{R}}_{yz} = \frac{1}{J} \sum_{n=1}^{J} \mathcal{Y}(n) \mathbf{z}_1^H(n)$.

Substituting $\hat{\mathbf{D}}$ into equation (5.9) yields

$$\hat{\mathbf{Q}} = \hat{\mathbf{R}}_{yy} - \hat{\mathbf{R}}_{yz}\, \hat{\mathbf{R}}_{zz}^{-1}\, \hat{\mathbf{R}}_{yz}^H.$$

with $\hat{\mathbf{R}}_{yy} = \frac{1}{J}\sum_{n=1}^{J} \mathcal{Y}(n)\,\mathcal{Y}^H(n)$. To find the estimations of $\boldsymbol{\tau}_1, \boldsymbol{\theta}_1, \mathbf{g}_1$, it now remains to minimize the following log-likelihood function

$$\ell(\boldsymbol{\tau}_1, \boldsymbol{\theta}_1, \mathbf{G}_1, \hat{\mathbf{Q}}) = J \log \mid \hat{\mathbf{Q}} \mid + constant, \tag{5.11}$$

with respect to channel parameters only. After some manipulations, it can be shown that the ML estimator of $\mathbf{G}_1$ for fixed non-linearly entered channel parameters $\boldsymbol{\tau}_1$ and $\boldsymbol{\theta}_1$ is given by

$$\hat{\mathbf{G}}_1 = (\mathbf{H}_1^H\,\hat{\mathbf{Q}}^{-1}\,\mathbf{H}_1)^{-1}\mathbf{H}_1^H\,\hat{\mathbf{Q}}^{-1}\,\hat{\mathbf{R}}_{yz}\,\hat{\mathbf{R}}_{zz}^{-1}, \tag{5.12}$$

with $\mathbf{H}_1 \triangleq \mathbf{H}_1(\tau_1, \theta_1)$ being parameterized by channel parameters. Substituted the above $\hat{\mathbf{G}}_1$ into equation (5.11), yields the estimations of $\boldsymbol{\tau}_1$ and $\boldsymbol{\theta}$ as

$$\left[\hat{\boldsymbol{\tau}}_1, \hat{\boldsymbol{\theta}}_1\right] = \arg\min_{\boldsymbol{\tau}_1, \boldsymbol{\theta}_1} \left|\mathbf{I} + \hat{\mathbf{Q}}^{-1}(\mathbf{H}_1\hat{\mathbf{G}}_1 - \hat{\mathbf{D}})\hat{\mathbf{R}}_{yy}(\mathbf{H}_1\hat{\mathbf{G}}_1 - \hat{\mathbf{D}})^H\right|. \tag{5.13}$$

According to the general theory of ML estimator, this estimator is asymptotically statistically efficient.

## 5.3 An Efficient Iterative Estimation Scheme

Getting the ML estimations of time delays and DOAs from equation (5.13) involves a $2L$ multi-dimensional search over the parameter space spanned $[\boldsymbol{\tau}_1, \boldsymbol{\theta}_1]$. Hence, it is computationally prohibitive even for moderate values of $L$. An iterative estimation scheme that approximates the ML estimator and is computationally efficient is presented next.

Before describing the estimator, some notations are introduced first. The formula (5.3) can be rewritten as

$$\begin{aligned}
\mathcal{Y}(n) &= \sum_{l=1}^{L} (\mathbf{U}_1(\tau_{1l}) \otimes \mathbf{I}_M) \cdot (g_1(l)\mathbf{I}_{2M}) \cdot \left[\ \mathbf{I}_2 \otimes \mathbf{a}(\theta_{1l})\ \right] \cdot \mathbf{z}_1(n) + \mathcal{N}_I(n) \\
&= \sum_{l=1}^{L} \boldsymbol{\Upsilon}(\tau_{1l}, g_1(l))\,\mathbf{r}(n; \theta_{1l}) + \mathcal{N}_I(n) \\
&= \sum_{l=1}^{L} \boldsymbol{\Pi}(\tau_{1l})\,\mathbf{x}(n; \theta_{1l}, g_1(l)) + \mathcal{N}_I(n)
\end{aligned}$$

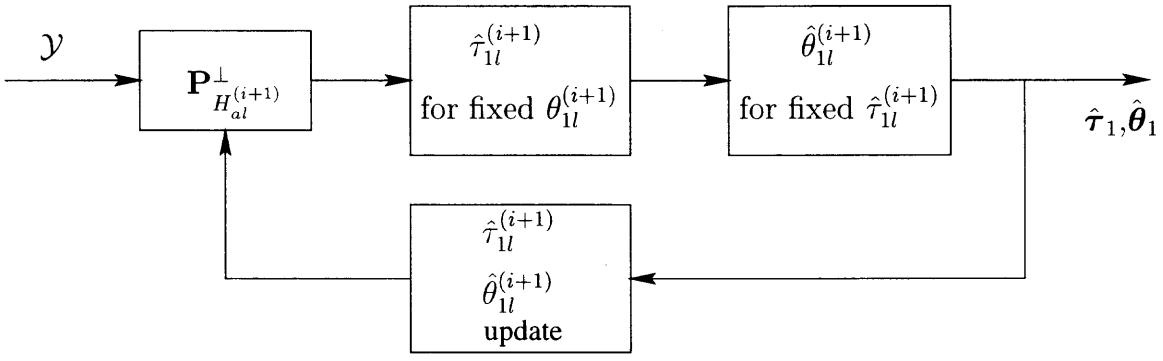


**Figure 5.2** Block diagram of the iterative estimation scheme.

where $\mathbf{U}_1(\tau_{1l}) = \left[\mathbf{u}_{1l}^{(r)}\ \mathbf{u}_{1l}^{(l)}\right]$, $\boldsymbol{\Upsilon}(\tau_{1l}, g_1(l)) = \boldsymbol{\Pi}(\tau_{1l})\,\Gamma(\mathbf{g}_1(l))$, with $\boldsymbol{\Pi}(\tau_{1l}) = \mathbf{U}_1(\tau_{1l}) \otimes \mathbf{I}_M$ and $\boldsymbol{\Gamma}(g_1(l)) = g_1(l)\mathbf{I}_{2M}$, $\mathbf{r}(n;\theta_{1l}) = \boldsymbol{\Psi}(\theta_{1l})\mathbf{z}_1(n)$, with $\boldsymbol{\Psi}(\theta_{1l}) = \left[\ \mathbf{I}_2 \otimes \mathbf{a}(\theta_{1l})\ \right]$, and $\mathbf{x}(n;\theta_{1l}, g_1(l)) = \boldsymbol{\Gamma}(g_1(l))\boldsymbol{\Psi}(\theta_{1l})\mathbf{z}_1(n) = \left[g_1(l)\mathbf{a}^T(\theta_{1l})b_1(n-1)\ \ g_1(l)\mathbf{a}^T(\theta_{1l})b_1(n)\right]^T$.

Figure 5.2 shows the block diagram of the proposed iterative estimation scheme. Instead of directly solving the multi-dimensional maximization problem in equation (5.13), the maximization problem is solved iteratively based on the alternating projection concept. The proposed iterative estimation scheme iterates between the DOA and the time delay parameter sets, and exploits the symmetry between them in the likelihood function. Each iteration involves two steps. First, the unstructured matrix $\boldsymbol{\Upsilon}(\tau_{1l}, g_1(l))$ or vector $\mathbf{x}(n;\theta_{1l}, g_1(l))$ that contains the information of $\tau_{1l}$ or $\theta_{1l}$ is estimated using ML estimator. Then, the parameter itself ,$\tau_{1l}$ or $\theta_{1l}$, is estimated using the structure of the estimated matrix $\hat{\boldsymbol{\Upsilon}}(\tau_{1l}, g_1(l))$ or the estimated vector $\hat{\mathbf{x}}(n;\theta_{1l}, g_1(l))$.

Start by initializing the estimations for a single path. First, an estimator for $\tau_{11}$ and $g_1(1)$ conditioned on $\theta_{11}$ is presented. To this end, fix $\theta_{11} = \hat{\theta}_{11}$ and rewrite the minimization problem (5.10) as

$$\left[\hat{\tau}_{11}^{(0)}, \hat{g}_1^{(0)}(1)\right] = \arg \min_{\tau_{11}, g_1(1)} F_1$$

$$= \arg \min_{\tau_{11}, g_1(1)} \left| \sum_{n=1}^{J} [\mathcal{Y}(n) - \boldsymbol{\Upsilon}(\tau_{11}, g_1(1)) \mathbf{r}(n; \hat{\theta}_{11})][\mathcal{Y}(n) - \boldsymbol{\Upsilon}(\tau_{11}, g_1(1)) \mathbf{r}(n; \hat{\theta}_{11})]^H \right|.$$

Instead of minimizing $F_1$ directly with respect to $\tau_{11}$ and $g_1(1)$, minimize $F_1$ first with respect to the unstructured matrix $\boldsymbol{\Upsilon}(\tau_{11}, g_1(1))$, which yields

$$\hat{\boldsymbol{\Upsilon}}^{(0)}(\tau_{11}, g_1(1)) = \hat{\mathbf{R}}_{yr,1}^{(0)} \hat{\mathbf{R}}_{rr,1}^{(0)-1},$$

where $\hat{\mathbf{R}}_{yr,1}^{(0)} = \frac{1}{J} \sum_{n=1}^{J} \mathcal{Y}(n) \mathbf{r}^H(n; \hat{\theta}_{11})$, and $\hat{\mathbf{R}}_{rr,1}^{(0)} = \frac{1}{J} \sum_{n=1}^{J} \mathbf{r}(n; \hat{\theta}_{11}) \mathbf{r}^H(n; \hat{\theta}_{11})$.

It is easy to show that $\hat{\mathbf{Q}}$ can be rewritten as

$$\hat{\mathbf{Q}}_1^{(0)} = \hat{\mathbf{R}}_{yy,1}^{(0)} - \hat{\mathbf{R}}_{yr,1}^{(0)} \hat{\mathbf{R}}_{rr,1}^{(0)-1} \hat{\mathbf{R}}_{yr,1}^{(0)H}, \tag{5.14}$$

with $\hat{\mathbf{R}}_{yy,1}^{(0)} = \frac{1}{J} \sum_{n=1}^{J} \mathcal{Y}(n) \mathcal{Y}^H(n)$.

The cost function $F_1$ in equation (5.14) may be rewritten as

$$\begin{aligned}
F_1 &= \left| \hat{\mathbf{R}}_{yy,1}^{(0)} - \boldsymbol{\Upsilon}(\tau_{11}, g_1(1)) \hat{\mathbf{R}}_{yr,1}^{(0)H} - \hat{\mathbf{R}}_{yr,1}^{(0)} \boldsymbol{\Upsilon}^H(\tau_{11}, g_1(1)) + \boldsymbol{\Upsilon}(\tau_{11}, g_1(1)) \hat{\mathbf{R}}_{rr,1}^{(0)} \boldsymbol{\Upsilon}^H(\tau_{11}, g_1(1)) \right| \\
&= \Bigg| \hat{\mathbf{R}}_{yy,1}^{(0)} - \hat{\mathbf{R}}_{yr,1}^{(0)} \hat{\boldsymbol{\Upsilon}}^H(\tau_{11}, g_1(1)) \\
&+ \left[ \boldsymbol{\Upsilon}(\tau_{11}, g_1(1)) - \hat{\boldsymbol{\Upsilon}}^{(0)}(\tau_{11}, g_1(1)) \right] \hat{\mathbf{R}}_{rr,1}^{(0)} \left[ \boldsymbol{\Upsilon}(\tau_{11}, g_1(1)) - \hat{\boldsymbol{\Upsilon}}^{(0)}(\tau_{11}, g_1(1)) \right]^H \Bigg| \\
&= \Bigg| \hat{\mathbf{R}}_{yy,1}^{(0)} - \hat{\mathbf{R}}_{yr,1}^{(0)} \hat{\mathbf{R}}_{rr,1}^{(0)-1} \hat{\mathbf{R}}_{yr,1}^{(0)H} \\
&+ \left[ \boldsymbol{\Upsilon}(\tau_{11}, g_1(1)) - \hat{\boldsymbol{\Upsilon}}^{(0)}(\tau_{11}, g_1(1)) \right] \hat{\mathbf{R}}_{rr,1}^{(0)} \left[ \boldsymbol{\Upsilon}(\tau_{11}, g_1(1)) - \hat{\boldsymbol{\Upsilon}}^{(0)}(\tau_{11}, g_1(1)) \right]^H \Bigg| \\
&= \left| \hat{\mathbf{Q}}_1^{(0)} + \left[ \boldsymbol{\Upsilon}(\tau_{11}, g_1(1)) - \hat{\boldsymbol{\Upsilon}}^{(0)}(\tau_{11}, g_1(1)) \right] \hat{\mathbf{R}}_{rr,1}^{(0)} \left[ \boldsymbol{\Upsilon}(\tau_{11}, g_1(1)) - \hat{\boldsymbol{\Upsilon}}^{(0)}(\tau_{11}, g_1(1)) \right]^H \right| \quad (5.15)
\end{aligned}$$

It is shown in [52] that minimizing $F_1$ defined in equation (5.15) is asymptotically equivalent to minimizing

$$\begin{aligned}
F_2 \;=\; & \mathrm{tr} \Bigg\{ \hat{\mathbf{R}}_{rr,1}^{(0)} \left[ \boldsymbol{\Upsilon}(\tau_{11}, g_1(1)) - \hat{\boldsymbol{\Upsilon}}^{(0)}(\tau_{11}, g_1(1)) \right]^H \hat{\mathbf{Q}}_1^{(0)-1} \\
& \left[ \boldsymbol{\Upsilon}(\tau_{11}, g_1(1)) - \hat{\boldsymbol{\Upsilon}}^{(0)}(\tau_{11}, g_1(1)) \right] \Bigg\}. \quad (5.16)
\end{aligned}$$

Let us now consider the structure of $\boldsymbol{\Upsilon}(\tau_{11}, g_1(1))$. For a given $\hat{\boldsymbol{\Upsilon}}(\tau_{11}, g_1(1))$, the $\hat{\boldsymbol{\Gamma}}(g_1(l))$ conditioned on $\tau_{11}$ is given by

$$\hat{\boldsymbol{\Gamma}}^{(0)}(g_1(1)) = \left[ \boldsymbol{\Pi}_1^H(\tau_{11}) \boldsymbol{\Pi}_1(\tau_{11}) \right]^{-1} \boldsymbol{\Pi}_1^H(\tau_{11}) \hat{\boldsymbol{\Upsilon}}^{(0)}(\tau_{11}, g_1(1)), \tag{5.17}$$

Now, substituting equation (5.17) back into equation (5.16), $\tau_{11}^{(0)}$ can be found by solving the following problem

$$\hat{\tau}_{11}^{(0)} = \arg\min_{\tau_{11}} \operatorname{tr}\left\{\hat{\mathbf{R}}_{rr,1}^{(0)}\left[\mathbf{\Pi}_1(\tau_{11})\hat{\mathbf{\Gamma}}^{(0)}(g_1(1)) - \hat{\mathbf{\Upsilon}}^{(0)}(\tau_{11}, g_1(1))\right]^H \hat{\mathbf{Q}}_1^{(0)-1} \left[\mathbf{\Pi}_1(\tau_{11})\hat{\mathbf{\Gamma}}^{(0)}(g_1(1)) - \hat{\mathbf{\Upsilon}}^{(0)}(\tau_{11}, g_1(1))\right]\right\}. \tag{5.18}$$

Next, develop an estimator for $\theta_{11}$ and $g_1(1)$ conditioned on $\tau_{11}$. To this end, fixing $\tau_{11} = \hat{\tau}_{11}$, equation (5.10) can be written as

$$\left[\hat{\theta}_{11}^{(0)}, \hat{g}_1^{(0)}(1)\right] = \arg\min_{\theta_{11}, g_1(1)} \left| \sum_{n=1}^{J} [\mathcal{Y}(n) - \mathbf{\Pi}(\hat{\tau}_{11})\,\mathbf{x}(n; \theta_{11}, g_1(1))] [\mathcal{Y}(n) - \mathbf{\Pi}(\hat{\tau}_{11})\,\mathbf{x}(n; \theta_{11}, g_1(1))]^H \right| \tag{5.19}$$

As above, first find the unstructured estimation of vectors $\mathbf{x}(n; \theta_{11}, g_1(1))$ as

$$\hat{\mathbf{x}}^{(0)}(n; \theta_{11}, g_1(1)) = \left(\mathbf{\Pi}^H(\hat{\tau}_{11})\hat{\mathbf{Q}}^{-1}\mathbf{\Pi}(\hat{\tau}_{11})\right)^{-1} \mathbf{\Pi}^H(\hat{\tau}_{11})\hat{\mathbf{Q}}^{-1}\mathcal{Y}(n). \tag{5.20}$$

The vector $\mathbf{q}_1^{(0)}(n) = \hat{\mathbf{x}}^{(0)}(n; \theta_{11}, g_1(1))./(\mathbf{z}_1(n) \otimes \mathbf{1}_M) = \left[\hat{g}_1(1)\mathbf{a}^T(\hat{\theta}_{11})\ \hat{g}_1(1)\mathbf{a}^T(\hat{\theta}_{11})\right]^T$ with $\mathbf{1}_M$ the $M \times 1$ all ones column vector. Thus, denoting

$$\hat{\mathbf{A}}_1^{(0)} = \left[\mathbf{q}_1^{(0)}(1) \cdots \mathbf{q}_1^{(0)}(J)\right], \tag{5.21}$$

$\theta_{11}$ and $g_1(1)$ can be estimated as follows

$$\hat{\theta}_{11}^{(0)} = \arg\max_{\theta} \left|\left|\left(\mathbf{1}_2 \otimes \mathbf{a}(\hat{\theta})\right)^H \hat{\mathbf{A}}_1^{(0)}\right|\right|_F^2, \tag{5.22}$$

and

$$\hat{g}_1^{(0)}(1) = \frac{\sum_{n=1}^{J}\left(\mathbf{1}_2 \otimes \mathbf{a}\left(\hat{\theta}_{11}^{(0)}\right)\right)^H \hat{\mathbf{A}}_1^{(0)}}{J \cdot \left(\left(\mathbf{1}_2 \otimes \mathbf{a}\left(\hat{\theta}_{11}^{(0)}\right)\right)^H \left(\mathbf{1}_2 \otimes \mathbf{a}\left(\hat{\theta}_{11}^{(0)}\right)\right)\right)}. \tag{5.23}$$

To describe the initialization of $\tau_{1l}, \theta_{1l}$, and $g_1(l)$ at the $l$th step, let $\mathbf{H}_{al}^{(0)} = [\hat{\mathbf{h}}_{11}^{(r,0)}\ \hat{\mathbf{h}}_{11}^{(l,0)} \cdots \hat{\mathbf{h}}_{1(l-1)}^{(r,0)}\ \hat{\mathbf{h}}_{1(l-1)}^{(l,0)}]$ contain all the estimated space-time signatures of the first $(l-1)$ paths with $\hat{\mathbf{h}}_{1l}^{(r,0)} = [\mathbf{u}_1^{(r)}(\hat{\tau}_{1l}^{(0)}) \otimes \mathbf{a}(\hat{\theta}_{1l}^{(0)})]$ and $\hat{\mathbf{h}}_{1l}^{(l,0)} = [\mathbf{u}_1^{(l)}(\hat{\tau}_{1l}^{(0)}) \otimes \mathbf{a}(\hat{\theta}_{1l}^{(0)})]$. After projecting the received data $\mathcal{Y}$ onto the null space spanned by $\mathbf{H}_{al}^{(0)}$, with the

projection matrix $\mathbf{P}^{\perp}_{H^{(0)}_{al}} = \mathbf{I} - \mathbf{H}^{(0)}_{al}(\mathbf{H}^{(0)H}_{al}\mathbf{H}^{(0)}_{al})^{-1}\mathbf{H}^{(0)H}_{al}$, $\tau_{1l}$ of the $l$th path conditioned on a fixed $\hat{\theta}_{1l}$ can be estimated by solving the following 1-D minimization problem

$$\begin{aligned}\hat{\tau}^{(0)}_{1l} &= \arg\min_{\tau_{1l}} \operatorname{tr}\left\{\hat{\mathbf{R}}^{(0)}_{rr,l}\left[\mathbf{\Pi}^{(0)}_1(\tau_{1l})\hat{\mathbf{\Gamma}}^{(0)}(g_1(l)) - \hat{\mathbf{\Upsilon}}^{(0)}(\tau_{1l}, g_1(l))\right]^H \hat{\mathbf{Q}}^{(0)-1}_l \right. \\ &\quad \left.\left[\mathbf{\Pi}^{(0)}_1(\tau_{1l})\hat{\mathbf{\Gamma}}^{(0)}(g_1(l)) - \hat{\mathbf{\Upsilon}}^{(0)}(\tau_{1l}, g_1(l))\right]\right\}, \end{aligned} \tag{5.24}$$

with

$$\mathbf{\Pi}^{(0)}_1(\tau_{1l}) = \mathbf{P}^{\perp}_{H^{(0)}_{al}}\mathbf{\Pi}_1(\tau_{1l}),$$

$$\hat{\mathbf{\Gamma}}^{(0)}(g_1(l)) = \left[\mathbf{\Pi}^{(0)H}_1(\tau_{1l})\mathbf{\Pi}^{(0)}_1(\tau_{1l})\right]^{-1}\mathbf{\Pi}^{(0)H}_1(\tau_{1l})\hat{\mathbf{\Upsilon}}^{(0)}(\tau_{11}, g_1(1)),$$

$$\hat{\mathbf{\Upsilon}}^{(0)}(\tau_{1l}, g_1(l)) = \hat{\mathbf{R}}^{(0)}_{yr,l}\hat{\mathbf{R}}^{(0)-1}_{rr,l},$$

and

$$\hat{\mathbf{Q}}^{(0)}_l = \hat{\mathbf{R}}^{(0)}_{rr,l} - \hat{\mathbf{R}}^{(0)}_{yr,l}\hat{\mathbf{R}}^{(0)-1}_{rr,l}\mathbf{R}^{(0)H}_{yr,l},$$

where $\hat{\mathbf{R}}^{(0)}_{yr,l} = \frac{1}{J}\sum_{n=1}^{J}\mathbf{P}^{\perp}_{H^{(0)}_{al}}\mathcal{Y}(n)\mathbf{r}^H(n;\hat{\theta}_{1l})$, $\hat{\mathbf{R}}^{(0)}_{rr,l} = \frac{1}{J}\sum_{n=1}^{J}\mathbf{r}(n;\hat{\theta}_{1l})\mathbf{r}^H(n;\hat{\theta}_{1l})$, and $\hat{\mathbf{R}}^{(0)}_{yy,l} = \frac{1}{J}\sum_{n=1}^{J}\mathbf{P}^{\perp}_{H^{(0)}_{al}}\mathcal{Y}(n)\mathcal{Y}^H(n)\mathbf{P}^{\perp H}_{H^{(0)}_{al}}$.

For a fixed $\hat{\tau}_{1l}$, the conditioned estimations of $\theta_{1l}$ and $g_{1l}$ are given by

$$\theta^{(0)}_{1l} = \arg\max_{\theta}\left|\left|\left(\mathbf{1}_2 \otimes \mathbf{a}(\theta)\right)^H \hat{\mathbf{A}}^{(0)}_l\right|\right|^2_F, \tag{5.25}$$

and

$$\hat{g}^{(0)}_1(l) = \frac{\sum_{n=1}^{J}\left(\mathbf{1}_2 \otimes \mathbf{a}\left(\hat{\theta}_{1l}\right)\right)^H \hat{\mathbf{A}}^{(0)}_l}{J\cdot\left(\left(\mathbf{1}_2 \otimes \mathbf{a}\left(\hat{\theta}_{1l}\right)\right)^H\left(\mathbf{1}_2 \otimes \mathbf{a}(\hat{\theta}_{1l})\right)\right)}, \tag{5.26}$$

where

$$\hat{\mathbf{A}}^{(0)}_l = \left[\mathbf{q}^{(0)}_l(1)\cdots\mathbf{q}^{(0)}_l(J)\right],$$

$$\hat{\mathbf{x}}^{(0)}(n;\theta_{1l}, g_1(l)) = (\mathbf{\Pi}^{(0)H}(\hat{\tau}_{11})\hat{\mathbf{Q}}^{(0)-1}_l\mathbf{\Pi}^{(0)}(\hat{\tau}_{11}))^{-1}\mathbf{\Pi}^{(0)H}(\hat{\tau}_{11})\hat{\mathbf{Q}}^{-1}_l\mathcal{Y}(n),$$

$$\mathbf{q}_l^{(0)}(n) = \hat{\mathbf{x}}^{(0)}(n;\theta_{1l}, g_1(l))./(\mathbf{z}_1(n) \otimes \mathbf{1}_M) = \left[\hat{g}_1(l)\mathbf{a}^T(\hat{\theta}_{1l})\ \hat{g}_1(l)\mathbf{a}^T(\hat{\theta}_{1l})\right]^T,$$

and

$$\mathbf{\Pi}^{(0)}(\hat{\tau}_{1l}) = \mathbf{P}^{\perp}_{H^{(0)}_{al}}\mathbf{\Pi}(\hat{\tau}_{1l}).$$

After obtaining the estimations of $\hat{\tau}_{1l}^{(0)}$, $\hat{\theta}_{1l}^{(0)}$ and $\hat{g}_1^{(0)}(l), l = 1, \cdots, L$, one need to improve the estimation accuracy as the estimation obtained at the initialization stage are biased ones. The refined path parameter estimations are obtained by iteration. Specifically, the estimations of $\tau_{1l}$, $\theta_{1l}$ and $g_1(l)$ at the $i+1$th iteration are obtained as follows:

Define

$$\mathbf{H}_{al}^{(i+1)} = [\hat{\mathbf{h}}_{11}^{(r,i+1)}\ \hat{\mathbf{h}}_{11}^{(l,i+1)} \cdots \hat{\mathbf{h}}_{1(l-1)}^{(r,i+1)}\ \hat{\mathbf{h}}_{1(l-1)}^{(l,i+1)}\ \hat{\mathbf{h}}_{1(l+1)}^{(r,i)}\ \hat{\mathbf{h}}_{1(l+1)}^{(l,i)} \cdots \hat{\mathbf{h}}_{1(L)}^{(r,i)}\ \hat{\mathbf{h}}_{1(L)}^{(l,i)}], \tag{5.27}$$

with $\hat{\mathbf{h}}_{1l}^{(r,i)} = \mathbf{u}_1^{(r)}(\hat{\tau}_{1l}^{(i)}) \otimes \mathbf{a}(\hat{\theta}_{1l}^{(i)})$ and $\hat{\mathbf{h}}_{1l}^{(l,i)} = \mathbf{u}_1^{(l)}(\hat{\tau}_{1l}^{(i)}) \otimes \mathbf{a}(\hat{\theta}_{1l}^{(i)})$. Projecting the received data $\mathcal{Y}$ onto the null space spanned by $\mathbf{H}_{a,l}^{(i+1)}$ with the projection matrix $\mathbf{P}^{\perp}_{H_{al}^{(i+1)}} = \mathbf{I} - \mathbf{H}_{al}^{(i+1)}(\mathbf{H}_{al}^{(i+1)H}\mathbf{H}_{al}^{(i+1)})^{-1}\mathbf{H}_{al}^{(i+1)H}$, the refined estimation $\hat{\tau}_{1l}^{(i+1)}$ is then given by

$$\begin{aligned}\hat{\tau}_{1l}^{(i+1)} = \arg\min_{\tau_{1l}} \mathrm{tr}\Bigg\{&\hat{\mathbf{R}}_{rr,l}^{(i+1)}\left[\mathbf{\Pi}_1^{(i+1)}(\tau_{1l})\hat{\mathbf{\Gamma}}^{(i+1)}(g_1(l)) - \hat{\mathbf{\Upsilon}}^{(i+1)}(\tau_{1l}, g_1(l))\right]^H \hat{\mathbf{Q}}_l^{(i+1)-1} \\ &\left[\mathbf{\Pi}_1^{(i+1)}(\tau_{1l})\hat{\mathbf{\Gamma}}^{(i+1)}(g_1(l)) - \hat{\mathbf{\Upsilon}}^{(i+1)}(\tau_{1l}, g_1(l))\right]\Bigg\},\end{aligned} \tag{5.28}$$

with

$$\mathbf{\Pi}_1^{(i+1)}(\tau_{1l}) = \mathbf{P}^{\perp}_{H_{al}^{(i+1)}}\mathbf{\Pi}_1(\tau_{1l}),$$

$$\hat{\mathbf{\Gamma}}(g_1(l)) = \left[\mathbf{\Pi}_1^{(i+1)H}(\tau_{1l})\mathbf{\Pi}_1^{(i+1)}(\tau_{1l})\right]^{-1}\mathbf{\Pi}_1^{(i+1)H}(\tau_{1l})\hat{\mathbf{\Upsilon}}^{(i+1)}(\tau_{11}, g_1(1)),$$

$$\hat{\mathbf{\Upsilon}}^{(i+1)}(\tau_{1l}, g_1(l)) = \mathbf{R}_{yr,l}^{(i+1)}\mathbf{R}_{rr,l}^{(i+1)-1},$$

and

$$\hat{\mathbf{Q}}_l^{(i+1)} = \mathbf{R}_{rr,l}^{(i+1)} - \mathbf{R}_{yr,l}^{(i+1)}\mathbf{R}_{rr,l}^{(i+1)-1}\mathbf{R}_{yr,l}^{(i+1)H},$$

where $\hat{\mathbf{R}}_{yr,l}^{(i+1)} = \frac{1}{J}\sum_{n=1}^{J} \mathbf{P}^{\perp}_{H_{al}^{(i+1)}} \mathcal{Y}(n)\mathbf{r}^H(n;\hat{\theta}_{1l})$, and $\hat{\mathbf{R}}_{rr,l}^{(i+1)} = \frac{1}{J}\sum_{n=1}^{J} \mathbf{r}(n;\hat{\theta}_{1l})\mathbf{r}^H(n;\hat{\theta}_{1l})$, and $\hat{\mathbf{R}}_{yy,l}^{(i+1)} = \frac{1}{J}\sum_{n=1}^{J} \mathbf{P}^{\perp}_{H_{al}^{(i+1)}} \mathcal{Y}(n)\mathcal{Y}^H(n)\mathbf{P}^{\perp H}_{H_{al}^{(i+1)}}$.

For a fixed $\hat{\tau}_{1l}$, the conditioned estimation of $\theta_{1l}$ is given by

$$\theta_{1l}^{(i+1)} = \arg\max_{\theta} \left|\left|(\mathbf{1}_2 \otimes \mathbf{a}(\theta))^H \hat{\mathbf{A}}_l^{(i+1)}\right|\right|_F^2, \tag{5.29}$$

where

$$\hat{\mathbf{A}}_l^{(i+1)} = \left[\mathbf{q}_l^{(i+1)}(1) \cdots \mathbf{q}_l^{(i+1)}(J)\right],$$

$$\hat{\mathbf{x}}^{(i+1)}(n;\theta_{1l}, g_1(1)) = \left(\mathbf{\Pi}^{(i+1)H}(\hat{\tau}_{11})\hat{\mathbf{Q}}_l^{(i+1)-1}\mathbf{\Pi}^{(i+1)}(\hat{\tau}_{11})\right)^{-1} \mathbf{\Pi}^{(i+1)H}(\hat{\tau}_{11})\hat{\mathbf{Q}}_l^{(i+1)-1}\mathcal{Y}(n),$$

$$\mathbf{q}_l^{(i+1)}(n) = \hat{\mathbf{x}}^{(i+1)}(n;\theta_{1l}, g_1(l))./(\mathbf{z}_1(n) \otimes \mathbf{1}_M) = \left[\hat{g}_1(l)\mathbf{a}^T(\hat{\theta}_{1l}) \;\; \hat{g}_1(l)\mathbf{a}^T(\hat{\theta}_{1l})\right]^T,$$

$$\mathbf{\Pi}^{(i+1)}(\hat{\tau}_{1l})) = \mathbf{P}^{\perp}_{H_{al}^{(i+1)}}\mathbf{\Pi}(\hat{\tau}_{1l})),$$

and

$$\hat{g}_1^{(i+1)}(l) = \frac{\sum_{n=1}^{J}\left(\mathbf{1}_2 \otimes \mathbf{a}\left(\hat{\theta}_{1l}\right)\right)^H \hat{\mathbf{A}}_l^{(i+1)}}{J \cdot \left(\left(\mathbf{1}_2 \otimes \mathbf{a}\left(\hat{\theta}_{1l}\right)\right)^H \left(\mathbf{1}_2 \otimes \mathbf{a}\left(\hat{\theta}_{1l}\right)\right)\right)}. \tag{5.30}$$

The algorithm continues to perform the iteration until no improvement in the likelihood function is attained. The number of iterations in most scenarios is between $5 - 10$. The algorithm can be easily extended to estimate all $K$ users' channel parameters.

## 5.4 A Fast Estimation Scheme

Another way to reduce the computational complexity of the multi-dimensional numerical search associated with the ML estimators is a fast iterative algorithm. The fast algorithm approximates the ML estimator and is computationally efficient. The fast algorithm starts by initializing the estimations for the strongest path and then proceeds to other paths. In figure 5.3, the mesh and contour plots of the

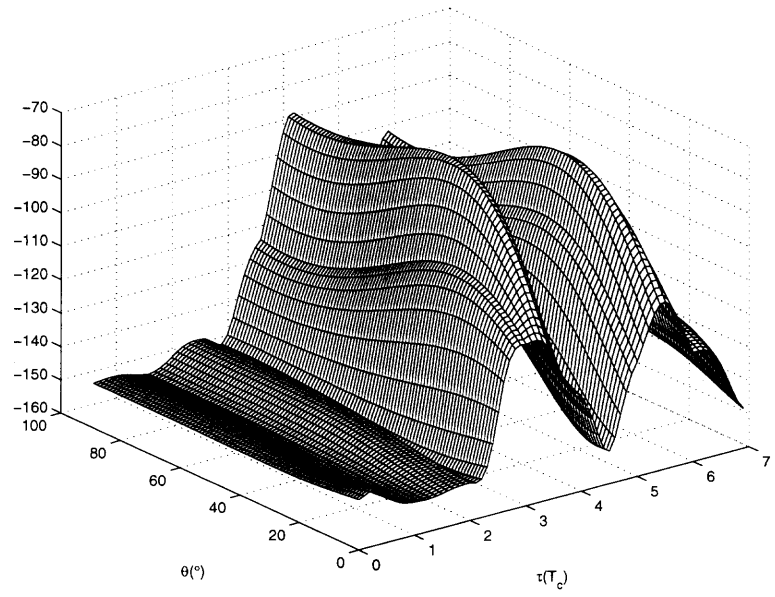


(a). $J(\tau, \theta)$

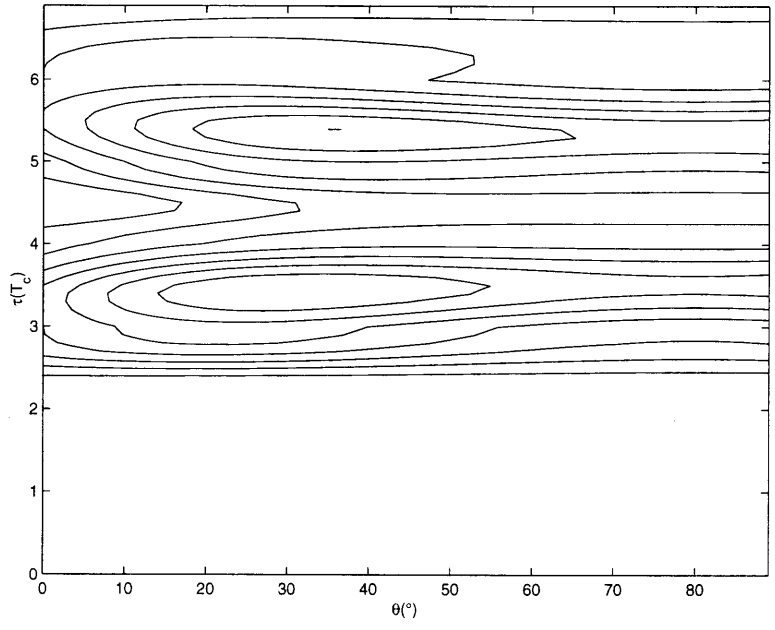


(b). $J(\tau, \theta)$

**Figure 5.3** Mesh and contour plots of the objective function $J(\tau, \theta)$ in 2-D parameter space. with $SNR_1 = 10dB$. $K = 3$, $N = 7$, $M = 2$, $\boldsymbol{\tau}_1 = [3.4 \quad 5.4]T_c$ and $\boldsymbol{\theta}_1 = [35° \quad 55°]$.

objective function in (5.13) are shown in a 2-D parameter space. The ridge structure of the objective function is revealed. As being pointed out in our previous work [88, 53], there exists an efficient way of estimating $\tau_{11}$ and $\theta_{11}$. The parameters for the strongest path of the desired user can be obtained as follows. First fix the value of $\theta_{11}$ to any value, say $\theta_{11} = 0°$, search only along the axis of $\tau$ to get $\hat{\tau}_{11}$ as in [53]. Once the $\hat{\tau}_{11}$ is obtained, come back to refine the value of $\theta_{11}$. That is

$$\begin{aligned} \hat{\tau}_{11} &= \arg \max_{\tau, \theta_{11}=0} J(\boldsymbol{\tau}_1, \boldsymbol{\theta}_1) \\ \hat{\theta}_{11} &= \arg \max_{\theta_{11}, \tau_{11}=\hat{\tau}_{11}} J(\boldsymbol{\tau}_1, \boldsymbol{\theta}_1) \end{aligned}$$

The second strongest path's parameters are then estimated in a similar way after removing the strongest path's effect by projecting the received data $\mathcal{Y}$ to the null space spanned by $\mathbf{H}_1(\hat{\tau}_{11}, \hat{\theta}_{11})$. Repeating this process until the parameters for all $L$ paths are obtained.

The refined parameter estimations for the $l$th path are then obtained via iteration. Specifically, fix the parameters of $L-1$ paths as the previous estimates and search for the more accurate estimates of $\tau_{1l}$ and $\theta_{1l}$ using the steps described above. The iteration is continued until there is no more improvement in the objection function in (5.13). The number of iterations in most scenarios is between $5-10$.

## 5.5 Simulation Results

In this section, the simulation results are presented in order to demonstrate the performance of the proposed algorithm. For comparison, the CRB for the joint estimation problem, which is derived in the Appendix A, is also presented. Assume that the system has $K = 3$ users, each user has $L = 2$ multipaths arriving at a half-wavelength uniformly spaced linear array with $M = 4$, so that $\mathbf{a}_{kl} = [1\, e^{-j\pi \sin(\theta_{kl})} \cdots e^{-j\pi(M-1)\sin(\theta_{kl})}]^T$ (i.e., having beam-width of 36°). Gold sequence of length $N = 7$ is used. The multipath fading coefficients for the desired

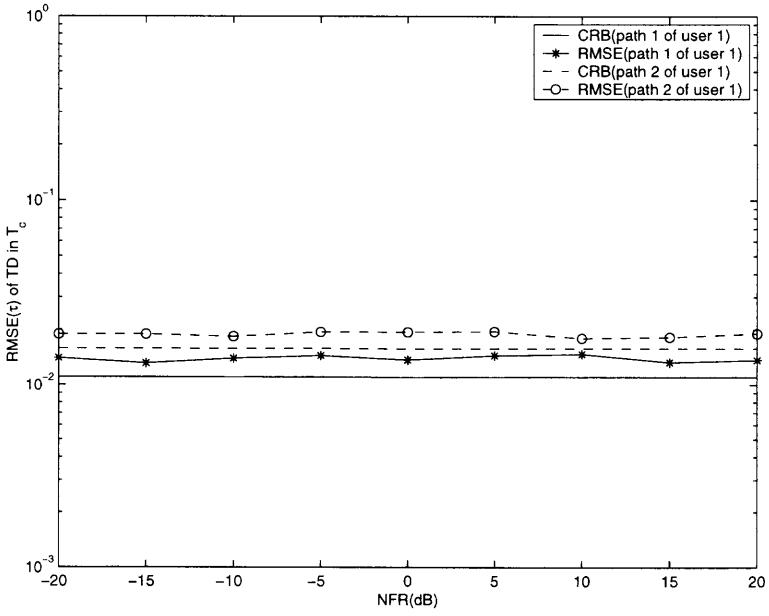


**Figure 5.4** RMSE of time delays of user 1 as a function of NFR, when $SNR_1 = 10dB$. Parameter used are: $K = 3$, $N = 7$, $M = 4$, $\boldsymbol{\tau}_1 = [3.4 \quad 5.2]T_c$ and $\boldsymbol{\theta}_1 = [34° \quad 16°]$.

user are normalized so that $|g_1(1)| > |g_1(2)|$. The observation time is fixed and $J = 100$ bits are used for channel estimation, and the root mean square error (RMSE) is obtained from 500 Monte Carlo runs.

The first case, set $\boldsymbol{\tau}_1 = [3.4 \ 5.2]T_c$ and $\boldsymbol{\theta}_1 = [34° \ 16°]$. Figures 5.4 and 5.5 present the time delay and DOA estimation accuracy of user 1 as a function of NFR. The SNR of the desired user is fixed as $SNR_1 = 10$dB. Figures 5.6 and 5.7 demonstrate the dependence of the time delay and DOA estimation accuracy on $SNR_1$ with $NFR = 0dB$. Clearly, the proposed algorithm approach to the CRB after convergence. The estimator can correctly separate the DOA of the two paths of the desired user even though the DOA difference of these two paths is much less than the beam-width of the receiving antenna array.

The second case, set $\boldsymbol{\tau}_1 = [3.4 \ 5.2]T_c$ and $\boldsymbol{\theta}_1 = [-34° \ -34°]$. Figure 5.8 demonstrates the dependence of the time delay estimation accuracy of user 1 on

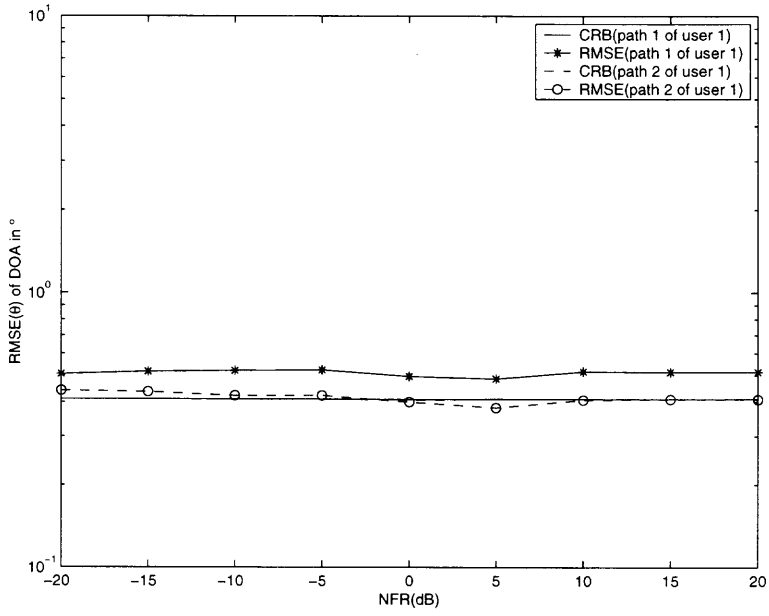


**Figure 5.5** RMSE of DOA's of user 1 as a function of NFR, with $SNR_1 = 10dB$. Parameter used are: $K = 3$, $N = 7$, $M = 4$, $\boldsymbol{\tau}_1 = [3.4 \;\; 5.2]T_c$ and $\boldsymbol{\theta}_1 = [34° \;\; 16°]$.

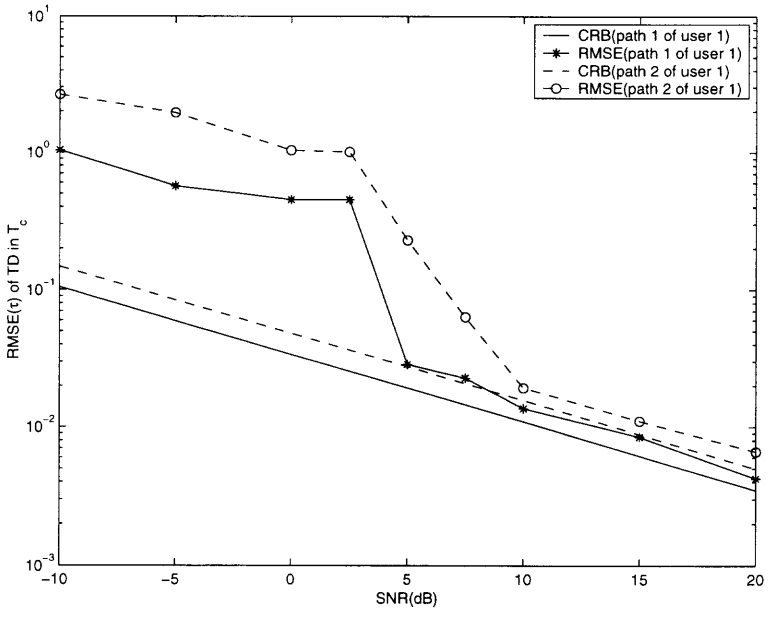


**Figure 5.6** RMSE of time delays of user 1 as a function of $SNR_1$, with $NFR = 0$dB. Parameter used are: $K = 3$, $N = 7$, $M = 4$, $\boldsymbol{\tau}_1 = [3.4 \;\; 5.2]T_c$ and $\boldsymbol{\theta}_1 = [34° \;\; 16°]$.

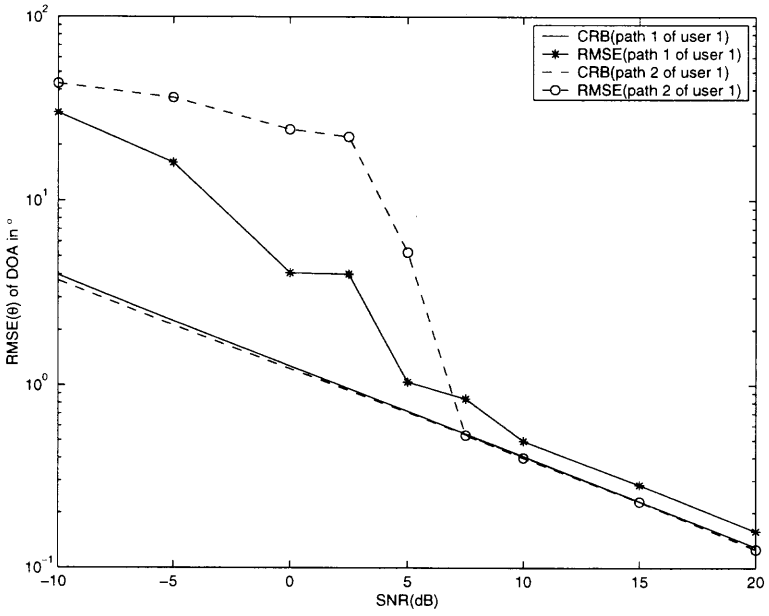


**Figure 5.7** RMSE of DOA's of user 1 as a function of $SNR_1$, with $NFR = 0$dB. Parameter used are: $K = 3$, $N = 7$, $M = 4$, $\boldsymbol{\tau}_1 = [3.4\ \ 5.2]T_c$ and $\boldsymbol{\theta}_1 = [34°\ 16°]$.

$SNR_1$ with $NFR = 0dB$. Although the two paths are not separable in space domain, the proposed algorithm can obtain the correct time delay estimations.

The third case, set $\boldsymbol{\tau}_1 = [3.4\ 3.4]T_c$ and $\boldsymbol{\theta}_1 = [-34°\ 50°]$. Figure 5.9 demonstrates the dependence of the DOA estimation accuracy of user 1 on $SNR_1$ with $NFR = 0dB$. Although the two paths are not separable in time domain, the proposed algorithm can obtain the correct DOA estimations.

Figure 5.10 demonstrates the average BER performance vs. SNR for each user ($NFR = 0$dB) for the single user bound, MMSE receiver when channel parameters are known and estimated. It is shown that the difference between the two MMSE receivers is less than 3dB. Figures 5.11 and 5.12 present the time delay and DOA estimation accuracy as a function of NFR for fast algorithm. The path is set to have equal power. The SNR of the desired user is fixed as $SNR_1 = 10$dB. Figures 5.13 and 5.14 demonstrate the dependence of the time delay and DOA estimation accuracy

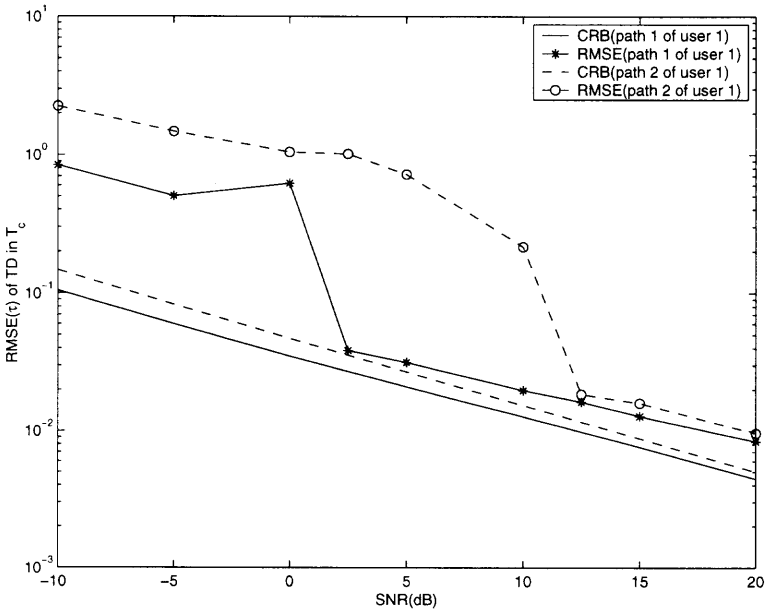


**Figure 5.8** RMSE of time delays of user 1 as a function of $SNR_1$, with $NFR$=0dB. Parameter used are: $K=3$, $N=7$, $M=4$, $\boldsymbol{\tau}_1=[3.4\ 5.2]T_c$ and $\boldsymbol{\theta}_1=[-34^\circ\ -34^\circ]$. *Note: two paths are non-separable in space, and separable in time.*

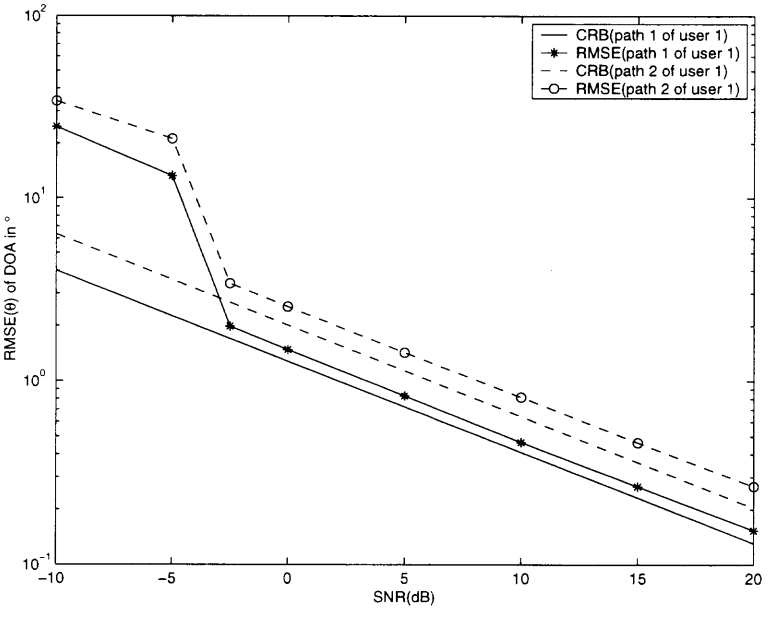


**Figure 5.9** RMSE of DOA's of user 1 as a function of $SNR_1$, with $NFR=0$dB. Parameter used are: $K=3$, $N=7$, $M=4$, $\boldsymbol{\tau}_1=[3.4\ 3.4]T_c$ and $\boldsymbol{\theta}_1=[-34^\circ\ 50^\circ]$.*Note: two paths are non-separable in time, and separable in space.*

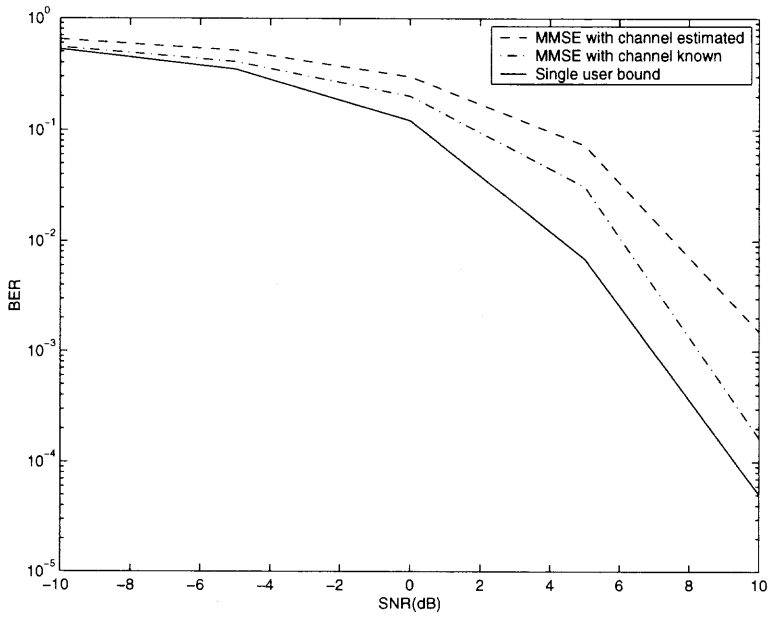


**Figure 5.10** Average BER performance vs. SNR for each user ($NFR = 0$dB). In this example, we treat 3 users as 3 independent parallel data streams coming from a transmit array, arriving at receiver array with different spatial-temporal multipath channels. Parameter used are: $K = 3$, $N = 7$, $M = 2$, $\boldsymbol{\tau}_1 = [3.4\ 5.2]T_c$, $\boldsymbol{\theta}_1 = [34^\circ\ 16^\circ]$; $\boldsymbol{\tau}_2 = [2.2\ 3.3]T_c$, $\boldsymbol{\theta}_2 = [2^\circ\ 42^\circ]$; and $\boldsymbol{\tau}_3 = [1.3\ 2.4]T_c$, $\boldsymbol{\theta}_3 = [-33^\circ\ -13^\circ]$.

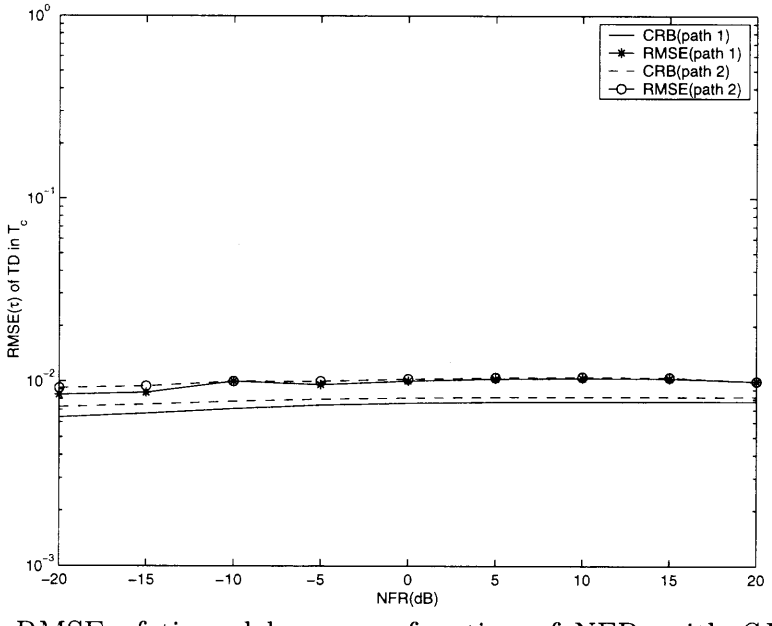


**Figure 5.11** RMSE of time delays as a function of NFR, with $SNR_1 = 10dB$. $K = 3$, $N = 7$, $M = 2$, $\boldsymbol{\tau}_1 = [3.4\ \ 5.2]T_c$ and $\boldsymbol{\theta}_1 = [16^\circ\ \ 34^\circ]$.

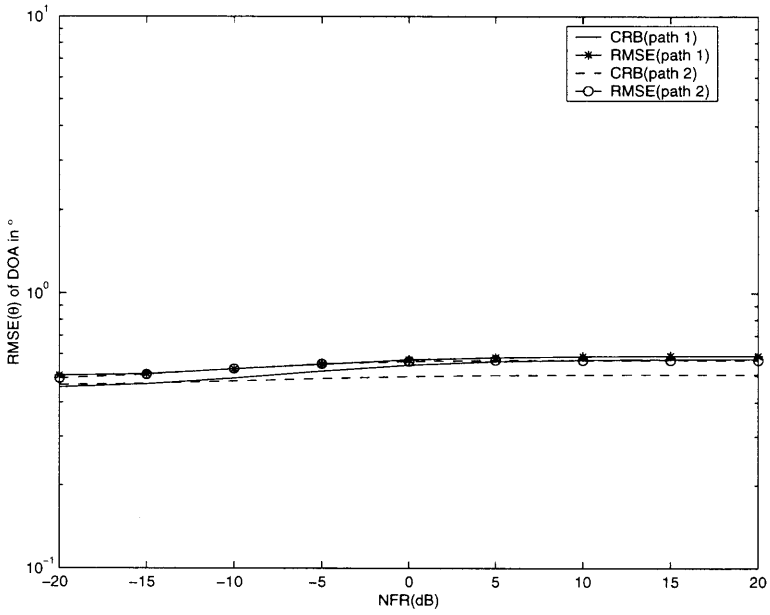


**Figure 5.12** RMSE of DOA's as a function of NFR, with $SNR_1 = 10dB$. $K = 3$, $N = 7$, $M = 2$, $\boldsymbol{\tau}_1 = [3.4 \;\; 5.2]T_c$ and $\boldsymbol{\theta}_1 = [16° \;\; 34°]$.

of the fast algorithm on the $SNR_1$. Clearly, RMSEs of the proposed fast estimators approach to their CRBs after convergence.

## 5.6 Conclusions

A joint time delays and DOA's ML estimator is presented for DS-CDMA systems over multipath Rayleigh fading channels. An iterative joint time delays and DOA's estimation scheme is developed to reduce the computational complexity associated with the proposed joint ML estimator. The proposed iterative algorithm, that transforms the multidimensional maximum likelihood estimation into two sets of simple 1-D maximization problems greatly reduces the computational expense of the multi-dimensional numerical search involved with the joint ML estimator. The resulted time delay and DOA accuracies can approach the corresponding CRBs after several iterations. For both time delay and DOA estimation, they are near-

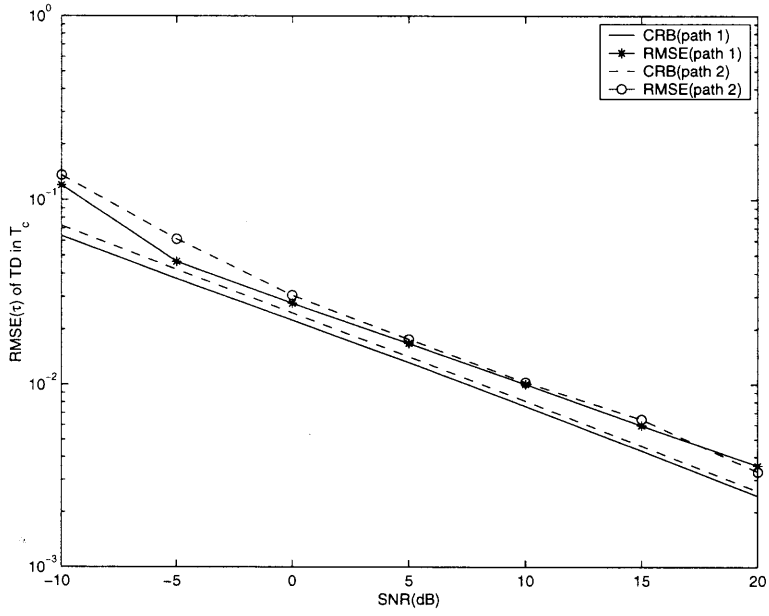


**Figure 5.13** RMSE of time delays as a function of $SNR_1$, with $NFR = 0$dB. $K = 3$, $N = 7$, $M = 2$, $\boldsymbol{\tau}_1 = [3.4 \;\; 5.2]T_c$ and $\boldsymbol{\theta}_1 = [16^\circ \;\; 34^\circ]$.

far resistant and there are no significant performance losses in comparison with the CRBs at reasonable SNRs.

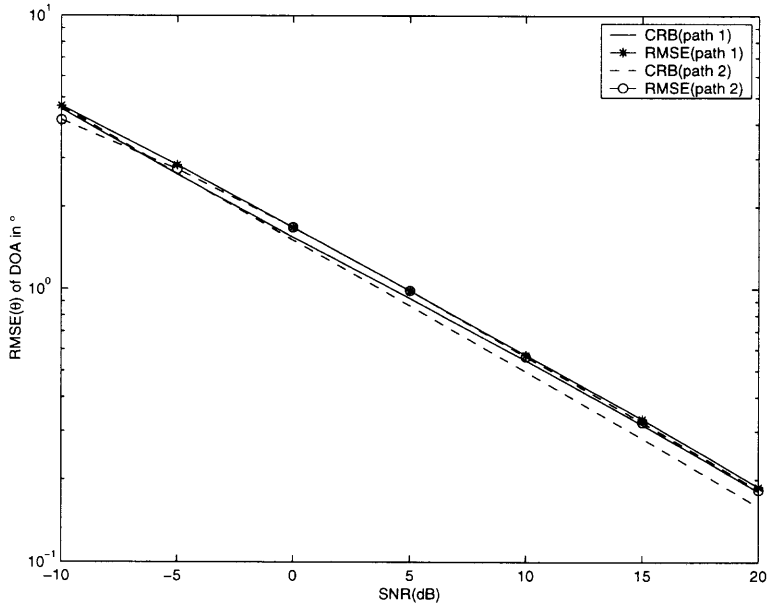


**Figure 5.14** RMSE of DOA's as a function of $SNR_1$, with $NFR = 0$dB. $K = 3$, $N = 7$, $M = 2$, $\boldsymbol{\tau}_1 = [3.4 \;\; 5.2]T_c$ and $\boldsymbol{\theta}_1 = [16^\circ \;\; 34^\circ]$.

# CHAPTER 6

# CONCLUSIONS

## 6.1 Bayesian Based Linear and Non-Linear Detectors for DS-CDMA Systems

The MUD problem is solved using Bayesian approach. The proposed detector is developed by minimizing the Bayes risk. When the cost function is chosen as the quadratic function, the optimal Bayes estimator results in the MMSE estimator. Due to the non-Gaussian nature of the problem, the MMSE estimator is quite non-linear. The multi-dimensional integrations need to be evaluated in order to get the exact form of MMSE estimator. To reduce the computational demanding inherent in the MMSE solution, LMMSE is derived under the linear constraint. When the cost function is hit-or-miss function, the solution is MAP estimator. To get the exact MAP estimate, non-linear multi-dimensional integration is also involved. The marginal MAP estimate gives the simplified solution. However, compared to the optimal detector, there are still performance losses coming along with the LMMSE and marginal MAP especially when the MAI is strong.

In order to bridge the performance gap between the LMMSE and the optimal detector, one step iterative optimization based on LMMSE receiver is proposed. The LMMSE estimator is first used as the initial starting point, then evaluate the objective function $J(\mathbf{b};\ \mathbf{A}, \mathbf{P})$ at the initial point as well as an alternative point. The estimated symbol of $b_k$ is the one that is corresponding to a larger value of objective function. The reason for the success of this approach is that: when the MAI is weaker compared to the desired user, the LMMSE detector itself provides detection performance comparable to the optimum detector, therefore, with high probability the one-step up-hill iteration will not change the initial estimate; when the MAI is stronger than the desired user, the *desired user*'s LMMSE estimate is less reliable than the interfering users'. Alternating the sign of the *desired user*'s information

allows us to seek margin for potential performance improvement by removing the effect of the MAI.

The multi-stage MAP solution is presented to bridge the performance gap between the marginal MAP and the optimal detector. The marginal Bayesian estimate is first calculated. In the second stage, the interferences from other users are removed by taking the noise correlation structure into consideration, and the refined information bit estimate based on the tentative estimate obtained by the marginal MAP is obtained. The performance of the presented non-linear multi-stage and iterative optimization approaches are close to that of the optimum detector after one iteration.

## 6.2 Space-Time Receivers for DS-CDMA systems

A S-T receiver operates simultaneously on all the antennas, processing signal samples in both space and time dimensions. The space domain enables interference cancellation in a way that is not possible with single-antenna receivers. The optimal S-T receiver that operates in the $M \times N$ S-T product space is very computational demanding. The suboptimal realizations include the decoupled and joint S-T RAKE receivers. However, conventional S-T RAKE receivers did not fully utilize the code information for MAI suppression. In order to better utilize the code signature, the MVDR filter instead of MF is chosen at the output of each receiving antenna sensor. The MVDR filter keeps the signal corresponding to each path of the desired user without distortion and eliminates the MAI and noise by minimizing the output power at each antenna sensor. For decoupled S-T receiver, the MVDR filter is followed by $L$ separate $M$-dimensional space beam-formers that corresponding to $L$ paths of the desired user. The output of the space beam-former is then combined before making the decision. For joint S-T receiver, the MVDR filter is followed by an $LM$-dimensional space beam-former to get the decision statistics. By combining the

MUD technique and the S-T processing, the proposed S-T receivers overcome the near-far problem existing in the conventional S-T RAKE receivers. The proposed S-T receivers significantly outperform the conventional ones without significant increase in complexity.

The phase ambiguity problem in channel estimation is solved in two ways. First, with the differential code, one can detect the information of the desired user blindly using the non-coherent receiver without the phase information. However, there exists $3dB$ SINR gap between it and the coherent receiver using the phase information. Secondly, with the training sequence, one can estimate the channel phase information and detect the information of the desired user coherently and the output SINR is increased around $1.5dB$. Simulation results show that both solutions work well even with high NFR and obviously outperform the conventional S-T RAKE receivers when NFR is high.

## 6.3 Differential Detection Scheme for DS-CDMA Systems with Transmit Diversity

TD is a technique where information is transmitted from multiple antenna in order to mitigate the effects of signal fading. Multiple transmit antennas at the base station will increase the downlink capacity with only minor increase in terminal implementation. Two TD schemes, OTD and STTD, are investigated for DS-CDMA system. According to OTD technique, each user's data stream is first split into two independent data streams, namely its odd and even substreams, respectively.

In OTD, the first antenna transmits the spread odd substream of the user's data during odd symbol periods and repeats the transmission of the spread odd substream of the user's data during even symbol periods. The second antenna transmits the spread even substream of the user's data during odd symbol periods and transmits the the spread negative even substream of the user's data during even symbol periods.

In STTD, the first antenna transmits the spread odd substream of the user's data $b_{k1}(n)$ during odd symbol periods and the spread even substream of the user's data $-b_{k2}^{*}(n)$ during even symbol periods. The second antenna transmits the spread even substream of the user's data $b_{k2}(n)$ during odd symbol periods and transmits the the spread odd substream of the user's data $b_{k1}^{*}(n)$ during even symbol periods.

To realize the blind detection, the differential encoding and decoding technique combining with the MVDR receiver are implemented when neither the transmitter nor the receiver has access to channel state information. Both transmission schemes provide full spatial diversity and require no channel state side information at the receiver. The performance of the proposed OTD+MVDR and STTD+MVDR receivers are much better than those conventionally used OTD+MF and STTD+MF receivers. The STTD+MVDR has a much better performance than OTD+MVDR at the price of the higher complexity receiver.

## 6.4 Joint Temporal and Spatial Channel Parameter Estimation for DS-CDMA Systems

In wireless communication systems, the multipath channel is characterized by both the time delays and the DOA's of different propagation paths. To estimate the time delays and the DOA's of a user's multipath signals arriving at a receiver antenna array, an approximate ML method for joint estimation of time delays and DOA's for the DS-CDMA systems over the multipath Rayleigh fading channels is developed. By modeling the known training sequence of the desired user as the desired signal and the MAI-plus-AWGN as unknown colored Gaussian noise uncorrelated with the desired signal, the joint ML time delays and the DOA's estimator is developed. Getting the ML estimations of time delays and DOAs from equation (5.13) involves a $2L$ multi-dimensional search over the parameter space spanned $[\boldsymbol{\tau}_1, \boldsymbol{\theta}_1]$. Hence, it is computationally prohibitive even for moderate values of $L$.

In order to reduce the computational complexity, an iterative estimation scheme that approximates the ML estimator is presented. The algorithm transforms the multi-dimensional maximization problem into two simple 1-D maximization problems based on the alternating projection concept. Instead of directly solving the multi-dimensional maximization problem in equation (5.13), the maximization problem is solved iteratively based on the alternating projection concept. The proposed iterative estimation scheme iterates between the DOA and the time delay parameter sets, and exploits the symmetry between them in the likelihood function. Each iteration involves two steps. First, the unstructured matrix $\boldsymbol{\Upsilon}(\tau_{1l}, g_1(l))$ or vector $\mathbf{x}(n; \theta_{1l}, g_1(l))$ that contains the information of $\tau_{1l}$ or $\theta_{1l}$ is estimated using ML estimator. Then, the parameter itself ,$\tau_{1l}$ or $\theta_{1l}$, is estimated using the structure of the estimated matrix $\hat{\boldsymbol{\Upsilon}}(\tau_{1l}, g_1(l))$ or the estimated vector $\hat{\mathbf{x}}(n; \theta_{1l}, g_1(l))$. After having the estimations of $\hat{\tau}_{1l}^{(0)}$,$\hat{\theta}_{1l}^{(0)}$ and $\hat{g}_1^{(0)}(l), l = 1, \cdots, L$, the refined estimation are obtained iteratively. Analytical and simulation results illustrate the performance of the proposed estimators in comparison with the CRBs. It is shown that the proposed algorithm is near-far resistant for both time delay and DOA estimation and little performance loss is observed in comparison with the CRBs at reasonable SNRs.

# APPENDIX A

## CRB DERIVATION FOR JOINT SPACE-TIME CHANNEL PARAMETER ESTIMATOR

The CRBs is derived for the joint estimation problem for the time delays, the DOA's, the amplitudes, and the phases of the desired user when the unknown covariance $\mathbf{Q}$ models both the thermal noise and all the MAI. Specifically, the elements of the Fisher information matrix (FIM) is derived, the diagonal elements of whose inverse matrix give the CRB.

Let $\boldsymbol{\xi} = [\boldsymbol{\alpha}^T \boldsymbol{\phi}^T \boldsymbol{\tau}^T \boldsymbol{\theta}^T \sigma^2]^T$, with $g_k(l) = \alpha_{kl} e^{j\phi_{kl}}$, $\boldsymbol{\alpha} = [\alpha_{11} \cdots \alpha_{1L} \cdots \alpha_{KL}]^T$, $\boldsymbol{\phi} = [\phi_{11} \cdots \phi_{1L} \cdots \phi_{KL}]^T$, $\boldsymbol{\tau} = [\tau_{11} \cdots \tau_{1L} \cdots \tau_{KL}]^T$, and $\boldsymbol{\theta} = [\theta_{11} \cdots \theta_{1L} \cdots \theta_{KL}]^T$.

For the likelihood function given by equation (5.6), the elements of the FIM $FIM_{ij}$ is given by

$$FIM_{ij} = M\, tr\left(\mathbf{Q}^{-1}\frac{\partial \mathbf{Q}}{\partial \boldsymbol{\xi}_i}\mathbf{Q}^{-1}\frac{\partial \mathbf{Q}}{\partial \boldsymbol{\xi}_j}\right) + 2\Re\left(\sum_{n=1}^{M}\frac{\partial \boldsymbol{\mu}(n)}{\partial \boldsymbol{\xi}_i}\mathbf{Q}^{-1}\frac{\partial \boldsymbol{\mu}(n)}{\partial \boldsymbol{\xi}_i}\right). \tag{A.1}$$

where $\Re(\cdot)$ stands for the real part.

Define $\mathbf{c}_k^{(r)1}(\tau_{kl}) = \frac{\partial \mathbf{u}_{kl}^{(r)}}{\partial \tau_{kl}} = \mathbf{c}_k^{(r)}(\nu_{kl}+1) - \mathbf{c}_k^{(r)}(\nu_{kl})$, $\mathbf{c}_k^{(l)1}(\tau_{kl}) = \frac{\partial \mathbf{u}_{kl}^{(l)}}{\partial \tau_{kl}} = \mathbf{c}_k^{(l)}(\nu_{kl}+1) - \mathbf{c}_k^{(l)}(\nu_{kl})$, and $\mathbf{a}^1(\theta_{kl}) = \frac{\partial \mathbf{a}(\theta_{kl})}{\partial \theta_{kl}}$, it is easily to show that for $l = 1, \cdots, L$

$$\frac{\partial \boldsymbol{\mu}(n)}{\partial \alpha_{1l}} = e^{j\,\phi_{1l}}\left(\mathbf{h}_{1l}^{(r)} b_1(n-1) + \mathbf{h}_{1l}^{(l)} b_1(n)\right), \tag{A.2}$$

$$\frac{\partial \boldsymbol{\mu}(n)}{\partial \phi_{1l}} = j\,\alpha_{1l}\, e^{j\,\phi_{1l}}\left(\mathbf{h}_{1l}^{(r)} b_1(n-1) + \mathbf{h}_{1l}^{(l)} b_1(n)\right), \tag{A.3}$$

$$\frac{\partial \boldsymbol{\mu}(n)}{\partial \tau_{1l}} = \alpha_{1l}\, e^{j\,\phi_{1l}}\left[\left(\mathbf{c}_1^{(r)1}(\tau_{1l}) \otimes \mathbf{a}(\theta_{1l})\right) b_1(n-1) + \left(\mathbf{c}_1^{(l)1}(\tau_{1l}) \otimes \mathbf{a}(\theta_{1l})\right) b_1(n)\right], \tag{A.4}$$

and

$$\frac{\partial \boldsymbol{\mu}(n)}{\partial \theta_{1l}} = \alpha_{1l}\, e^{j\,\phi_{1l}}\left[\left(\mathbf{u}_{1l}^{(r)} \otimes \mathbf{a}^1(\theta_{1l})\right) b_1(n-1) + \left(\mathbf{h}_{1l}^{(l)} \otimes \mathbf{a}^1(\theta_{1l})\right) b_1(n)\right]. \tag{A.5}$$

For $k = 2, \cdots, K$, $l = 1, \cdots, L$, $\frac{\partial \boldsymbol{\mu}(n)}{\partial \alpha_{kl}} = \mathbf{0}$, $\frac{\partial \boldsymbol{\mu}(n)}{\partial \phi_{kl}} = \mathbf{0}$, $\frac{\partial \boldsymbol{\mu}(n)}{\partial \tau_{kl}} = \mathbf{0}$, and $\frac{\partial \boldsymbol{\mu}(n)}{\partial \theta_{kl}} = \mathbf{0}$. Also $\frac{\partial \boldsymbol{\mu}(n)}{\partial \sigma^2} = \mathbf{0}$.

As

$$\begin{aligned}\mathbf{Q} &= \sum_{k=2}^{K} \mathbf{H}_k(\boldsymbol{\tau}_k, \boldsymbol{\theta}_k)\, \mathbf{G}_k(\mathbf{g}_k)\, \mathbf{G}_k^H(\mathbf{g}_k) \mathbf{H}_k^H(\boldsymbol{\tau}_k, \boldsymbol{\theta}_k) + 2\,\sigma^2\,\mathbf{I} \\ &= \sum_{k=2}^{K} \sum_{l_1=1}^{L} \sum_{l_2=1}^{L} \alpha_{kl_1} \alpha_{kl_2} e^{j(\phi_{kl_1} - \phi_{kl_2})} \left[ \mathbf{h}_{kl_1}^{(r)}(\tau_{kl_1}, \theta_{kl_1}) \mathbf{h}_{kl_2}^{(r)H}(\tau_{kl_2}, \theta_{kl_2}) \right. \\ &\quad \left. + \mathbf{h}_{kl_1}^{(l)}(\tau_{kl_1}, \theta_{kl_1}) \mathbf{h}_{kl_1}^{(l)H}(\tau_{kl_2}, \theta_{kl_2}) \right] + 2\,\sigma^2\,\mathbf{I}, \end{aligned} \tag{A.6}$$

it can be easily shown that for $l = 1, \cdots, L$, $\frac{\partial \mathbf{Q}}{\partial \alpha_{1l}} = \mathbf{0}$, $\frac{\partial \mathbf{Q}}{\partial \phi_{1l}} = \mathbf{0}$, $\frac{\partial \boldsymbol{\mu}(n)}{\partial \tau_{1l}} = \mathbf{0}$ and $\frac{\partial \boldsymbol{\mu}(n)}{\partial \theta_{1l}} = \mathbf{0}$. And for $k = 2, \cdots, K$, $l = 1, \cdots, L$,

$$\frac{\partial \mathbf{Q}}{\partial \alpha_{kl}} = \sum_{l_1=1}^{L} \Re \left\{ \alpha_{kl_1} e^{j(\phi_{kl} - \phi_{kl_1})} \left[ \mathbf{h}_{kl}^{(r)} \mathbf{h}_{kl_1}^{(r)H} + \mathbf{h}_{kl}^{(l)} \mathbf{h}_{kl_1}^{(l)H} \right] \right\}, \tag{A.7}$$

$$\frac{\partial \mathbf{Q}}{\partial \phi_{kl}} = -2 \sum_{l_1=1, l_1 \neq l}^{L} \Im \left\{ \alpha_{kl} \alpha_{kl_1} e^{j(\phi_{kl} - \phi_{kl_1})} \left[ \mathbf{h}_{kl}^{(r)} \mathbf{h}_{kl_1}^{(r)H} + \mathbf{h}_{kl}^{(l)} \mathbf{h}_{kl_1}^{(l)H} \right] \right\}, \tag{A.8}$$

$$\begin{aligned}\frac{\partial \mathbf{Q}}{\partial \tau_{kl}} &= 2 \sum_{l_1=1}^{L} \Re \left\{ \alpha_{kl} \alpha_{kl_1} e^{j(\phi_{kl} - \phi_{kl_1})} \left[ \mathbf{c}_k^{(r)1}(\tau_{kl}) \otimes \mathbf{h}_{kl_1}^{(r)H} \right. \right. \\ &\quad \left. \left. + \mathbf{c}_k^{(l)1}(\tau_{kl}) \otimes \mathbf{h}_{kl_1}^{(l)H} \right] \right\}, \end{aligned} \tag{A.9}$$

$$\begin{aligned}\frac{\partial \mathbf{Q}}{\partial \theta_{kl}} &= 2 \sum_{l_1=1}^{L} \Re \left\{ \alpha_{kl} \alpha_{kl_1} e^{j(\phi_{kl} - \phi_{kl_1})} \left[ (\mathbf{u}_{kl}^{(r)} \otimes \mathbf{a}^1(\theta_{kl}) \mathbf{h}_{kl_1}^{(r)H} \right. \right. \\ &\quad \left. \left. + (\mathbf{u}_{kl}^{(r)} \otimes \mathbf{a}^1(\theta_{kl}) \mathbf{h}_{kl_1}^{(l)H} \right] \right\}, \end{aligned} \tag{A.10}$$

and

$$\frac{\partial \mathbf{Q}}{\partial \sigma^2} = 2\mathbf{I}. \tag{A.11}$$

$\Im(\cdot)$ stands for the imaginary part.

After having the elements of the FIM, the CRBs are easily obtained as

$$CRBs = diag\left\{ FIM^{-1} \right\} \tag{A.12}$$

## REFERENCES


1. T. S. Rappaport, *Wireless Communications: Principle & Practice.* Prentice Hall, 1996.

2. A. Paulraj and C. B. Papadias, "Space-time processing for wireless communications," *IEEE Signal Processing Magazine*, pp. 49–83, Nov. 1997.

3. J. G. Proakis, *Digital Communications.* McGraw-Hill, 3rd ed., 1995.

4. S. Verdú, "Minimum probability of error for asynchronous Gaussian multiple-access channel," *IEEE Trans. on Information Theory*, vol. 32, pp. 85–96, Jan. 1986.

5. S. Verdú, *Multiuser Detection.* Cambridge, U.K.: Cambridge Univ. Press, 1998.

6. R. Lupas and S. Verdú, "Linear multiuser detector for synchronous code division multiple access channels," *IEEE Trans. on Information Theory*, vol. 35, pp. 123–136, Jan. 1989.

7. R. Lupas and S. Verdú, "Near-far resistance of multiuser detectors in asynchronous channels," *IEEE Trans. on Communications*, vol. 38, pp. 496–508, Apr. 1990.

8. U. Madhow and M. Honig, "MMSE interference suppression for direct-sequence spread-spectrum CDMA," *IEEE Trans. on Communications*, vol. 42, pp. 3178–3188, Dec. 1994.

9. M. Honig, U. Madhow, and S. Verdú, "Blind adaptive multiuser detection," *IEEE Trans. on Information Theory*, vol. 41, pp. 944–960, Jul. 1995.

10. M. Honig and M. Tsatsanis, "Adaptive techniques for multiuser CDMA receivers," *IEEE Signal Processing Magazine*, vol. 17, pp. 49–61, May 2000.

11. H. Ge, "The LMMSE estimate-based multiuser detector: performance analyses and adaptive implementation," in *Proceedings of ICASSP*, pp. 571–574, 1997.

12. H. Ge, "Adaptive schemes of implementing the LMMSE multiuser detector for cdma," in *Proceedings of ICC*, pp. 615 –619, 1997.

13. A. J.Viterbi, "Very low rate convolutional codes for maximum theoretical performance of spread-spectrum multiple-access channels," *IEEE J. on Selected Areas in Communications*, vol. 8, pp. 641–649, May 1990.

14. A. Duel-Hallen, "Decorrelating decision-feedback multiuser detector for synchronous code-division multiple-access channel," *IEEE Trans. on Communications*, vol. 41, pp. 285–290, Feb. 1993.

15. A. Duel-Hallen, "A family of multiuser decision-feedback detectors for asynchronous code-division multiple-access channels," *IEEE Trans. on Communications*, vol. 43, pp. 421–434, Feb./Mar./Apr. 1995.

16. P. Patel and J. Holtzman, "Analysis of a simple successive interference cancellation scheme in a DS/CDMA system," *IEEE J. on Selected Areas in Communications*, vol. 12, pp. 796–807, Jun. 1994.

17. M. K. Varanasi and B. Aazhang, "Multistage detection for asynchronous code-division multiple-access communications," *IEEE Trans. on Communications*, vol. 38, pp. 509–519, Apr 1990.

18. M. K. Varanasi and B. Aazhang, "Near-optimum detection in synchronous code-division multiple-access systems," *IEEE Trans. on Communications*, vol. 39, pp. 725–736, May 1991.

19. U. Madhow, "Blind adaptive interference suppression for the near-far resistant acquisition and demodulation of the direct-sequence CDMA signals," *IEEE Trans. on Signal Processing*, vol. 45, pp. 124–136, Jan. 1997.

20. J. H. Winters, J. Salz, and R. D. Gitlin, "The impact of antenna diversity on the capacity of wireless communication systems," *IEEE Trans. on Communications*, vol. 42, pp. 1740–1751, Feb./Mar./Apr. 1994.

21. G. J. Foschni and M. J. Gans, "On limits of wireless communications in a fading environment when using multiple antennas," *Wireless Personal Communications*, vol. 6, pp. 311–335, 1998.

22. B. Suard, A. F. Naguib, G. Xu, and A. Paulraj, "Performance analysis of CDMA mobile communication systems using antenna arrays," in *Proceedings of ICASSP*, pp. 2140–2150, 1993.

23. A. F. Naguib and A. Paulraj, "Performance of CDMA cellular networks with base-station antenna arrays," in *Proceedings International Zurich Seminar on Digital Communications*, pp. 87–100, 1994.

24. A. F. Naguib, *Adaptive Antennas for CDMA Wireless Networks.* PhD thesis, Stanford University, CA, Aug. 1996.

25. M. D. Zoltowski and J. Ramo, "Blind adaptive beamforming for CDMA-based PCS/cellular," in *Proceedings of the 29th IEEE Asilomar Conference*, pp. 378–381, 1995.

26. H. Liu and M. D. Zoltowski, "Blind equalization in antenna array CDMA systems," *IEEE Trans. on Signal Processing*, vol. 45, pp. 161–172, Jan. 1997.

27. A. F. Naguib and A. Paulraj, "Performance enhancement and trade-offs of smart antennas in CDMA cellular networks," in *Proceeding of VTC*, pp. 40–44, 1995.

28. A. F. Naguib, A. Paulraj, and T. Kailath, "Capacity improvement with base-station antenna arrays in cellular CDMA," *IEEE Trans. on Vehicular Technology*, vol. 43, pp. 691–698, Aug. 1994.

29. J. Ramos, M. Zoltowski, and H. Liu, "Low-complexity space-time processor for DS-CDMA communications," *IEEE Trans. on Signal Processing*, vol. 48, pp. 39–52, January 2000.

30. Y.Chen, M. Zoltowski, J. Ramos, C. Chatterjee, and V. Roychowdhury, "Reduced-dimension blind space-time 2-D RAKE receivers for DS-CDMA communication systems," *IEEE Trans. on Signal Processing*, vol. 48, pp. 1521 –1536, June 2000.

31. X. Wu and A. M. Haimovich, "Space-time processing for CDMA communications," in *Proceedings of 31st Annual Conf. on Information Sciences and Systems*, pp. 371–376, 1995.

32. X. Bernstein and A. M. Haimovich, "Space-time optimum combining for CDMA communications," *Wireless Personal Communications*, vol. 3, pp. 73–89, Mar. 1996.

33. S. Affes and P. Mermelstein, "A new receiver structure for asynchronous CDMA: STAR-the spatio-temporal array-receiver," *IEEE J. on Selected Areas in Communications*, vol. 16, pp. 1411–1422, Oct. 1998.

34. X. Wang and H. V. Poor, "Space-time multiuser detection in multipath CDMA channels," *IEEE Trans. on Signal Processing*, vol. 47, pp. 2356–2374, Sep. 1999.

35. C. Brunner, M. Haardt, and J. A. Nossek, "On space-time RAKE receiver structures for WCDMA," in *Proceedings of the 33rd IEEE Asilomar Conference*, pp. 1546–1551, 1999.

36. D. A. Pados and S. N. Batalama, "Joint space-time auxiliary-vector filtering for DS/CDMA systems with antenna arrays," *IEEE Trans. on Communications*, vol. 47, pp. 1405–1415, Sep. 1999.

37. G. G. Raleigh, S. N. Diggavi, V. K. Jones, and A. Paulraj, "A blind adaptive transmit antenna algorithm for wireless communication," in *Proceeding of ICC*, pp. 1494–1499, 1995.

38. A. Wittneben, "A new bandwidth efficient transmit antenna modulation diversity scheme for linear digital modulation," in *Proceedings of ICC*, pp. 1630–1634, May 1993.

39. N. Seshadri and J. H. Winters, "Two signaling schemes for improving the error performance of frequency-division-duplex FDD transmission systems using transmitter antenna diversity," in *Proceedings of VTC*, pp. 508–511, 1994.

40. J. H. Winters, "The diversity gain of transmit diversity in wireless systems with rayleigh fading," in *Proceedings of ICC*, pp. 1121 –1125, 1994.

41. J. H. Winters, "The diversity gain of transmit diversity in wireless systems with rayleigh fading," *IEEE Trans. on Vehicular Technology*, vol. 47, pp. 119–123, Feb. 1998.

42. K. Rohani and L. Jalloul, "Orthogonal transmit diversity for direct spread CDMA," in *ETSI SMG2 Wideband CDMA Concept Group*, 1997.

43. K. Rohani, M. Harrison, and K. Kuchi, "A comparison of base station transmit diversity methods for third generation cellular standards," in *Proceedings of VTC*, pp. 351–355, 1999.

44. D. Rajan and S. D. Gray, "Transmit diversity schemes for CDMA-2000," in *Proceedings of WCNC*, pp. 669–673, 1999.

45. J. Guey, "Concatenated coding for transmit diversity systems," in *Proceedings of VTC*, pp. 2500–2504, 1999.

46. S. M. Alamouti, "A simple transmit diversity technique for wireless communications," *IEEE J. on Selected Areas in Communications*, vol. 16, pp. 1451–1458, Oct. 1998.

47. T. Lo and V. Tarokh, "Space-time block coding - from a physical perspective," in *Proceedings of WCNC*, pp. 150–153, 1999.

48. V. Tarokh, H. Jafarkhani, and A. R. Calderbank, "Space-time block coding for wireless communications: Performance results," *IEEE J. on Selected Areas in Communications*, vol. 17, pp. 451–460, Mar. 1999.

49. V. Tarokh, H. Jafarkhani, and A. R. Calderbank, "Space-time block codes from orthogonal designs," *IEEE Trans. on Information Theory*, vol. 45, pp. 1456–1467, Jul. 1999.

50. S. E. Bensley and B. Aazhang, "Maximum-likelihood synchronization of a single user for code devision multiple-access communication system," *IEEE Trans. on Communications*, vol. 46, pp. 393–399, Mar. 1998.

51. E. G. Ström and F. Malmsten, "A maximum likelihood approach for estimating DS-CDMA multipath fading channels," *IEEE J. on Selected Areas in Communications*, vol. 18, pp. 132–140, Jan. 2000.

52. D. Zheng, J. Li, S. L. Miller, and E. G. Ström, "An efficient code-timing estimator for DS-CDMA signals," *IEEE Trans. on Signal Processing*, vol. 45, pp. 82–89, Jan. 1997.

53. H. Ge, K. Wang, and K. Hong, "Fast delay estimation for asynchronous CDMA communications system," in *Proceedings of the 33rd IEEE Asilomar Conference*, pp. 1589–1593, Oct. 1999.

54. B. H. Khalaj, A. Paulraj, and T. Kailath, "Spatio-temporal channel estimation techniques for multiple access spread spectrum systems with antenna arrays," in *Proceeding of ICC*, pp. 1520–1524, 1995.

55. R. O. Schmidt, "Multiple emitter location and signal parameter estimation," *IEEE Trans. on Antennas Propagation*, vol. 36, pp. 1553–1560, Oct. 1986.

56. I. Ziskind and M. Wax, "Maximum likelihood localization of multiple sources by alternating projection," *IEEE Trans. on Signal Processing*, vol. 36, pp. 1553–1560, Oct. 1988.

57. K. M. Buckley and X. Xu, "Spatial-spectrum estimation in a location sector," *IEEE Trans. on Acoustics, Speech, and Signal Processing*, vol. 38, pp. 1842–1852, Nov. 1990.

58. M. Viberg and B. Ottersten, "Sensor array processing based on subspace fitting," *IEEE Trans. on Signal Processing*, vol. 39, pp. 1110–1121, May 1991.

59. P. Stoica and K. C. Sharman, "Maximum likelihood methods for direction-of-arrival estimation," *IEEE Trans. on Acoustics, Speech, and Signal Processing*, vol. 38, pp. 1132–1143, Jul. 1990.

60. M. Wax and A. Leshem, "Joint estimation of time delay and directions of arrival of multiple reflections of a known signal," *IEEE Trans. on Signal Processing*, vol. 45, pp. 2477–2484, Oct. 1997.

61. M. C.Vanderveen, A. L. van der Veen, and A. Paulraj, "Estimation of multipath parameters in wireless communications," *IEEE Trans. on Signal Processing*, vol. 46, pp. 682–691, Mar. 1998.

62. G. G. Raleigh and T. Boros, "Joint space-time parameter estimation for wireless communication channels," *IEEE Trans. on Signal Processing*, vol. 46, pp. 1333–1343, May 1998.

63. R. Madyastha and B. Aazhang, "Antenna arrays for joint maximum likelihood parameter estimation in CDMA systems," in *Proceedings of 31st Annual Conf. on Information Sciences and Systems*, (Baltimore, MD), pp. 984–988, Mar. 1997.

64. C. Sengupta, J. R. Cavallaro, and B. Aazhang, "Maximum likelihood multipath channel estimation in CDMA systems using antenna arrays," in *Proceedings of PIMRC*, pp. 1406–1410, 1998.

65. C. Sengupta, J. R. Cavallaro, and B. Aazhang, "On multipath channel estimation for CDMA systems using multiple sensors," *IEEE Trans. on Communications*, vol. 49, pp. 543–553, Mar. 2001.

66. H. Ge and K. Wang, "Bayesian based linear and non-linear detectors for CDMA communications," in *Proceeding of HOS'99*, pp. 135–139, 1999.

67. K. Wang, X. Cai, and H. Ge, "A novel space-time RAKE receiver for DS-CDMA systems," in *Proceeding of the 34th Annual Conf. on Information Sciences and Systems*, vol. II, (Princeton, NJ), pp. FA3–12–FA3–16, Mar. 2000.

68. K. Wang and H. Ge, "New space-time receivers for DS-CDMA systems," *submitted to IEEE Communications Letters*, 2001.

69. K. Wang and H. Ge, "Differential transceiver design for DS-CDMA system with transmit diversity," *accepted by VTC*, 2001.

70. K. Wang and H. Ge, "Differential detection scheme for DS-CDMA system with transmit diversity," *accepted by MILCOM*, 2001.

71. K. Wang and H. Ge, "Joint Space-Time channel parameter estimation for DS-CDMA system in multipath Rayleigh fading channels," *IEE Electronics Letters*, vol. 37, pp. 458–460, Mar. 2001.

72. K. Wang and H. Ge, "Joint estimation of time delays and DOA's for DS-CDMA system over multipath Rayleigh fading channels," *accepted by ICC*, Jun. 2001.

73. K. Wang and H. Ge, "Estimating temporal and spatial channel parameters for DS-CDMA system over multipath Rayleigh fading channels," in *Proceeding of ICASSP 2001*, vol. 4, pp. SPCOM–P2.2, May 2001.

74. K. Wang and H. Ge, "Joint channel parameter estimation for ds-cdma system over multipath rayleigh fading channels," *submitted to IEEE Transactions on Vehicular Technology*, 2001.

75. H. Ge and Y. Bar-Ness, "Bayesian approach to multiuser separation and interference suppression in CDMA communications," in *Proceeding of the 29th Asilomar Conf. on Signals, Systems, and Computer*, pp. 295–299, Oct. 1995.

76. H. Ge, "On the non-linear operators in the multiuser detectors for CDMA," in *Proceedings of 31st Annual Conf. on Information Sciences and Systems*, (Baltimore, MD), Mar. 1997.

77. S. M. Kay, *Fundamentals of Statistical Signal Processing: Estimation Theory*, vol. I. Prentice Hall, 1993.

78. J. S. Thompson, P. M. Grant, and B. Mulgrew, "Smart antenna arrays for CDMA systems," *IEEE Personal Communication Magazine*, pp. 16–25, Oct. 1996.

79. M. K. Tsatsanis and Z. Xu, "Performance analysis of minimum variance CDMA receivers," *IEEE Trans. on Signal Processing*, vol. 46, pp. 3014–3022, Nov. 1998.

80. Y. Chen and M. D. Zoltowski, "Convergence analysis and tracking ability of reduced dimension blind space-time RAKE receivers for DS-CDMA," in *Proceedings of VTC*, pp. 2333–2337, 1998.

81. R. A. Monzingo and T. W. Miller, *Introduction to Adaptive Arrays*, ch. 3. New York: Wiley-Interscience, 1980.

82. S. Haykin and A. Steinhardt, eds., *Adaptive RADAR Detection and Estimation*, ch. 4. New York: Wiley-Interscience, 1992.

83. H. Liu and K. Li, "A decorrelating RAKE receiver for CDMA communications over frequency-selective fading channels," *IEEE Trans. on Communications*, vol. 47, pp. 1036–1045, Jul. 1999.

84. B. H. Khalaj, A. Paulraj, and T. Kailath, "Antenna arrays for CDMA systems with multipath," in *Proceeding of MILCOM*, pp. 624–628, 1993.

85. A. F. Naguib and A. Paulraj, "Recursive adaptive beamforming for wireless CDMA," in *Proceeding of ICC*, pp. 1515–1519, 1995.

86. X. Cai, H. Ge, and A. N. Akansu, "Low-rank minimum variance CDMA receiver in multipath channels," in *Proceedings of ICASSP*, pp. 2877–2880, Jun. 2000.

87. V. Tarokh and H. Jafarkhani, "A differential detection scheme for transmit diversity," *IEEE J. on Selected Areas in Communications*, vol. 18, pp. 1169–1174, Jul. 2000.

88. D. W.Tufts, H. Ge, and S. Umesh, "Fast maximum likelihood estimation of single parameters using the shape of the compressed likelihood function," *IEEE Journal of Oceanic Engineering*, vol. 18, pp. 388–400, Oct. 1993.